Point and Probabilistic Forecasts for Day-Ahead Battery Scheduling

Zur Erlangung des akademischen Grades einer

Doktorin der Ingenieurwissenschaften

von der KIT-Fakultät für Informatik
des Karlsruher Instituts für Technologie (KIT)

genehmigte

Dissertation

von

Dorina Werling

Tag der mündlichen Prüfung: 27.10.2025

1. Referent: Prof. Dr. Veit Hagenmeyer
2. Referent: Prof. Dr. Antonello Monti

Acknowledgement

This thesis marks the end of a long journey, during which I have met many people to whom I am deeply grateful and without whom this work would not have been possible.

First, I want to thank my supervisors Veit Hagenmeyer and Ralf Mikut. I thank Veit Hagenmeyer for giving me the opportunity of this journey, believing in me, and supporting me throughout. I thank Ralf Mikut for having my back, the many valuable discussions and constructive feedback, and helping me to find my way when I felt lost. Additionally, I thank Antonello Monti for being my reviewer and Barbara Bruno for being a member of the committee.

Second, I thank Ben, Frederik and Max for their emotional and professional support. Specifically, Ben – my "Research-Buddy", but really so much more – without you, I would have remained stuck in a dead end. Frederik – a steady wave in the surf – thank you for your calm presence and for the proofreading. Max thank you for all the technical support and programming help.

Third, I thank my favorite OC group for all the deep and light-hearted talks, the serious and fun activities. We went through so many phases together, shaping a time I will always remember. This includes Adrian, Ben, Frederik, Henni, Janik, Rebecca, Tillmann, Xinliang, Yanlin.

Fourth, I thank the colleagues at IAI. In particular, I thank Kaleb for the professional and non-professional conversations, and my "Schreib-Buddy" Moritz for the exchange and keeping an eye on the process steps.

Fifth, I thank the people outside of IAI who accompanied me on this journey – my friends and family. Above all, I thank my parents for supporting my decisions and carrying my emotions with me. And Tobi, thank you for always being by my side and for being whatever I needed you to be: masseur, therapist, motivator, protector… and, most importantly, simply yourself.

Abstract

The global energy transition towards renewable energy sources (RES) poses challenges due to their inherent uncertainty, which reduces the energy system's flexibility and stability. Battery energy storage systems (BESS) offer a solution by increasing flexibility and making aggregated RES and loads dispatchable, enabling them to meet day-ahead dispatch schedules communicated with the grid through effective BESS management. This concept is implemented in a so-called dispatchable feeder (DF), which represents a system consisting of RES generation, loads, and a BESS, working together as a single controllable unit. The operation of the DF is formulated as a stochastic optimisation problem (OP) using forecasts of RES generation and loads as inputs. This thesis focuses on two main aspects affecting the performance of the DF: the forecasts and the mathematical formulation of the OP. In the first half of this thesis, the impact of different point forecasts with different characteristics on the performance of the DF via the so-called forecast value is investigated. Using a dataset of 300 residential buildings, the results show that the forecast characteristics affect the performance of the DF depending on problem-specific parameters. Based on these results, a meta-learning framework is proposed that automates the selection of the value-oriented forecast for the DF. The evaluation shows that the proposed framework outperforms existing forecast method selection heuristics in performance and accuracy. Additionally, it achieves comparable results to a manual selection with noticeably lower computational effort. In the second half of this thesis, probabilistic forecasts with different characteristics are evaluated with respect to the forecast value for the DF, showing again that the forecast characteristics in combination with the problem-specific parameters affect the performance of the DF. Additionally, a head-to-head performance comparison is made between the DF considering point forecasts and the DF considering probabilistic forecasts. This evaluation is carried out using both standard and the best value-oriented forecasts resulting from the aforementioned forecast evaluations. This allows for a comprehensive analysis of the impact of the forecast characteristics and the integration of the uncertainty of the RES generation and loads on the DF's performance. Finally, a modification to the mathematical formulation of the DF considering probabilistic forecasts is introduced, incorporating a line restriction to prevent line overloads in low-voltage distribution grids. Evaluations show that the modified DF can improve line usage and mitigate grid overloads.

Publications

Main Publications

- D. Werling et al. “Towards line-restricted dispatchable feeders using probabilistic forecasts for PV-dominated low-voltage distribution grids”. *Proceedings of the 13th ACM International Conference on Future Energy Systems, e-Energy ’22, Association for Computing Machinery* (June 2022), pp. 395–400. DOI: 10.1145/3538637.3538868
- D. Werling et al. “The Impact of Forecast Characteristics on the Forecast Value for the Dispatchable Feeder”. *Companion Proceedings of the 14th ACM International Conference on Future Energy Systems, e-Energy ’23, Association for Computing Machinery* (June 2023), pp. 59–71. DOI: 10.1145/3599733.3600251
- D. Werling et al. “Automating Value-Oriented Forecast Model Selection by Meta-learning: Application on a Dispatchable Feeder”. *Energy Informatics, Lecture Notes in Computer Science, Springer Nature Switzerland* (2024), pp. 95–116. DOI: 10.1007/978-3-031-48649-4_6

Further Publications

- S. Beichter et al. “Towards a Real-World Dispatchable Feeder”. *2023 8th IEEE Workshop on the Electronic Grid (eGRID)*. Oct. 2023, pp. 1–6. DOI: 10.1109/eGrid58358.2023.10380834
- M. Beichter et al. “Decision-Focused Retraining of Forecast Models for Optimization Problems in Smart Energy Systems”. *Proceedings of the 15th ACM International Conference on Future and Sustainable Energy Systems, Association for Computing Machinery*. e-Energy ’24 (2024), pp. 170–181. DOI: 10.1145/3632775.3661952
- M. Beichter et al. “Decision-focused fine-tuning of time series foundation models for dispatchable feeder optimization”. *Energy and AI* 21, 100533 (2025). DOI: 10.1016/j.egyai.2025.100533

Contents

List of Important Symbols

General Conventions for a Random Variable Z

s_Z	Statistical quantity of Z
$\hat{s}_Z$	Forecast of the statistical quantity of Z
z	Realisation of Z
$\mathbf{z}/\mathbf{Z}$	Vector of the realisation of Z / random variable Z
$\bar{z}/\mathbb{E}[Z]$	Mean of Z
$\mathrm{Var}[Z]$	Variance of Z
$F_Z(\cdot)$	Cumulative distribution function of Z
$f_Z(\cdot)$	Probability densitiy function of Z
$\mathbb{P}_Z$	Probability measure of Z
$q_Z(p)$	Quantile of random variable Z at probability p
ΔZ	Random variable representing the deviation from the mean of Z

Greek Symbols

α	Imbalance cost factor in the total cost
β_{load}, β_{PV}	Factors in the calculation of the prosumption
Δt	Duration of scheduling time intervals
δ	Parameter in the Huber metric
ϵ	Security level parameter
ϵ_{fix}	Relaxation decision variable for the security level of the energy chance constraint with no time-varying cost
ϵ_{var}	Relaxation decision variable for the security level of the energy chance constraint with time-varying cost
ϵ_E	Security level parameter of the energy chance constraint
ϵ_P	Security level parameter of the power chance constraint
$\hat{\xi}_j$	Vector of samples of the random parameters
μ	Loss coefficient of the BESS

Ω	Sample space
ω	Outcome within the sample space
τ	Parameter in the pinball loss
Θ	Parameter set
$\theta/\hat{\theta}$	Vector of (estimated) parameters
ξ	Parameter vector
ξ^{det}	Vector of deterministic parameters
Ξ^{rand}	Vector of random parameters
ζ	Relaxation parameter in the dispatchable feeder optimisation problem

Mathematical Sets

$\mathbb{N}$	Set of natural numbers
$\mathbb{N}_0$	Set of natural numbers including 0
$\mathbb{R}$	Set of real numbers
$\mathbb{R}_{\geq 0}$	Set of real numbers bigger or equal to zero
$\mathbb{Z}$	Set of integers
$n, n_1, u, v, v_1, w \in \mathbb{N}_0$	Dimension parameter

Other Symbols

$\bar{e}_s^{k_b}$	Estimated BESS' SoE for time interval k_b
$\Delta t \in \mathbb{R}$	Duration of scheduling time interval
$\hat{m}_i$	Output of the classifier for instance i
$\hat{x}_j$	Vector of samples of the random decision variables
$\mathcal{F}$	Function space
$\mathcal{I}$	Set of instances
$\mathcal{K}$	Discrete scheduling horizon
$\mathcal{K}_{\text{MPC}}$	Discrete rescheduling horizon
$\mathcal{M}$	Set of forecast methods
$\mathcal{T}$	Time index set
$\mathbf{Y}_{t+h}$	Vector of random variables $Y_{t+1}, Y_{t+2}, ..., Y_{t+h}$
$\mathbf{y}_{t-k}$	Vector of realisations $y_{t-k+q}, y_{t-k+2}, ..., y_t$
CRPS$(\cdot)$	Continuous ranked probability score
err$(\cdot)$	General function to measure the forecast error

$\mathrm{fem}(\cdot)$	General forecast evaluation metric function
$\mathrm{Value}(\cdot)$	Forecast value function
a	Downstream application
$c(\cdot)$	Classifier
$c(\cdot;\xi)$	Parameterised function with parameter ξ
$c_{\mathrm{DS}}(\cdot)$	Energy costs function of the dispatch schedule
c_{fix}, c_{var}	Cost coefficients of the relaxation for the security level of the energy chance constraints
$c_{\mathrm{imb}}(\cdot)$	Imbalance cost function
c^{+}_{quad}, c^{-}_{quad}, c^{+}_{lin}, c^{-}_{lin}	Cost coefficients of the energy costs
$c^{\Delta}_{\mathrm{quad}}$, $c^{\Delta}_{\mathrm{lin}}$	Cost coefficients of the imbalance cost
$c_{\mathrm{total}}(\cdot)$	Total cost function
d	Parameter for the modification of probabilistic forecasts
D_i	Data of instance i
$E_l(k+1)$	Random variable of the prosumption energy between the beginning of the time interval with index k_0 and the beginning of the time interval with index $k+1$
$E_s(k+1)$	Random variable of the BESS' SoE at the beginning of time interval with index $k+1$
$e_s^{\min}, e_s^{\max}$	Lower and upper BESS energy capacity
$f(\cdot;\theta)$	Parameterised function with parameter θ
$g(\cdot;\xi)$	Parameterised function with parameter ξ
h	Forecast horizon
$h(\cdot;\xi)$	Parameterised function with parameter ξ
i	Instance
j	Sample index in the context of sampling-based stochastic optimisation problems; Index of time intervals in the context of dispatchable feeder optimisation problem
k	Length of time series in the context of time series; Index of time interval in the context of dispatchable feeder
k_0	Index of time interval of the dispatch schedule computation
k_b	Index of time interval of the start of the dispatch schedule

m	Forecast method
$m_i^\star$	Forecast method leading to the forecast with the highest forecast value for instance i
md_i	Metadata from the data of instance i
N	Sample size
p	Probability
$p_{\text{load}}(k)$	Actual load averaged over the time interval with index k
$p_{\text{PV}}(k)$	Actual PV power generation averaged over the time interval with index k
$p_{g_{DS}}(k)$	Power dispatch schedule averaged over the time interval with index k
$p_{g_{reDS}}(k)$	Rescheduled power dispatch averaged over the time interval with index k
$p_g(k)$	Actual power dispatch averaged over the time interval with index k
$P_l(k)$	Random variable of the prosumption power averaged over the time interval with index k
$P_s(k)$	Random variable of the BESS' power input average over the time interval with index k
$p_s^{\text{min}}, p_s^{\text{max}}$	Lower and upper BESS power capacity
R	Feasible region of an optimisation problem
S	Original set of an optimisation problem
s	Number of time intervals for dispatch schedule extension
S'	Subset of the original set S of an optimisation problem
t, t_l, t_m, t'	Time index
w	Weight parameter
w_j	Weight
$x(k) \in \mathbb{R}^n$	Vector of decision variables for the time interval with index k
x^{det}	Vector of deterministic decision variables
X^{rand}	Vector of random decision variables
$Y / \{Y_t\}_{t \in \mathcal{T}}$	Time series
Y_t	Random variable at time index t of time series Y

Part I

Motivation

1 Introduction

The global energy transition towards a more sustainable and low-carbon-emissions energy system transforms the existing energy landscape. One such transformation is the massive integration of distributed renewable energy sources (RES) such as PV power generation. For example, the German government aims to achieve at least 80% share of RES by 2050 [25]. The challenge of such a massive integration is the uncertainty of generation inherent in the RES, which increases the inflexibility of the energy system. To counteract the inflexibility and thus maintain the energy system's stability, measures providing flexibility are necessary.

Flexibility in the energy system thereby refers to its ability to adapt and respond to changes in supply and demand, grid constraints, and market signals [45]. Different services provided by flexibility include frequency regulation, voltage support, and peak shaving, with various sources contributing to these services, such as demand-side management and battery energy storage systems (BESS) [66, 74]. With respect to the integration of RES, BESSs in particular become more and more relevant because of their strongly decreasing costs and fast improving efficiency [71, 81]. A promising way in which BESSs can contribute to a better integration of RES is by making systems containing aggregated RES and loads dispatchable through a proper BESS operation [12]. Dispatchability is thereby a subtype of flexibility and refers to the ability of a system to strictly follow a day-ahead dispatch schedule [149]. As renewable energy sources are not dispatchable per se due to their inherent uncertainty, the flexibility of the BESS enables following the dispatch schedule. Such a commitment to a dispatch schedule leads to a better reliability for the energy system operator and thus a better integration into the existing market, allowing the energy system operator to plan the energy supply and communicate with the consumer primarily through price signals. This idea is implemented in virtual power plants and microgrids [12, 104], which aggregate various distributed RESs and BESSs into a single dispatchable system. However, both virtual power plants and microgrids face limitations, such as the complexity of coordinating all system components and thus the need for advanced control systems. By focusing on the dispatch of active power only, this thesis aims to simplify the control and coordination challenges. In accordance with [8, 126] such a concept is referred to as dispatchable feeder (DF).

The DF operates hierarchically on multiple time scales, starting with the computation of the day-ahead dispatch schedule. This can be followed by an intra-day rescheduling via model predictive control (MPC) based on current information. Finally, the actual dispatch is calculated based on the actual data in real time. Mathematically, this hierarchical operation is formulated as a stochastic optimisation problem, which uses forecasts of the RES and the loads as input for a proper operation. Consequently, the forecasts have a direct impact on the performance of the stochastic optimisation problem, which is referred to as the value of the forecast. How the forecasts influence the performance depends, inter alia, on the integration of the uncertainty in the mathematical formulation of the stochastic optimisation problem. While a mathematical formulation considering probabilistic forecasts such as in [8] can account for the uncertainty, a mathematical formulation considering point forecasts does not include this uncertainty. Additionally, the mathematical formulation determines, which physical aspects of the real world are taken into account. Thus, both the used mathematical formulation of the stochastic optimisation problem and the forecasts are two important aspects for the dispatchable feeder and are central focuses of this thesis.

The remainder of this Part I is structured as follows. First, Chapter 2 provides the foundation of forecasting in Section 2.1, the foundation of optimisation in Section 2.2, the foundation of the dispatchable feeder in Section 2.3, and the experimental setup for the experiments in this thesis in Section 2.4. Finally, Chapter 3 specifies the research questions addressed in Section 3.1 and the further structure of this thesis in Section 3.2.

2 Forecasting and Optimisation for Dispatchable Feeder

This chapter provides the foundations relevant for this thesis. This includes the foundation of forecasting, the foundation of optimisation, and the foundation of the dispatchable feeder. Finally, the experimental setup is described.

2.1 Foundation of Forecasting

As forecasts are essential for the dispatchable feeder, this section presents the foundation of forecasting. First, forecasting is introduced. Second, different types of time series forecasts are described, which are particularly relevant as the dispatchable feeder relies on such forecasts. Finally, different aspects of the evaluation of forecasts are explained.

2.1.1 Introduction to Forecasting

The general task in **forecasting** is to predict uncertain future quantities based on knowledge that may affect the future [70]. While the difficulty of accurate forecasting depends on the target being forecasted and the knowledge in the form of data, an exact forecast and thus the elimination of the future's uncertainty can not be expected in relevant tasks [107]. Instead, forecasting aims to quantify this uncertainty by determining statistical quantities $s_Z \in \mathbb{R}^n, n \in \mathbb{N}$, of the to be forecasted target variable Z [49], such as the mean. The result is a forecast

$$\hat{s}_Z = f(x; \hat{\theta}) \tag{2.1}$$

of Z using knowledge in the form of data x, called features. Note that throughout this thesis, the symbol $\hat{}$ is used to indicate a forecast. To approximate the relationship between the statistical quantity of Z and x, typically a parameterised function f with parameters θ from an assumed function space $\mathcal{F}$ and parameter set Θ is used. During training, the parameters are then estimated, denoted as $\hat{\theta}$, with respect to

the chosen forecasting specifications. In this thesis, we consider forecasting in the context of real-valued time series.

A **time series** is, mathematically, a sequence of random variables on a common probability space, also called a stochastic process, over equidistant time indices, i.e.

$$Y = \{Y_t\}_{t \in \mathcal{T}} \tag{2.2}$$

with random variables Y_t and time index set[1] $\mathcal{T} = \mathbb{Z}$, see [22, 83]. In practice, one observes data of the time series $\mathbf{y}_{t-k} = (y_{t-k+1}, y_{t-k+2}, ..., y_t), t \in \mathcal{T}$, of length $k \in \mathbb{N}$, which are considered as realisations of the random variables. In **time series forecasting**, the target variables are then the future realisations of the time series [56]. Because the future realisations of the time series are influenced by both historical realisations of the time series and exogenous factors, typical features consist of both. The forecast of $\mathbf{Y}_{t+h} = (Y_{t+1}, Y_{t+2}, ..., Y_{t+h})$ with forecast horizon $h \in \mathbb{N}$ can then be written as

$$\hat{s}_{\mathbf{Y}_{t+h}} = f(\mathbf{y}_{t-k}, \{Y^{exog}_{t'}\}_{t' \in \mathcal{T}}; \hat{\theta}) \tag{2.3}$$

with the time series of the exogenous factors[2] $\{Y^{exog}_{t'}\}_{t' \in \mathcal{T}}$.

2.1.2 Types of Time Series Forecasts

Because of the huge interest in forecasting the future, there is a wide variety of forecasts and ways to generate them to meet different needs. These forecasts can be grouped according to different aspects, some of which are outlined below[3].

Statistical Quantity Forecasts can be grouped according to the type of statistical quantity they forecast, namely as point forecasts or probabilistic forecasts. A **point forecast** is a single-valued forecast for each time step. In doing so, typically centre-oriented statistical quantities, often called location, such as the mean or the median

[1] A time series can also be defined with $\mathcal{T} = \mathbb{N}_0$. However, the definition with $\mathcal{T} = \mathbb{Z}$ is more common.
[2] Note that the time indices of $\mathbf{y}_{t-k}$ and $\{Y^{exog}_{t'}\}_{t' \in \mathcal{T}}$ do not have to be the same, as indicated by the usage of t'
[3] This section provides an introduction to key terms relevant to this thesis and does not aim to provide a comprehensive overview of all types. For an in-depth exploration, see [56].

are considered [56]. For the mean $\bar{\mathbf{y}}_{t+h} = \mathbb{E}[\mathbf{Y}_{t+h}]$, Equation (2.3) can be written as

$$\hat{s}_{\mathbf{Y}_{t+h}} = \hat{\bar{\mathbf{y}}}_{t+h} = \hat{\mathbb{E}}[\mathbf{Y}_{t+h}|\mathbf{y}_{t-k}, \{Y_{t'}^{exog}\}_{t' \in \mathcal{T}}; f, \hat{\theta}]. \tag{2.4}$$

In contrast, a **probabilistic forecast** aims for the full information of the uncertainty [99]. While several statistical quantities fulfil this property, the following statistical quantities are relevant for this thesis:

- *Distribution forecast*: A distribution forecast attempts to forecast the probability density function (PDF) $f_{\mathbf{Y}_{t+h}} : \mathbb{R}^h \to \mathbb{R}_{\geq 0}, h \in \mathbb{N}$, or cumulative distribution function (CDF) $F_{\mathbf{Y}_{t+h}} : \mathbb{R}^h \to [0, 1]$ in its entirety [99]. The result is a forecasted conditional PDF or CDF, which is denoted as $\hat{f}_{\mathbf{Y}_{t+h}}$ and $\hat{F}_{\mathbf{Y}_{t+h}}$. However, this approach can be computationally expensive. One strategy to overcome this challenge is to discretise the distribution, often using methods such as quantiles.

- *Quantile forecast*: The quantile $q_{\mathbf{Y}_{t+h}} : (0, 1) \to \mathbb{R}^h, h \in \mathbb{N}$, for the CDF $F_{\mathbf{Y}_{t+h}}$ and probability $p \in (0, 1)$ is defined as [123]

  $$q_{\mathbf{Y}_{t+h}}(p) = \inf\{z \in \mathbb{R}^h : F_{\mathbf{Y}_{t+h}}(z) \geq p\}. \tag{2.5}$$

  If the inverse of the CDF exists, the quantile can be written as $q_{\mathbf{Y}_{t+h}}(p) = F^{-1}_{\mathbf{Y}_{t+h}}(p)$. The resulting forecast is written as $\hat{q}_{\mathbf{Y}_{t+h}}(p)$. While a single quantile forecast is a (biased) point forecast, with the quantile at $p = 0.5$ representing the median, multiple quantile forecasts with different probabilities can contain sufficient information to derive the PDF and CDF [108].

Probabilistic forecasts, although beneficial for modeling uncertainty, present challenges as they are more computationally expensive and not straightforward to incorporate into applications.
In between probabilistic and point forecasts, further approaches exist, such as **scenario forecasts**. These forecasts consist of multiple point forecasts of possible time trajectories to capture the uncertainty of future outcomes [36]. Each time trajectory can be equipped with a weight, in some cases corresponding to probabilities. The time trajectories can be generated using various approaches, including scenario trees, sampling from pre-generated ensembles (often obtained using the Monte-Carlo method), and directly sampling out of distribution or quantile forecasts. In contrast to probabilistic forecasts, scenario forecasts can easily incorporate considerations of correlations between timestamps and other random variables. This can be particularly beneficial for multivariate forecasts.

Tab. 2.1.: The suitability to forecast different types of statistical quantities, the required dataset size, and the computational effort for training of common machine learning methods in time series forecasting [9, 33, 52, 61, 62, 63, 70, 109, 120, 135]. Note that this comparison is intended to provide a general understanding rather than absolute validity, as the determination of the required dataset size and the computational effort for training depends heavily on the specific data and application.

Method	Point	Probabilistic		Non-parametric	Dataset size	Computational effort
		Distribution	Quantiles			
Linear regression	✓	✗	✗	✗	Small to medium	Low
XGBoost	✓	✗	✓	✗	Medium to large	Medium to high
General NNs	✓	✗	✓	✓	Small to large	High to very high
Transformers	✓	✗	✓	✓	Large	Very high
DeepAR	✓[4]	✓	✓	✗	Medium	High
Invertible NNs	✓	✗	✓	✓	Large	High

Further categorisations, especially for probabilistic forecasts, are parametric or non-parametric. **Parametric** approaches assume that the distribution of a random variable belongs to a specific parametric family of functions such as the normal distribution [56]. The parameters uniquely define the distribution and are unknown, but may be forecasted [107]. In contrast, **non-parametric** approaches forecast the statistical quantity without making assumptions about the underlying distribution, relying solely on the available data. This makes non-parametric approaches less restrictive but more computationally expensive, as the forecasting of the distribution is not limited to the forecasting of the distribution's parameters [32].

Forecast Method Forecasts are often categorised according to the method used. While there are many forecast methods, they can be divided into statistical and machine learning methods. More specifically, **statistical methods** assume a fixed dependency structure and make use of statistical models. Their results are easy to interpret and fast to compute. In time series forecasting, typical statistical methods are moving average (MA) [150], exponential smoothing (ES) [23, 65], and autoregressive integrated moving average (ARIMA) [20]. On the other hand, **machine learning methods** use algorithms and computing power to identify complex patterns and relationships in data [61]. As such, they operate without the assumption of a fixed dependency structure and their learning may not be easy to understand. Due to advances in hardware and the exponential growth of available data, machine learning methods are becoming increasingly important. Commonly used machine

[4] DeepAR is primarily a method for probabilistic forecasting. However, point forecasts can be derived from the probabilistic forecasts.

learning methods include linear regression, XGBoost [33] and neural networks (NN). For NNs, advanced methods have been developed under the term deep learning [88], which involves NNs with many layers. Examples of deep learning methods are transformers [135], DeepAR [120], and invertible neural networks [42]. These advanced methods can effectively describe complex patterns in large amounts of data. However, they can perform worse than simpler methods when less data is available due to overfitting and the high computational effort required for training. A comparison of the forecast methods mentioned, including their suitability to forecast the statistical quantities described above, their dataset size requirements, and their computational effort for training, can be found in Table 2.1.

2.1.3 Forecast Evaluation

When evaluating forecasts, there are many aspects [98] that form the basis for the selection of the forecast method, its hyperparameters and features. Two of these aspects are described below.

Data Data is the foundation of all time series forecasting. When working with real-world data, a pre-processing of the data with a comprehensive inspection and analysis is essential. This includes the detection and handling of anomalies [132] and missing values [142]. Depending on the forecast method and the data's nature, transformation and normalisation may prove beneficial. For example, the lognormal transformation adapts the data to the assumption of a normal distribution. Common normalisation approaches include the min-max scaler, which normalises the data to a range between 0 and 1, and the standard scaler, which scales the data to have a mean of 0 and a variance of 1. Once the data is clear and prepared, the choice of the data for training, validation, and testing the forecast method is important to avoid over-fitting to the training data and to enable reliable forecasts on new, unseen data. While simple data splitting produces single training, validation, and testing sets, cross-validation involves iterative training and testing over different subsets of the data, called folds. This process often eliminates the need for a separate validation set.

Forecast Evaluation Metric The forecast evaluation metric defines what constitutes a "good" forecast and is thus a key aspect in forecast evaluation. According to [100], forecasts can be evaluated based on their quality as well as their value they provide. The **forecast quality** assesses the forecast solely from the perspective of

accurate forecasting, neglecting its further usage. Consequently, the forecast quality depends on the to be forecasted statistical quantity. For point forecasts, quality is often expressed in terms of the forecast error, i.e.

$$\text{fem}(\hat{\mathbf{s}}, \mathbf{y}) = \frac{1}{(m-l+1)\cdot h} \sum_{j=l}^{m} \sum_{i=1}^{h} \text{err}(y_{t_j+i} - \hat{s}_{\mathbf{Y}_{t_j+h},i}) \tag{2.6}$$

for the forecasts $\hat{\mathbf{s}} = (\hat{s}_{\mathbf{Y}_{t_l+h}}, \hat{s}_{\mathbf{Y}_{t_{l+1}+h}}, ..., \hat{s}_{\mathbf{Y}_{t_m+h}})$, $h \in \mathbb{N}$, $t_l < t_{l+1} < ... < t_m \in \mathcal{T}, l < m \in \mathbb{N}$, the actual realisations $\mathbf{y} = (\mathbf{y}_{t_l+h}, \mathbf{y}_{t_{l+1}+h}, ..., \mathbf{y}_{t_m+h})$, $\hat{s}_{\mathbf{Y}_{t_j+h},i}$ the ith entry of $\hat{s}_{\mathbf{Y}_{t_j+h}}$, and the function $\text{err} : \mathbb{R} \to \mathbb{R}$ determining how the forecast error is measured. This function can be tailored to give different weighting to different characteristics. Typical point forecast evaluation metrics are the mean squared error (MSE) with

$$\text{err}(z) = z^2 \tag{2.7}$$

and the mean absolute error (MAE) with

$$\text{err}(z) = |z|. \tag{2.8}$$

While the first weights larger absolute forecast errors stronger, the latter weights all forecast errors equally. Other point forecast evaluation metrics take a composite approach through a piecewise error function, such as the Huber metric [69], which is defined as

$$\text{err}(z;\delta) = \begin{cases} \frac{1}{2}\cdot z^2, & \text{for } |z| < \delta \\ \delta \cdot (|z| - \frac{1}{2}\delta), & \text{otherwise} \end{cases} \tag{2.9}$$

for $\delta > 0$. The Huber metric is equal to the MSE for absolute forecast errors smaller to δ, and otherwise a function based on the absolute forecast error. In contrast, probabilistic forecasts require metrics considering different characteristics than the forecast error, such as calibration and sharpness. Calibration refers to the alignment of the forecasted distribution with their true values ensuring the reflection of the true likelihood. A common metric for calibration is the coverage rate. It is the proportion of times that the true values fall within a forecasted interval. In contrast, sharpness measures the spread of the forecasted distribution, focusing on the uncertainty inherent in the forecast itself, without considering the actual realisations. A metric for sharpness is the interquartile range and the interdecile range. The interquartile range is the difference between the quantile forecast at $p = 0.75$ and the quantile forecast at $p = 0.25$, while the interdecile range is the difference between the quantile forecast at $p = 0.9$ and the quantile forecast at $p = 0.1$. A metric that

considers both calibration and sharpness is the continuous ranked probability score (CRPS) [49], which is defined as

$$\text{CRPS}(\hat{\mathbf{F}}, \mathbf{y}) = \frac{1}{(m-l+1)\cdot h} \sum_{j=l}^{m} \sum_{i=1}^{h} \int_{\mathbb{R}} (\hat{F}_{\mathbf{Y}_{t_j+h},i}(u) - \mathbb{1}_{\{u \leq y_{t_j+i}\}})^2 du \tag{2.10}$$

with CDF forecast $\hat{\mathbf{F}} = (\hat{F}_{\mathbf{Y}_{t_l+h}}, \hat{F}_{\mathbf{Y}_{t_{l+1}+h}}, ..., \hat{F}_{\mathbf{Y}_{t_m+h}})$, $h \in \mathbb{N}$, $t_l < t_{l+1} < ... < t_m \in \mathcal{T}, l < m \in \mathbb{N}$, the actual realisations $\mathbf{y} = (\mathbf{y}_{t_l+h}, \mathbf{y}_{t_{l+1}+h}, ..., \mathbf{y}_{t_m+h})$, $\hat{F}_{\mathbf{Y}_{t_j+h},i}$ the ith entry[5] of $\hat{F}_{\mathbf{Y}_{t_j+h}}$, and indicator function $\mathbb{1}$. The last probabilistic forecast metric we want to mention is the pinball loss. It evaluates the probabilistic forecast point-wise and can be written in the form of Equation (2.6) with

$$\text{err}(z) = \max\{\tau \cdot z, (\tau - 1) \cdot z\} \tag{2.11}$$

for a $\tau \in (0, 1)$. It is typically used as loss function to forecast quantiles of probability τ. If a CDF forecast is evaluated with the pinball loss, $\hat{\mathbf{s}}$ specifies to $\hat{\mathbf{F}}(\tau)$. Additionally, the pinball loss can be calculated over several τ values and then average over all τ values.

As opposed to the forecast quality, the **forecast value** considers the benefit that the forecast provides when used for a downstream application, as the forecast may affect the performance of the downstream application [100]. Given the broad range of downstream applications, the performance of the downstream application, and thus the forecast value, can be measured in several ways. A typical metric for evaluating the performance of the downstream application is economic cost [107]. While the consideration of the forecast value can be important when using forecasts in downstream applications, forecast quality metrics dominate both the literature and practice.

2.2 Foundation of Optimisation

Optimisation plays a crucial role for the dispatchable feeder as its operation is formulated as a stochastic optimisation problem. Therefore, this section first introduces optimisation in general and then presents different categories of optimisation problems. Afterwards, stochastic optimisation problems and their challenges are explained and finally, how to solve optimisation problems is described.

[5] Note that this formulation implies that the forecast for $\mathbf{Y}_{t_j+h}$ consists of h marginal CDFs for each time step. However, it is also possible to forecast one multivariate CDF, particularly when the random variables in $\mathbf{Y}_{t_j+h}$ are correlated.

2.2.1 Introduction to Optimisation

In optimisation, one aims to minimise an objective function over a given region of feasible solutions [46]. The general form can be expressed as

$$\begin{aligned} \min_{x \in S} \quad & c(x;\xi) \\ \text{s.t.} \quad & h(x;\xi) \leq 0 \\ & g(x;\xi) = 0 \end{aligned} \tag{2.12}$$

with the original set $S \subset \mathbb{R}^n, n \in \mathbb{N}_0$, the objective function[6] $c : \mathbb{R}^n \to \mathbb{R}$, the vector of decision variables $x \in \mathbb{R}^n$, the vector of parameters $\xi \in \mathbb{R}^u, u \in \mathbb{N}_0$, the vector of inequality constraints $h(x;\xi) \leq 0$ given ξ with $h : \mathbb{R}^n \to \mathbb{R}^v, v \in \mathbb{N}_0$, the vector of equality constraints $g(x;\xi) = 0$ given ξ with $g : \mathbb{R}^n \to \mathbb{R}^w, w \in \mathbb{N}_0$, and the feasible region $R = \{x \in S : h(x;\xi) \leq 0, g(x;\xi) = 0\}$. Based on specifications such as the nature of the functions and the feasible region, the optimisation problem (OP) can be categorised into different categories. This category influences the solution approach, leading to either local or global solutions. While the former minimises the objective function only in its local neighbourhood within the feasible region, the latter represents a point within the feasible region where the objective function reaches its minimum over all other points.

2.2.2 Categories of Optimisation Problems

Optimisation problems come in various forms. To derive theoretical statements and develop fitting solution approaches, OPs can be categorised based on different aspects, some of which are outlined below.

Decision Variable OPs can be categorised according to the nature of the decision variables, namely as continuous or discrete. In **continuous** optimisation, the feasible region is uncountable, allowing the decision variables to take on any real value within a given range. On the other hand, in **discrete** optimisation, the feasible region must be countable, leading to problems commonly referred to as integer OPs. There is also a hybrid category known as mixed-integer OPs, where some decision variables are restricted to integer values while others are not.

[6] This formulation addresses commonly considered single-criteria optimisation problems, unlike multi-criteria optimisation problems with objective function $c : \mathbb{R}^n \to \mathbb{R}^m, m \in \mathbb{N}$.

Objective Function and Constraints An important categorisation of OPs is based on the nature of the objective function and the constraints. Common categories are linear, non-linear, convex, and non-convex. An OP is **linear** if both the objective function and the functions describing the constraints are linear, otherwise it is non-linear. Further, if the objective function is convex and the constraints describe a feasible region that forms a convex set, the OP is **convex**, otherwise it is non-convex. A notable advantage of convex OPs is that every local minimum is a global minimum, which is exploited during solving. While the theoretical complexity lies between convex and non-convex OPs, the practical complexity can already lie between linear and non-linear OPs as there is no universal solution approach for non-linear OPs [54].

Structure While a simple structure of an OP can be formulated using the general form in Equation (2.12), many real-world problems have a more complex structure, such as hierarchical OPs. A **hierarchical** OP consists of multiple nested OPs [134]. Each of these nested OPs, called levels, can have its own objective function, decision variables and constraints. To solve a hierarchical OP, each level must be solved iteratively, respecting the hierarchy.

Parameters To formulate an OP, various parameters must be defined, some of which may not be known in advance. Such OPs are subject to uncertainty and are called **stochastic** OPs. In contrast, in **deterministic** OPs all parameters are known in advance.

2.2.3 Stochastic Optimisation Problems

In many real-world OPs, not all parameters can be defined in advance. Stochastic OPs deal with this aspect by modelling these parameters as random variables, introducing uncertainty and potentially making decision variables random. However, a random decision variable is counterintuitive. For better understanding, the concept of **stages** is introduced [68]. The idea is to break down the OP into stages, each referring to a different point in time when new information arises and decisions are made [36, 78]. I.e., within each stage, a subset of decision variables and parameters become deterministic, while others remain random. Decisions associated with

the deterministic variables are made at that specific stage. The general form in Equation (2.12) can then be written as

$$\begin{aligned} \min_{\substack{x^{\text{det}} \in S' \\ X^{\text{rand}}}} \quad & c(x^{\text{det}}, X^{\text{rand}}; \xi^{\text{det}}, \Xi^{\text{rand}}) \\ \text{s.t.} \quad & h(x^{\text{det}}, X^{\text{rand}}; \xi^{\text{det}}, \Xi^{\text{rand}}) \leq 0 \\ & g(x^{\text{det}}, X^{\text{rand}}; \xi^{\text{det}}, \Xi^{\text{rand}}) = 0 \end{aligned} \tag{2.13}$$

with the subset of the original set $S' \subset \mathbb{R}^{n_1}, n_1 \in \mathbb{N}_0$, the vector of the deterministic decision variables $x^{\text{det}} \in \mathbb{R}^{n_1}$, the vector of the deterministic parameters $\xi^{\text{det}} \in \mathbb{R}^{u_1}, u_1 \in \mathbb{N}_0$, the vector of the random decision variables $X^{\text{rand}} : \Omega \to \mathbb{R}^{n-n_1}$ with sample space Ω, and the vector of the random parameters $\Xi^{\text{rand}} : \Omega \to \mathbb{R}^{u-u_1}$. However, this formulation is not well defined as the minimum operator over a random variable and the inequality constraints involving random variables are not clear and therefore require interpretation [72]. Moreover, a random variable with infinite support potentially leads to an infinite-dimensional OP that is computationally intractable [7]. However, it is important to note that even a random variable with finite support can lead to an infinite-dimensional OP, depending on the structure of the OP. Therefore, a reformulation into a deterministic OP that can be solved with numerical algorithms is necessary. In doing so, several approaches exist that can be categorised as sampling-based and non-sampling-based. In the following, we further describe existing approaches within these two categories and explain their interpretation and how they achieve computational tractability.

Sampling-Based One common approach is to restrict the random variables to a finite number of possible realisations [29]. Therefore, samples $\hat{\xi}_j = \Xi^{\text{rand}}(\hat{\omega}_j)$ and $\hat{x}_j = X^{\text{rand}}(\hat{\omega}_j)$ with $\hat{\omega}_j \in \Omega, j = 1, ..., N \in \mathbb{N}$ are generated, assigned with a weight w_j. The benefit of this approach is that no extensive reformulation of the OP is needed:

$$\begin{aligned} \min_{x^{\text{det}} \in S'} \quad & \sum_{j=1}^{N} w_j \cdot c(x^{\text{det}}, \hat{x}_j; \xi^{\text{det}}, \hat{\xi}_j) \\ \text{s.t. for all } j = 1, ..., N \quad & \\ & h(x^{\text{det}}, \hat{x}_j; \xi^{\text{det}}, \hat{\xi}_j) \leq 0 \\ & g(x^{\text{det}}, \hat{x}_j; \xi^{\text{det}}, \hat{\xi}_j) = 0 \end{aligned} \tag{2.14}$$

As samples, typically scenario forecasts are used.

Non-Sampling-Based In non-sampling-based approaches, the OP is reformulated using statistical quantities of the random variables such as moments, quantiles, and CDFs. These statistical quantities are then usually forecasted with suitable forecasting specifications. Because the reformulations depend on many aspects such as the problem-specific structure and the modelling choice, a standard way is not given. In the following, some existing approaches for the reformulation are presented.

The first is the reformulation of the OP using single moments of the random variable. The simplest yet often used specification is to use the first moment – the mean – only. The resulting OP shows similarity to Equation (2.14) with $N = 1$. This reformulation can be extended by the consideration of other moments such as the variance [8, 10]. Using single moments limits the inclusion of the random variable to single points neglecting the uncertainty.

To include the uncertainty, the OP can be reformulated using (full) information on the uncertainty. Such a reformulation is not straightforward and must be well thought out. One widely used reformulation for inequality constraints is the interpretation as chance constraint [31]. This interpretation ensures that the inequality constraints are met with a predetermined probability, often referred to as security level, thus introducing a probabilistic perspective. To achieve computational tractability, the chance constraint can be reformulated under certain conditions via the CDF or quantile of the random variable $H = h(x^{\text{det}}, X^{\text{rand}}; \xi^{\text{det}}, \Xi^{\text{rand}})$:

$$\begin{aligned} & \mathbb{P}_H(H \leq 0) \geq 1 - \epsilon \\ \Rightarrow \quad & F_H(0) \geq 1 - \epsilon \\ \Rightarrow \quad & q_H(1 - \epsilon) \leq 0 \end{aligned} \tag{2.15}$$

with probability measure $\mathbb{P}_H$, CDF F_H, and quantile q_H of random variable H and security level parameter $\epsilon \in (0, 1)$. If the distribution of the random variable H is assumed to follow a parametric distribution, the chance constraints can be further reformulated using the parameters of this distribution. A probabilistic interpretation is also achievable for the objective function with the (conditional) value at risk [10].

2.2.4 Solving Optimisation Problems

Depending on the category of the OP, theoretical statements and solution approaches, often implemented as numerical algorithms, exist for solving it. Therefore, it is crucial to formulate the OP appropriately according to its category, ensuring reasonable

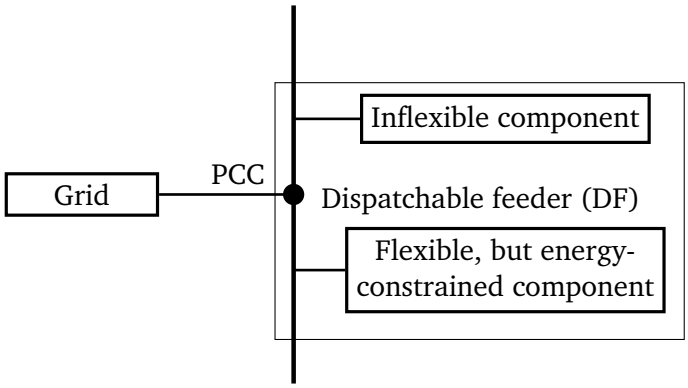

Fig. 2.1.: The dispatchable feeder combines inflexible generation – as PV power generation – and load with a flexible, but energy constrained component – as a BESS. These two components are connected to the grid via one bus at the point of common coupling (PCC) (adapted from [8] and [17]).

theoretical statements and available stable numerical algorithms [54]. Because even if an OP can be solved analytically, the solution is often found numerically due to the low computational effort. The variety of such numerical algorithms is large and can be divided into exact and approximate. The first category describes algorithms that find the exact global minimum by exploring the entire feasible region, e.g. branch-and-bound algorithm [86]. However, exploring the entire feasible region is not computationally tractable for most OP categories. Therefore, approximate algorithms efficiently provide solutions close to the optimal solution. Subcategories of such approximate algorithms are heuristic algorithms, e.g. interior-point method [75] and particle swarm optimisation [76], and meta-heuristic algorithms, e.g. evolutionary algorithm [117].

For implementation, various numerical solvers supporting commonly used programming languages are available that implement these numerical algorithms, e.g. Ipopt [137], Gurobi, and CPLEX. Additionally, these solvers and other optimisation-relevant features are supported in modelling languages such as Pyomo [27, 59], CasADi [6], YALMIP [92], and JuMP [93].

2.3 Foundation of Dispatchable Feeder

This section describes the foundation of the dispatchable feeder, starting with an introduction. Afterwards, the different aspects of the optimisation problem for the dispatchable feeder are described, followed by the forecasting for the dispatchable feeder. Finally, the framework of the dispatchable feeder is presented.

2.3.1 Introduction to Dispatchable Feeder

Numerous studies investigate the concept of coupling inflexible renewable generation with a flexible battery energy storage system (BESS) to provide ancillary services to the grid, e.g. [2, 8, 37, 55, 73, 87, 102, 103, 126, 146, 148, 157]. In this thesis, we focus on the day-ahead scheduling of portions of active power exchange, called dispatch, between the grid and a coupled system consisting of inflexible renewable generation and load and a flexible, but energy-constrained BESS, as illustrated in Figure 2.1. Within this framework, we introduce the term **prosumption**, defined as load minus renewable generation. The aim of the day-ahead scheduling is to achieve dispatchability of the inflexible prosumption with the help of the flexible BESS. We denote such a coupled system with the aim of following a day-ahead dispatch schedule (DS) as a **dispatchable feeder** (DF) [8, 126]. The operation of the DF is hierarchical, beginning with the computation of the day-ahead DS based on prosumption forecasts and concluding with the calculation of actual dispatch considering the actual prosumption data. This hierarchical operation can be formulated as stochastic OP. Depending on the setting specifications, such as the ownership of the BESS, this operation can be performed by either the grid operator or the prosumption producer. To facilitate its operation, the DF utilises a smart grid infrastructure enabled by the Internet of Things (IoT), which communicates through information and communication technology (ICT) [41]. In this setup, smart meters ensure the collection and transmission of necessary real-time data to enable the management of necessary information flows. More precisely, externally, the DF receives a price signal from the grid operator, such as from a time-of-use price tariff [138], influencing the DS [80]. This DS is then communicated back to the grid operator. Additionally, the actual dispatch is coordinated between the grid operator and the DF. Internally, the DF manages information flows between its components, including monitoring of renewable generation and the BESS.

2.3.2 Optimisation Problem for Dispatchable Feeder

Having introduced the concept of the DF, a closer look is taken at how it is achieved. Therefore, a mathematical model of the DF and its operation is required. Such a mathematical model is typically formulated - as is common for scheduling problems [26, 115] - as a stochastic OP. Therefore, the operation of the DF is discretised with time intervals of duration $\Delta t \in \mathbb{R}$ indexed by $k \in \mathbb{N}$. When formulating the stochastic OP, relevant physical aspects of the real world should be considered while maintaining the ability to be efficiently solvable. Among others, three aspects are

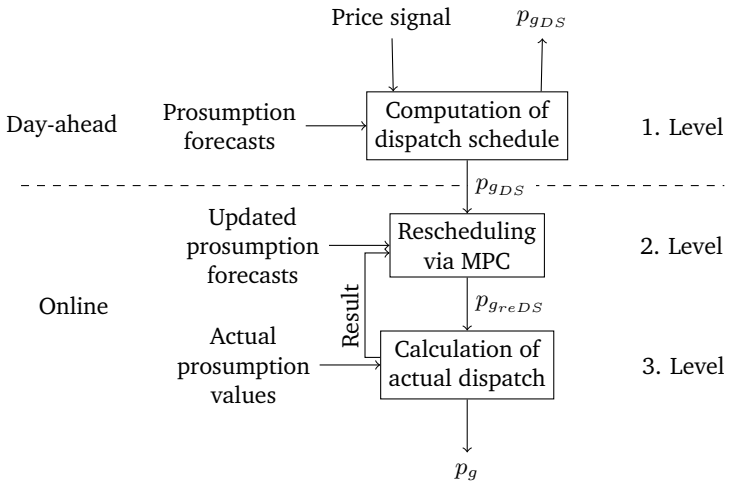

Fig. 2.2.: The hierarchical operation of the dispatchable feeder with three levels: the day-ahead computation of the dispatch schedule, the rescheduling via MPC, and the calculation of the actual dispatch. The dispatch schedule is denoted as $p_{g_{DS}}$, the rescheduled dispatch as $p_{g_{reDS}}$, an the actual dispatch as p_g (adapted from [8]).

important for the DF: One is how to set up the scheduling framework. Another is how to model the electrical system components. And finally, how to interpret the stochastic OP and reformulate it deterministically. Despite the interconnection between these aspects, we look further into each of them separately in the following.

Scheduling Framework The scheduling framework refers to all the characteristics of the scheduling. In this thesis, we refer to the scheduling as the process from the computation of the DS until the calculation of the actual dispatch. Thereby, each of the task in this process defines a new level in the hierarchical optimisation problem, see Subsection 2.2.2. The computation of the DS is the first level and the calculation of the actual dispatch is the last level. Between these two levels, another level can be added that adjusts the DS via model predictive control (MPC) as illustrated in Figure 2.2 [8, 85, 126]. We refer to these two approaches as two-level DF and three-level DF.

Other relevant characteristics of the scheduling relate to temporal specifications as illustrated in Figure 2.3. These include the time setting, i.e. when a task is to be performed, and the temporal resolution, i.e. the duration of the time interval Δt. Thereby, the concept of the DF can be found in the literature for the medium- or long-term control at temporal resolutions of a few minutes to hours, compared to primary control approaches that operate at temporal resolutions of milliseconds to seconds [148]. More precisely, the temporal resolution can vary between the different levels,

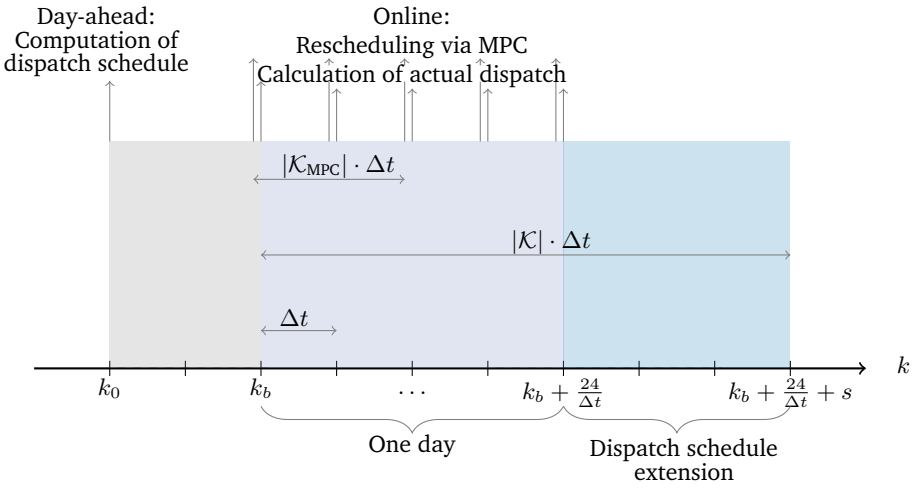

Fig. 2.3.: The temporal scheme of the hierarchical operation of a three-level dispatchable feeder including the time interval index of the dispatch schedule computation $k_0 \in \mathbb{N}$, the time interval index of the start of the dispatch schedule $k_b \in \mathbb{N}$, the number of time intervals for the dispatch schedule extension $s \in \mathbb{N}$, the discrete rescheduling horizon $\mathcal{K}_{\text{MPC}}$, the discrete scheduling horizon $\mathcal{K}$ and the duration of the time interval Δt (adapted from [7]). Note that the figure shows the temporal scheme resulting in a one-day dispatch. For a multi-day dispatch, the time intervals overlap.

with values found in the literature ranging from five minutes [103, 126, 127] to 15 minutes [87, 128], and up to one hour [7, 82, 85] for the computation of the DS. Additionally, efforts are being made to extend the DF for primary control [7, 127]

Electrotechnical System Components For the DF, two important electrotechnical system components are the grid and the BESS. With respect to the grid, there are a variety of grid models with different levels of detail to represent the components, such as buses and lines, and the electrotechnical quantities, including power, voltage, and current, of the grid. Commonly used grid models are formulated as AC power flow and DC power flow. While the former involves the consideration of AC power flows in the grid including reactive power and all losses, the latter approximates the AC power flows by e.g. neglecting the reactive power and assuming constant voltage magnitudes. Additionally, even simpler grid models exist, concentrating solely on active power. For the DF, a simple grid model is used in several works, such as [7, 82, 85, 87, 103, 126, 127], while [128] considers AC power flows. Additionally, in [126], the grid model varies betwenn the levels, using a simple grid model for the computation of the DS and a DC power flow for the rescheduling via MPC and the calculation of the actual dispatch.
The BESS can be modelled including electrical, thermal, and aging aspects [121,

122]. Thereby, the BESS model has to be tailored to the specific hardware used. From the electrical aspect, the discharge and charge characteristics of the BESS are described by its power input and a quantity related to its energy. This can be the state of energy (SoE) or state of charge (SoC). To model the transformation of the power input into the energy quantity of interest, there are several models whose parameters can be specified using look-up tables for the specific hardware used, or estimated using data-driven methods. For this transformation, the thermal and aging aspects play a role.

Deterministic Reformulation Different ways to reformulate a stochastic OP into a deterministic OP are described in Subsection 2.2.3, some of which are approached in the literature for the DF. For example, for the computation of the DS, [87, 126] use sampling-based reformulations. While [126] considers worst-case scenario forecasts, [87] generates scenario forecasts via the Monte-Carlo method. A simple non-sampling-based reformulation is done in [82, 85], which uses mean forecasts. In contrast, [7] approaches a non-sampling-based reformulation that takes the uncertainty into account and reformulates the OP in several steps. This includes the consideration of the mean and the deviation from the mean of the random decision variables and random parameters, as well as the use of chance constraints, which are reformulated using quantiles and CDFs.

2.3.3 Forecasting for Dispatchable Feeder

Once the OP has its final mathematical formulation, the forecasting can be set up. This involves the evaluation steps in Subsection 2.1.3. As the forecasts have a direct impact on the performance of the OP, the selection of the forecasting specifications should be carefully considered. In the literature, different forecasting specifications can be found including machine learning methods [8], statistical methods [87], parametric approaches [82], and non-parametric approaches [8, 87, 126]. However, an extensive evaluation of the resulting forecasts especially with respect to the forecast value for the DF is lacking.

2.3.4 Framework of Dispatchable Feeder

The use of the DF is encapsulated in a general framework illustrated in Figure 2.4, which includes forecasting, stochastic optimisation, and all the necessary data flows. More precisely, data is used to generate forecasts. Using these forecasts

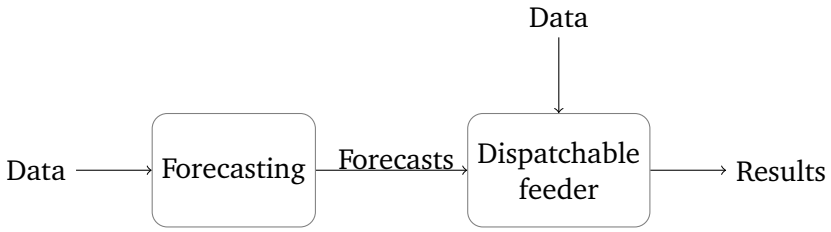

Fig. 2.4.: The general framework for the dispatchable feeder, which is applicable to a variety of downstream applications.

and additional data, the OP of the DF is solved to obtain the results detailed in Figure 2.2.

2.4 Experimental Setup

The following section describes the basic experimental setup that is based on previous works found in the literature and used throughout this thesis. More precisely, we take a close look at the considered dispatchable feeder specifications, the used data, and the used hard- and software. Further specifications, which include novelty such as the forecasting specifications, are described in the respective chapters.

2.4.1 Dispatchable Feeder Specifications

We position the DF at the low-voltage distribution grid level, a specification resulting from the scope of this thesis rather than a limitation. Furthermore, our focus extends to residential buildings with rooftop photovoltaic (PV) panels and a residential BESS. The building's prosumption then consists of the residential load and the PV power generation. Additionally, we consider each building separately in a single-building scenario, thus omitting potential correlations that are apparent in neighbourhoods. This simplification allows for a better interpretation of the results.
For the mathematical formulation, we consider the OP adapted from the works [7, 8], which enables the use of non-parametric probabilistic forecasts. In this formulation, chance constraints are used to ensure that the BESS keeps power and energy reserves for the prosumption power and energy uncertainty. These chance constraints are reformulated using quantiles and CDFs[7]. They show that the integration of the

[7]Note that the reformulation of the chance constraint using CDFs allows a more flexible satisfaction of the chance constraint, allowing the considered uncertainty to be asymmetric with respect to its mean [7].

uncertainty can lead to a higher reliability of the DS and lower costs compared to using point forecasts via a single moment reformulation and scenario forecasts via a sample-based reformulation. Therefore, even when the OP is simplified by considering point forecasts, we stay with this general formulation for consistency. This general formulation has the following specifications:

- Scheduling framework:
  - Levels: two or three
  - Time setting: at 12 PM computation of the DS starting at 12 AM of the next day
  - Temporal resolution: $\Delta t = 1$ h
- Electrotechnical system components:
  - BESS:
    - active power input $P_s(k) \in [p_s^{\min}, p_s^{\max}]$ with power capacity $p_s^{\min} \in \mathbb{R}_{<0}, p_s^{\max} \in \mathbb{R}_{>0}$
    - SoE $E_s(k) \in [e_s^{\min}, e_s^{\max}]$ with energy capacity $e_s^{\min}, e_s^{\max} \in \mathbb{R}_{\geq 0}$
    - simple transformation of active power input to SoE neglecting thermal and aging aspects via[8]

$$E_s(k+1) = E_s(k) + \Delta t \cdot \left(P_s(k) - \mu |P_s(k)|\right) \tag{2.16}$$

      with loss coefficient $\mu \geq 0$

    - Grid: active power only with lossless connections, i.e. the net power exchange between the grid and the DF is the sum of the prosumption and the BESS' active power input
- Deterministic reformulation:
  - Computation of DS: mean (referred to as considering point forecasts) or mean, quantiles and CDF (referred to as considering probabilistic forecasts)
  - Rescheduling: mean

[8] For computational reasons, Equation (2.16) is rewritten as $E_s(k+1) = E_s(k) + \Delta t \cdot \left(P_s(k) - \mu P_s(k)^+ + \mu P_s(k)^-\right)$ with positive and negative directions of the BESS' active power input $P_s^+(k) \in \mathbb{R}_{\geq 0}$ and $P_s^-(k) \in \mathbb{R}_{\leq 0}$ fulfilling $P_s(k) = P_s^+(k) + P_s^-(k)$ and $P_s^+(k) \cdot P_s^-(k) \geq -\zeta$ with $\zeta \geq 0$, $\zeta \approx 0$.

Next, we describe the mathematical formulations of the OPs for each level and all considered deterministic reformulations in detail, namely the computation of the DS considering point forecasts, the computation of the DS considering probabilistic forecasts, the rescheduling via MPC, and the calculation of the actual dispatch. All of these OPs are continuous and non-convex[9]. Further, as described above, the computation of the DS and the rescheduling via MPC are stochastic OPs with non-sampling based deterministic reformulation. In contrast, the calculation of the actual dispatch is a deterministic OP. The specifications of the parameters used can be found in Appendix A.2, unless otherwise specified.

Computation of the DS Starting with the computation of the DS, the OP computes the day-ahead DS $p_{g_{DS}}(k) \in \mathbb{R}$ with respect to minimising the energy cost for the following day making $p_{g_{DS}}(k)$ a deterministic decision variable. Thereby, the energy cost is

$$\begin{aligned} c_{DS}(p^+_{g_{DS}}(k), p^-_{g_{DS}}(k)) = c^+_{\text{quad}} \cdot (p^+_{g_{DS}}(k) \cdot \Delta t)^2 + c^+_{\text{lin}} \cdot p^+_{g_{DS}}(k) \cdot \Delta t \\ + c^-_{\text{quad}} \cdot (p^-_{g_{DS}}(k) \cdot \Delta t)^2 + c^-_{\text{lin}} \cdot p^-_{g_{DS}}(k) \cdot \Delta t, \end{aligned} \tag{2.17}$$

with positive and negative directions of the DS $p^+_{g_{DS}}(k) \in \mathbb{R}_{\geq 0}$ and $p^-_{g_{DS}}(k) \in \mathbb{R}_{\leq 0}$, $p_{g_{DS}}(k) = p^+_{g_{DS}}(k) + p^-_{g_{DS}}(k)$, and cost coefficients c^+_{quad}, c^+_{lin}, c^-_{quad}, $c^-_{\text{lin}} \in \mathbb{R}_{\geq 0}$. The energy cost takes into account both self-consumption and peak shaving. In contrast to the DS, the uncertain active power of the prosumption $P_l(k) \in \mathbb{R}$, modelled as random parameter, makes the decision variables for the BESS' power input $P_s(k)$ and the SoE $E_s(k)$ uncertain. In the computation of the DS considering probabilistic forecasts, the random variables are represented by their mean, denoted as $\bar{\cdot}$, and their deviation from the mean, denoted as Δ, as follows:

$$P_l(k) = \bar{p}_l(k) + \Delta P_l(k), \tag{2.18}$$

$$P_s(k) = \bar{p}_s(k) + \Delta P_s(k), \tag{2.19}$$

$$E_s(k) = \bar{e}_s(k) + \Delta E_s(k) \tag{2.20}$$

Additionally, to take into account the temporal correlation of the prosumption power, the prosumption energy $E_l(k+1) \in \mathbb{R}$ is considered. Specifically, for this random parameter, the deviation from its mean $\Delta E_l(k+1)$ is considered, which is expressed as

$$\Delta E_l(k+1) = \Delta t \sum_{i=k_0}^{k} \Delta P_l(i), \tag{2.21}$$

[9] See Appendix A.1 for further details on how to deal with the non-convexity.

$$\Delta E_l(k_0) = 0 \tag{2.22}$$

with the time index of the DS computation $k_0 \in \mathbb{N}$. To reformulate the OP deterministically, chance constraints are employed, see [8] for a detailed description of the reformulation. In contrast, the computation of the DS considering point forecasts uses only the means $\bar{p}_l(k)$, $\bar{p}_s(k)$, and $\bar{e}_s(k)$.
Next, we formulate[10] the OP for the **computation the DS considering point forecasts** as

$$\begin{aligned}
&\min_{\{x(k)\}_{k\in\mathcal{K}}} \sum_{k\in\mathcal{K}} c_{DS}(p^+_{g_{DS}}(k), p^-_{g_{DS}}(k)) \\
&\quad \text{s.t. for all } k \in \mathcal{K} \\
&\bar{e}_s(k+1) = \bar{e}_s(k) + \Delta t \cdot \left(\bar{p}_s(k) - \mu\bar{p}^+_s(k) + \mu\bar{p}^-_s(k)\right) \\
&\bar{e}_s(k_b) = \bar{e}^{k_b}_s \\
&p_{g_{DS}}(k) = \bar{p}_s(k) + \bar{p}_l(k) \\
&p_{g_{DS}}(k) = p^+_{g_{DS}}(k) + p^-_{g_{DS}}(k) \\
&p^+_{g_{DS}}(k) \geq 0 \\
&p^-_{g_{DS}}(k) \leq 0 \\
&\bar{p}_s(k) = \bar{p}^+_s(k) + \bar{p}^-_s(k) \\
&\bar{p}^+_s(k) \geq 0 \\
&\bar{p}^-_s(k) \leq 0 \\
&\bar{p}^+_s(k) \cdot \bar{p}^-_s(k) \geq -\zeta \\
&p^{\min}_s \leq \bar{p}_s(k) \leq p^{\max}_s \\
&e^{\min}_s \leq \bar{e}_s(k+1) \leq e^{\max}_s
\end{aligned} \tag{2.23}$$

with discrete scheduling horizon $\mathcal{K}$, decision vector[11]

$$x(k) = \left(p_{g_{DS}}(k), p^+_{g_{DS}}(k), p^-_{g_{DS}}(k), \bar{e}_s(k+1), \bar{p}_s(k), \bar{p}^+_s(k), \bar{p}^-_s(k)\right)^T$$

and parameters $\bar{e}^{k_b}_s$, $p^{\min}_s$, $p^{\max}_s$, $e^{\min}_s$, $e^{\max}_s$, ζ. The prosumption is forecasted as mean point forecast $\hat{\bar{p}}_l(k)$.

[10] Note that it is not necessary to include the constraint $p^+_{g_{DS}}(k) \cdot p^-_{g_{DS}}(k) \geq -\zeta$ with $\zeta \geq 0$, $\zeta \approx 0$ as the minimisation of the energy cost in Equation (2.17) already ensures that either $p^+_{g_{DS}}(k)$ or $p^-_{g_{DS}}(k)$ is almost zero.

[11] Note that not all decision variables are free, but are determined by equality constraints. For the implementation, however, we use all specified decision variables as the number of decision variables is not critical in our case for the numerical solving. The free decision variables are $p^+_{g_{DS}}(k)$ and $p^-_{g_{DS}}(k)$.

In contrast, the **computation of the DS considering probabilistic forecasts** is formulated as

$$
\begin{aligned}
&\min_{\{x(k)\}_{k\in\mathcal{K}}} \sum_{k\in\mathcal{K}} c_{DS}\left(p^{+}_{g_{DS}}(k), p^{-}_{g_{DS}}(k)\right) + c_{\text{fix}} \cdot \epsilon_{\text{fix}}(k) + c_{\text{var}}(k) \cdot \epsilon_{\text{var}}(k) \\
&\text{s.t. for all } k \in \mathcal{K} \\
&\bar{e}_s(k+1) = \bar{e}_s(k) + \Delta t \cdot \left(\bar{p}_s(k) - \mu\bar{p}^{+}_s(k) + \mu\bar{p}^{-}_s(k)\right) \\
&\bar{e}_s(k_b) = \bar{e}^{k_b}_s \\
&p_{g_{DS}}(k) = \bar{p}_s(k) + \bar{p}_l(k) \\
&p_{g_{DS}}(k) = p^{+}_{g_{DS}}(k) + p^{-}_{g_{DS}}(k) \\
&p^{+}_{g_{DS}}(k) \geq 0 \\
&p^{-}_{g_{DS}}(k) \leq 0 \\
&\bar{p}_s(k) = \bar{p}^{+}_s(k) + \bar{p}^{-}_s(k) \\
&\bar{p}^{+}_s(k) \geq 0 \\
&\bar{p}^{-}_s(k) \leq 0 \\
&\bar{p}^{+}_s(k) \cdot \bar{p}^{-}_s(k) \geq -\zeta \\
&p_{g_{DS}}(k) - p^{\max}_s \leq q_{P_l(k)}(0.5 - 0.5 \cdot (1 - \epsilon_P)) \\
&p_{g_{DS}}(k) - p^{\min}_s \geq q_{P_l(k)}(0.5 + 0.5 \cdot (1 - \epsilon_P)) \\
&1 - \epsilon_E - \epsilon_{\text{fix}}(k) - \epsilon_{\text{var}}(k) \leq F_{\Delta E_l(k+1)}\left(\bar{e}_s(k+1) - e^{\min}_s\right) - \\
&\qquad\qquad F_{\Delta E_l(k+1)}\left(\bar{e}_s(k+1) - e^{\max}_s\right) \\
&\epsilon_{\text{fix}}(k) \geq 0 \\
&\epsilon_{\text{var}}(k) \geq 0
\end{aligned}
\tag{2.24}
$$

with discrete scheduling horizon $\mathcal{K}$, decision vector[12]

$$
x(k) = \left(p_{g_{DS}}(k), p^{+}_{g_{DS}}(k), p^{-}_{g_{DS}}(k), \bar{e}_s(k+1), \bar{p}_s(k), \bar{p}^{+}_s(k), \bar{p}^{-}_s(k), \zeta, \epsilon_{\text{fix}}(k), \epsilon_{\text{var}}(k)\right)^T
$$

and parameters $\bar{e}^{k_b}_s$, $p^{\min}_s$, $p^{\max}_s$, $e^{\min}_s$, $e^{\max}_s$, c_{fix}, $c_{\text{var}}(k)$, ϵ_P, ϵ_E. The latter two parameters are security level parameters of the reformulated power and energy chance constraints[13]. The security level of the energy chance constraint can be relaxed via the decision variables $\epsilon_{\text{fix}}(k)$ and $\epsilon_{\text{var}}(k)$. In accordance with the reformulation of the chance constraints, the prosumption is forecasted as probabilistic forecasts in forms

[12] Note that not all decision variables are free, but are determined by equality constraints. For the implementation, however, we use all specified decision variables as the number of decision variables is not critical in our case for the numerical solving. The free decision variables are $p^{+}_{g_{DS}}(k)$, $p^{-}_{g_{DS}}(k)$, $\epsilon_{\text{fix}}(k)$ and $\epsilon_{\text{var}}(k)$.

[13] There are other approaches that include the prosumption power uncertainty in the objective function such as [112]

of power quantile forecasts $\hat{q}_{P_l(k)}(0.5+0.5\cdot(1-\epsilon_P))$ and $\hat{q}_{P_l(k)}(0.5-0.5\cdot(1-\epsilon_P))$ for $P_l(k)$ and energy CDF forecasts $\hat{F}_{\Delta E_l(k+1)}$ for $\Delta E_l(k+1)$.
Note that in both OPs it is necessary to estimate $\bar{e}_s^{k_b}$, the SoE at the time index of the start of the DS $k_b \in \mathbb{N}$. This estimation is done with the OP described in Appendix A.3.

Rescheduling via MPC In the rescheduling via MPC, we iteratively adjust the pre-computed DS $p_{g_{DS}}(k)$ online just before the calculation of the actual dispatch at each time step $k \in \mathbb{N}$, with the aim to minimise the deviations from the DS. While only the rescheduled dispatch $p_{g_{reDS}}(k) \in \mathbb{R}$ in k is utilised in the subsequent level, the rescheduling process considers the horizon $\mathcal{K}_{\text{MPC}} = \{k, k+1, ..., k+m\}, m \in \mathbb{N}$, which is a typical characteristic of MPC problems. Thus, besides the deterministic decision variables $p_{g_{reDS}}(j), j \in \mathcal{K}_{\text{MPC}}$, the OP consists of the uncertain prosumption power $P_l(j)$, modelled as random parameter, and the BESS' power input $P_s(j)$ and SoE $E_s(j)$, modelled as random decision variables, except for the known SoE in k, which is a deterministic parameter. For the rescheduling via MPC, we reformulate the random variables using the mean denoted with $\bar{p}_l(j), \bar{p}_s(j)$, and $\bar{e}_s(j)$. The OP for the **rescheduling via MPC** is then formulated as

$$
\begin{aligned}
\min_{\{x(j)\}_{j\in\mathcal{K}_{\text{MPC}}}} \quad & \sum_{j\in\mathcal{K}_{\text{MPC}}} \left(p_{g_{DS}}(j) - p_{g_{reDS}}(j)\right)^2 \\
\text{s.t. for all } j \in \mathcal{K}_{\text{MPC}} \quad & \\
\bar{e}_s(j+1) &= \bar{e}_s(j) + \Delta t \cdot \left(\bar{p}_s(j) - \mu\bar{p}_s^+(j) + \mu\bar{p}_s^-(j)\right) \\
\bar{e}_s(k) &= e_s(k) \\
p_{g_{reDS}}(j) &= \bar{p}_s(j) + \bar{p}_l(j) \\
\bar{p}_s(j) &= \bar{p}_s^+(j) + \bar{p}_s^-(j) \\
\bar{p}_s^+(j) &\geq 0 \\
\bar{p}_s^-(j) &\leq 0 \\
\bar{p}_s^+(j)\cdot\bar{p}_s^-(j) &\geq -\zeta \\
p_s^{\min} \leq \bar{p}_s(j) &\leq p_s^{\max} \\
e_s^{\min} \leq \bar{e}_s(j+1) &\leq e_s^{\max}
\end{aligned}
\tag{2.25}
$$

with discrete rescheduling horizon $\mathcal{K}_{\text{MPC}}$, decision vector[14]

$$x(j) = \left(p_{g_{reDS}}(j), \bar{e}_s(j+1), \bar{p}_s(j), \bar{p}_s^+(j), \bar{p}_s^-(j)\right)^T$$

[14] Note that not all decision variables are free, but are determined by equality constraints. For the implementation, however, we use all specified decision variables as the number of decision variables is not critical in our case for the numerical solving. The free decision variable is $p_{g_{reDS}}(j)$.

and parameters $p_{g_{DS}}(j)$, $e_s(k)$, $p_s^{\min}$, $p_s^{\max}$, $e_s^{\min}$, $e_s^{\max}$, ζ. The prosumption is forecasted as mean point forecast $\hat{\bar{p}}_l(j)$ based on new information.

Calculation of Actual Dispatch The objective during the calculation of the actual dispatch $p_g(k) \in \mathbb{R}$ is to minimise the deviation $\Delta p_g(k) \in \mathbb{R}$ to a reference schedule $p_{g_{\text{ref}}}(k)$, taking into account the actual prosumption $p_l(k) \in \mathbb{R}$ and the technical constraints of the BESS. The reference schedule is the DS, i.e.

$$p_{g_{\text{ref}}}(k) = p_{g_{DS}}(k),$$

in the two-level framework and the rescheduled dispatch, i.e.

$$p_{g_{\text{ref}}}(k) = p_{g_{reDS}}(k),$$

in the three-level framework. Since all parameters are known, this OP is deterministic. We formulate the **calculation of the actual dispatch** then as

$$\begin{aligned}
\min_{x(k)} \quad & \left(\Delta p_g(k)\right)^2 \\
e_s(k+1) &= e_s(k) + \Delta t \cdot \left(p_s(k) - \mu p_s^+(k) + \mu p_s^-(k)\right) \\
p_g(k) &= p_s(k) + p_l(k) \\
p_g(k) &= p_{g_{\text{ref}}}(k) + \Delta p_g(k) \\
p_s(k) &= p_s^+(k) + p_s^-(k) \\
p_s^+(k) &\geq 0 \\
p_s^-(k) &\leq 0 \\
p_s^+(k) \cdot p_s^-(k) &\geq -\zeta \\
p_s^{\min} \leq & p_s(k) \leq p_s^{\max} \\
e_s^{\min} \leq & e_s(k+1) \leq e_s^{\max}
\end{aligned} \tag{2.26}$$

with decision vector[15]

$$x(k) = \left(\Delta p_g(k), p_g(k), e_s(k+1), p_s(k), p_s^+(k), p_s^-(k)\right)^T$$

and parameters $p_{g_{\text{ref}}}(k)$, $p_l(k)$, $e_s(k)$, $p_s^{\min}$, $p_s^{\max}$, $e_s^{\min}$, $e_s^{\max}$, ζ.

[15] Note that not all decision variables are free, but are determined by equality constraints. For the implementation, however, we use all specified decision variables as the number of decision variables is not critical in our case for the numerical solving. The free decision variable is $\Delta p_g(k)$.

Tab. 2.2.: The hardware specification of different servers used for the evaluations.

	Server 1	Server 2	Server 3
CPU cores	12	76	96
CPU base clock rate	2.1GHz	2.4 GHz	1.5 GHz
CPU maximum clock rate	4.7 GHz	4.0 GHz	2.8 GHz
RAM	32 GB	512 GB	128 GB
GPU	Inter(R) Iris(R) Xe Graphics	4x NVIDIA A100-40	ASPEED Graphics Family

2.4.2 Data

For all our evaluations, we use the "Ausgrid - Solar home electricity data" set [116]. This dataset contains real-world load and PV power generation data from 300 residential buildings located in New South Wales, Australia, over the period from 1st July 2010 to 30th June 2013 in a 30-minute resolution. As we consider a duration of the time interval Δt of one hour, the data is adjusted to an hourly temporal resolution. Due to missing values in the dataset for buildings 2, 68, 95, 161, 187, 248, 272, 284, 289, 293, and 294, we exclude these buildings. We also exclude building 138, which has long periods of 0 values and is therefore anomalous, and buildings 75 and 157, for which the optimisation has convergence problems. For the remaining 286 buildings, the prosumption of time interval k is calculated by

$$p_l(k) = \beta_{\text{load}} \cdot p_{\text{load}}(k) - \beta_{\text{PV}} \cdot p_{\text{PV}}(k). \tag{2.27}$$

with load $p_{\text{load}}(k) \in \mathbb{R}_{\geq 0}$, PV power generation $p_{\text{PV}}(k) \in \mathbb{R}_{\geq 0}$, and factors $\beta_{\text{load}}, \beta_{\text{PV}} \in \mathbb{R}_{\geq 0}$. Unless otherwise specified, we set $\beta_{\text{load}} = 1, \beta_{\text{PV}} = 1$ as in the dataset. Furthermore, this dataset does not contain BESS data. Therefore, we consider a BESS with the specifications comparable to [17], i.e. $p_s^{\min} = -5$ kW, $p_s^{\max} = 5$ kW, $e_s^{\min} = 0$ kWh, and $e_s^{\max} = 19.5$ kWh, unless otherwise specified.
In addition, when presenting detailed results for a single building, we use the building 109 in accordance with [7, 8].

2.4.3 Hardware and Software

The evaluations are performed on servers with different hardware specifications, depending on the scope of the evaluation and the computational effort required. The hardware specifications are provided in Table 2.2.
With respect to the software, the evaluations are implemented in Python and multiple Python libraries. For data handling, we specially make use of NumPy [58] and Pandas

[97]. The forecasts are generated with PyTorch [105] and Scikit-learn [106]. To implement and solve the OPs, we use Pyomo [27, 59] with Ipopt [137] as solver as interior point methods are effective in solving non-linear OPs, including non-convex ones [13, 19]. For tracking our evaluations, we log the results with Weights and Biases[16].

[16]https://www.wandb.com/ [accessed: 2024-07-25]

3 Thesis Focus

This chapter describes the focus of this thesis. Therefore, we first formulate the considered research questions, and finally present the outline of this thesis.

3.1 Research Questions

This section describes the five research questions addressed in this thesis, see Figure 3.1 for an overview. The description of these research questions is as follows. First, the respective context is introduced. Second, the existing literature in this context is presented. Finally, the resulting research question is formulated.

3.1.1 Evaluation of Forecast Value for Dispatchable Feeder

Forecasts play a crucial role in the performance of the DF as they serve as input to the stochastic OP. The impact of these forecasts can be quantified by a representative forecast value that measures the performance of the OP, e.g. economic costs. Therefore, an extensive evaluation of the forecasts especially with respect to the forecast value is of interest.

Related Work[1] Several works examine the difference between forecast value and forecast quality for different OPs, such as [18, 35, 39, 114]. While [39, 114] show that the forecast value does not directly correspond to the forecast quality, [18, 35] show that the forecast value depends not only on the forecast error but also on problem-specific factors. Therefore, [18] analyses the impact of different forecasts on the forecast value for different system viewpoints.
In addition, while the aforementioned works consider point forecasts, there are several works that evaluate different probabilistic forecasts with respect to their forecast value for different OPs, such as [24, 28, 90, 94, 111, 156]. Among these, [90, 94, 111] focus on the renewable energy sector. More specifically, they consider

[1] This paragraph is adapted from [144].

the market trading of renewable generation, with [90] focusing specifically on forecasts of aggregated renewable generation. Additionally, several works compare the forecast value between point forecasts and probabilistic forecasts, such as [4, 91, 101]. Of these, [4, 91] consider OPs in a comparable context to the DF, but use a sample-based approach via scenario forecasts and do not consider different forecast characteristics.

Research Question An extensive evaluation of different forecast characteristics with respect to the forecast value in the context of DFs, covering both point forecasts and probabilistic forecasts, is lacking. This includes exploring the impact of problem-specific parameters. The resulting research questions are:

RQ1: *How do different point forecast characteristics influence the forecast value for the dispatchable feeder, and how does this influence depend on problem-specific parameters?*

RQ2: *How do different probabilistic forecast characteristics influence the forecast value for the dispatchable feeder, and how does this influence depend on problem-specific parameters?*

3.1.2 Automated Value-Oriented Forecast Method Selection by Meta-Learning

To generate forecasts for the DF, a tremendous amount of forecast methods exists. Commonly, the selection of the forecast method is based on the forecast quality, which does not include the performance of the DF based on the resulting forecasts. In addition, since the selection of the forecast method can be computationally expensive, the consideration of the computational effort required for the forecast method selection is crucial for a real-world implementation. Therefore, the selection of the forecast method with respect to the forecast value for the DF with low computational effort is of interest.

Related Work[2] In the literature, several works exist that either focus on the design of forecast methods for a specific OP or approach the selection of forecast methods with low computational effort with respect to the forecast quality. In the following, we present works within these two categories.

[2]This paragraph is adapted from [16] and [143].

One approach to designing forecast methods for a specific OP is to incorporate information from the OP into the forecasting. In the context of machine learning, there are several works that address such an end-to-end training of forecasting and optimisation known under the term decision-focused learning [95, 119]. This end-to-end learning necessitates differentiation through the OP, which poses challenges. Although analytical approaches exist, these are tailored to specific categories of OPs. For instance, [5, 43, 153, 154] focus on strongly convex and quadratic OPs. To avoid the differentiation through the OP, further approaches use differentiable surrogate loss functions [11, 34, 44, 124, 125, 152, 155]. In more detail, while [44] approximates the analytical description for linear OPs, several other works rely on specific parametric loss function families. These approaches learn the parameters of these loss function families based on the forecast value, e.g. [11, 34, 124, 125]. Among the parametric loss function families is the cost-oriented loss function [53, 77, 89, 141, 152]. The cost-oriented loss function is a piecewise function assigning different weights to forecast errors, introducing bias into the forecasts. While [77, 89] require the explicit form of the cost-oriented loss function, [141, 152] approximate it in a computationally expensive manner. However, for complex OPs such as the DF, the forecast value is not solely determined by the forecast error. The strategy of tailoring the loss function to fit the specific OP is also explored in [1, 57]. However, these approaches are tailored to specific OPs and are not readily applicable for generating forecasts with a high forecast value for other OPs.
While the above presented decision-focused learning approaches can be computationally expensive, meta-learning approaches for the forecast method selection can reduce this computational effort. However, in literature such a meta-learning forecast method selection can only be found based on the forecast quality [129, 139, 140]. Another approach in [30] is to use meta-learning to forecast the RMSE of a forecast. Summarising, these meta-learning approaches lack the consideration of the performance of the OP based on the forecast.

Research Question While decision-focused learning approaches are computationally expensive and make restrictive assumptions such as the category of the OP or the parametric loss function family, a meta-learning approach for selecting the forecast method is solely approached with respect to the forecast quality. Therefore, a solution to automatically select the forecast method with respect to the forecast value using meta-learning is lacking. The respective research question is:

RQ3: *How to automatically select the forecast method with respect to the forecast value with low computational effort using meta-learning?*

3.1.3 Comparison of Dispatchable Feeder Considering Point and Probabilistic forecasts

As both the integration of the prosumption uncertainty in the mathematical formulation of the OP and the forecasts play a crucial role for the performance of the DF, an evaluation comparing the DF considering point forecasts and the DF considering probabilistic forecasts with different forecast characteristics is of interest.

Related Work Several studies evaluate the integration of the prosumption uncertainty for the DF, including [7, 8, 87, 126]. Of these, [7] evaluates the performance of the DF considering point forecasts and the DF considering probabilistic forecasts. However, this study is limited to a single building and considers quality-oriented forecasts. Other works compare the forecast value between point forecasts and probabilistic forecasts for an OP in a comparable context, using a sample-based approach with scenario forecasts, such as [4, 91]. These works use quality-oriented forecasts.

Research Question A comparative evaluation of the DF considering point forecasts and the DF considering probabilistic forecasts with different forecast characteristics is lacking. This includes the evaluation on several buildings. In this context, it is of interest whether the consideration of value-oriented point forecasts can compensate for the lack of integration of the prosumption uncertainty. The corresponding research question is:

RQ4: *How does the performance of the dispatchable feeder considering point forecasts compare to the performance of the dispatchable feeder considering probabilistic forecasts for difference forecast characteristics?*

3.1.4 Line Restriction for Dispatchable Feeder considering Probabilistic Forecasts

Addressing the technical restrictions imposed by the electrotechnical system components is essential for a seamless real-world implementation of the DF. In particular, the inclusion of the line restriction becomes crucial as the energy transition increases both the residential load and the distributed renewable generation. With such a high power exchange between the grid and the DF, it is important to consider the technical restrictions of the line to mitigate line overloadings.

Related Work[3] In the following, works within two categories are presented. First, DFs considering the line restriction are reviewed, and afterwards, works approaching the line overloadings during PV power generation hours are explained.
The mathematical formulations for the DF from [87, 126] consider the line restriction. For this mathematical formulation, both works use scenario forecasts as input. However, as can be seen in [8], the mathematical formulation of the DF considering probabilistic forecasts as input in the computation of the DS significantly enhance the dispatchability of the DF. For this mathematical formulation, the inclusion of the line restriction is lacking.
The motivation to mitigate line overloadings is discussed in [55, 73, 102, 146]. In response to this challenge, [55, 73, 102] propose an MPC problem for residential buildings using point forecasts as input. However, all three works do not consider the scheduling level and thus do not aim for the dispatchability of their considered systems. Instead of using residential BESSs, [146] propose the usage of a community BESS. However, while community BESSs offer a promising solution, they introduce new challenges such as optimal placement and may not fully address line overloads within the community.

Research Question A mathematical formulation of the DF that takes into account both probabilistic forecasts and the restriction of the power exchange between the grid and the DF imposed by the technical constraints of the line is lacking. The resulting research question is:

RQ5: *How to consider the line restriction and mitigate line overloadings for the dispatchable feeder considering probabilistic forecasts?*

3.2 Outline

Based on the research questions reported in Section 3.1, the remainder of this thesis is structured as follows. In Part II, point forecasts are evaluated for the DF considering point forecasts with respect to the forecast value in Chapter 4 (RQ1), and an automated value-oriented forecast method selection using meta-learning is presented in Chapter 5 (RQ3). These research questions extend the general framework in Figure 2.4 to Figure 3.1a and Figure 3.1b respectively, with the novelty marked in orange. In Part III, probabilistic forecasts are evaluated for the DF considering probabilistic forecasts with respect to the forecast value in Chapter 6

[3] This paragraph is adapted from [145].

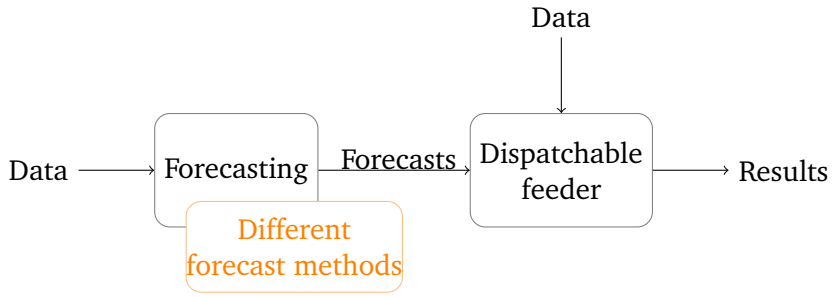

(a) The specified framework for Chapter 4 addressing research question RQ1 and Chapter 6 addressing research question RQ2 of this thesis. Different forecasts are used and the performance of the dispatchable feeder for each forecast is evaluated.

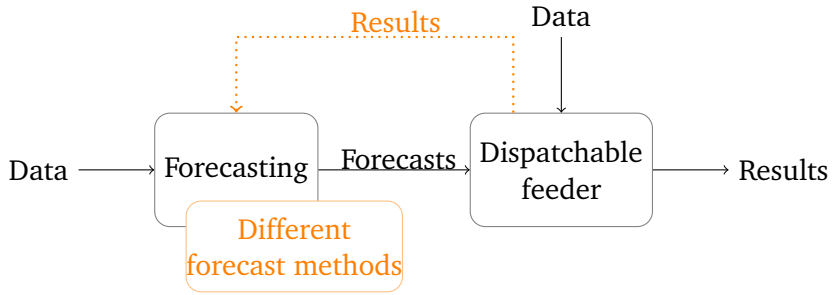

(b) The specified framework for Chapter 5 addressing research question RQ3 of this thesis. An automated forecast method selection is proposed with respect to the performance of the dispatchable feeder.

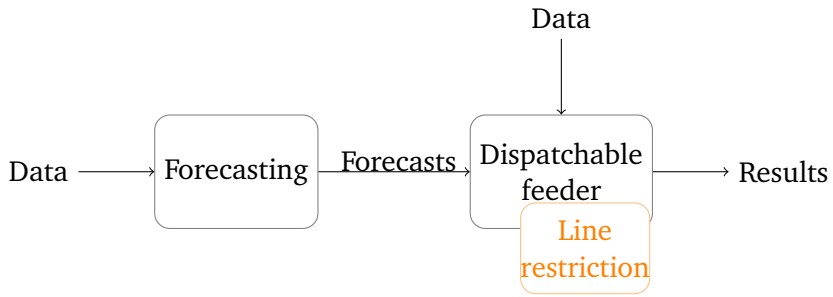

(c) The specified framework for Chapter 8 addressing research question RQ5 of this thesis. The mathematical formulation of the optimisation problem for the dispatchable feeder is modified.

Fig. 3.1.: The specific frameworks of Figure 2.4 considered in the different chapters of this thesis, with the addressed research question specified and the novelty marked in orange.

(RQ2). While the structure of this chapter and the specific framework in Figure 3.1a is the same as in Chapter 4, the difference lies in the mathematical formulation of the OP for the DF and the consideration of probabilistic forecasts. Additionally, in Chapter 7, the DF considering point forecasts and the DF considering probabilistic forecasts are evaluated with both value-oriented and standard forecasts and it is assessed whether value-oriented point forecasts can compensate for the lack of integration of the prosumption uncertainty (RQ4). Further, in Chapter 8, the

mathematical formulation of the OP for the DF considering probabilistic forecasts is modified by including a line restriction (RQ5) resulting in the specific framework shown in Figure 3.1c.

Part II

Forecast Evaluation for Dispatchable Feeder Considering Point Forecasts

4 Point Forecast Evaluation

This chapter evaluates point forecasts with respect to the forecast value for the two-level dispatchable feeder (DF) considering point forecasts[1]. For this evaluation, different point forecasts with different characteristics are considered. More precisely, they are generated to have different locations, i.e. we intentionally introduce bias. For these different forecasts, we analyse the relation between the considered forecast value and the considered forecast quality. Additionally, we evaluate the forecast value for the different forecasts depending on problem-specific parameters. Therefore, this chapter deals with the research question:

RQ1: *How do different point forecast characteristics influence the forecast value for the dispatchable feeder, and how does this influence depend on problem-specific parameters?*

The chapter is structured as follows. First, Section 4.1 describes the approach. Second, Subsection 4.2.1 presents the experimental setup. This includes the description of the generation of the point forecasts with different characteristics and the considered forecast value and the considered forecast quality. Then, Subsection 4.2.2 presents the results of the evaluation. Finally, Section 4.3 discusses the results.

4.1 Approach

In this section, an overview of the evaluation of prosumption point forecasts $\hat{\overline{p}}_l(k)$ with different characteristics with respect to the forecast value for the DF is given, see Figure 4.1. This evaluation involves the following steps for each set of forecasts: First, the point forecasts are generated. Then, based on these forecasts, the day-ahead dispatch schedule is computed by solving the first level optimisation problem (OP). Afterwards, the actual dispatch is calculated using the actual prosumption values by solving the second level OP, which aims to minimise the deviations from the dispatch schedule. Finally, the forecast value for the DF is measured and compared

[1]The content of this chapter is based on [144]. While the concept of the evaluation is the same, the experimental setup differs, including the forecasting specifications, the used prosumption data, and the used BESS energy capacity.

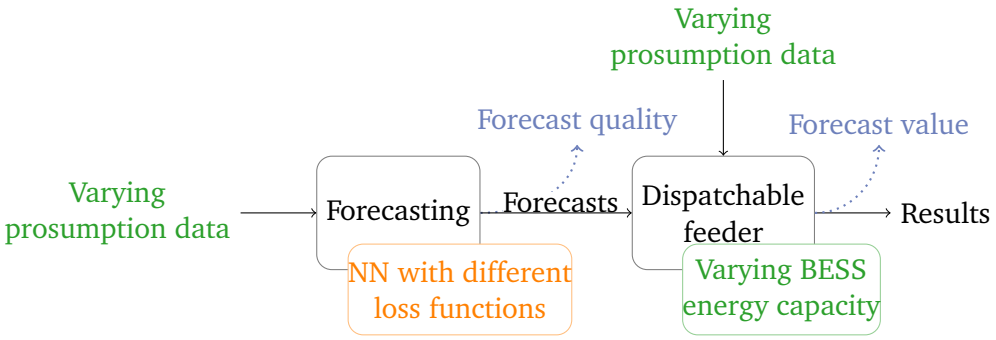

Fig. 4.1.: The framework to evaluate point forecasts with different characteristics with respect to the forecast quality and the forecast value (marked in blue) for the two-level dispatchable feeder considering point forecasts. The point forecasts with different characteristics are generated via neural networks (NN) with different loss functions (marked in orange). Additionally, varying problem-specific parameters, namely the prosumption data and the BESS energy capacity, are considered (marked in green).

with the forecast values of other point forecasts.

For the generation of the point forecasts, we use a non-parametric machine learning method, namely a neural network (NN). The reason for this choice is that machine learning methods are well established for power forecasting [67] and we do not want to make any assumptions about the distribution or the statistical model. Such assumptions are necessary for statistical methods and would need to be validated, which would require a large computational effort given the scale of this evaluation. Additionally, compared to other machine learning methods in Table 2.1, the complexity of the NN architecture can be tailored to the application considered. Therefore, NNs can be designed to perform adequately with smaller dataset sizes and to be computationally efficient, both of which are valuable characteristics for this evaluation. Note that since our focus is on evaluating the impact of different forecast characteristics on the performance of the DF, we chose not to compare point forecasts generated by different machine learning methods, but only to use NNs to generate point forecasts with different characteristics.

To achieve these different characteristics, we employ different loss functions inside the NN. The choice of the loss function plays a crucial role in shaping the characteristics of the resulting forecast as the loss function evaluates how well the forecast aligns with the actual value. During training of the NN, the loss function is minimised so that the NN generates forecasts reflecting the characteristic of the chosen loss function, see Figure 4.2. Commonly used loss functions are the MSE in Equation (2.7) and MAE in Equation (2.8). Both loss functions produce unbiased forecasts. While the former weights larger absolute forecast errors stronger, the latter weights all forecast errors equally. Besides these two loss functions, we further

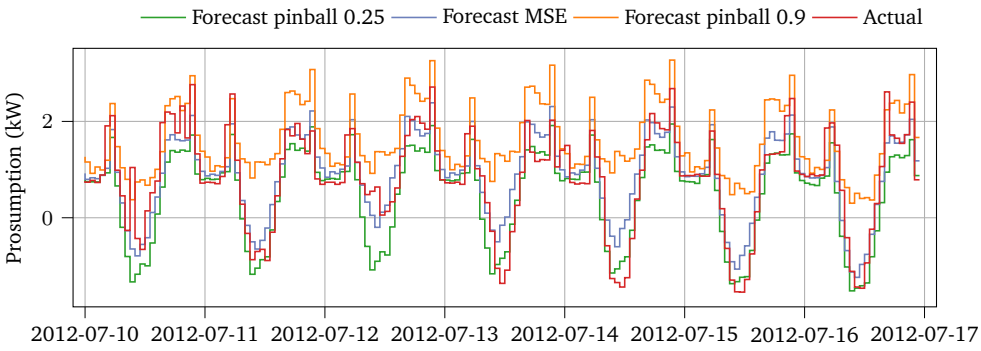

Fig. 4.2.: The actual prosumption p_l and the prosumption point forecasts of $\overline{p}_l$ with different characteristics, generated with different loss functions inside the neural network, namely pinball 0.25, MSE, and pinball 0.9, for the prosumption data original ($\beta_{\text{load}} = 1, \beta_{\text{PV}} = 1$) and an exemplary week.

consider the Huber metric in Equation (2.9) with $\delta = 1$. This loss function is a mixture between MSE and MAE. To generate biased forecasts, we use the pinball loss function in Equation (2.11) with different τ values of 0.1, 0.25, 0.75, and 0.9. If τ is smaller than 0.5, the forecasts are expected to be smaller than forecasts generated with centre-oriented loss functions such as the MSE and MAE. Therefore, the prosumption is what we call underestimated. In contrast, if τ is greater than 0.5, the prosumption is overestimated, i.e. the forecasts are expected to be greater than forecasts generated with centre-oriented loss functions.

The point forecasts with different characteristics generated at 12 PM are then used for the computation of the dispatch schedule (DS) at 12 AM. To estimate the state of energy (SoE) of the BESS at 12 AM, we use the MSE point forecast generated at 12 PM, unlike in [144], where the point forecasts with different characteristics are also used to estimate the BESS' SoE. This allows us to focus our evaluation on the impact of different point forecasts on the forecast value, rather than on the impact of different estimates of the SoE at 12 AM.

In order to evaluate the forecast value for a specific forecast characteristic, it is important to consider other problem-specific parameters that may affect this performance and thus the forecast value. For the DF, one such parameter is a building's prosumption data, i.e. the scale and fluctuation of the building's prosumption. As the prosumption data in the considered Ausgrid dataset is limited and does not include future scenarios, we synthetically extend the dataset by using different ratios of load and PV power generation via β_{load} and β_{PV} in Equation (2.27). More specifically, to account for the increase in load and PV power generation due to the energy transition, we consider **load5** with $\beta_{\text{load}} = 5, \beta_{\text{PV}} = 1$, and **PV5** with $\beta_{\text{load}} = 1, \beta_{\text{PV}} = 5$. To account for energy efficient buildings with lower loads, we extend the dataset by **load1/2** with $\beta_{\text{load}} = \frac{1}{2}, \beta_{\text{PV}} = 1$. In addition to the prosump-

Tab. 4.1.: The general and detailed neural network architectures to generate the point forecasts. Note that the forecast horizon is 42 hours.

(a) The general architecture of the used neural networks.

Input features	Architecture	Output
historical data[3] calendar features, weather features[10]	three-layer NN	Mean $\hat{\hat{p}}_l(k)$, $k = k_0, ..., k_0 + 41$

(b) The detailed architecture of the used three-layer neural network.

Layer	Activation function	Layer size
Input	Linear	267
Hidden	ReLU	20
	ReLU	50
Output	Linear	42

tion data, the problem-specific parameter of the BESS energy capacity $e_s^{\max}$ may also influence the forecast value. As the BESS is added to the Ausgrid dataset, we use different BESS energy capacities to account for differences in installed BESS. Specifically, we consider the BESS energy capacities $e_s^{\max}$ of 3, 6, 13.5[2], and 19.5 kWh to account for the increase in affordable BESSs.
With these specifications, we aim to analyse whether the expectation that point forecasts with higher forecast quality lead to a higher forecast value for the DF holds true across all considered forecast values and all problem-specific parameters.

4.2 Evaluation

This section evaluates the forecast value for the two-level DF considering point forecasts described in Subsection 2.4.1. Therefore, Subsection 4.2.1 describes the further experimental setup beyond the specifications in Section 2.4, while Subsection 4.2.2 presents the results.

4.2.1 Experimental Setup

The following two aspects are relevant for the evaluation and are presented in the remainder. First, the generation of the point forecasts with different characteristics is explained. Second, the considered forecast value and forecast quality are outlined.

[2]https://www.tesla.com/support/energy/powerwall/documents/documents [accessed: 2024-05-15]
[3]This input feature is scaled with SKLearn's min-max scaler [106].

Forecast Method In the following, we first describe the used forecast specifications and the NN architecture. Afterwards, the considered input features and the splitting of the data in training, validation, and testing are described.

Regarding the forecasting specifications, we forecast the prosumption directly, as opposed to [8], which forecasts the load and the PV power generation separately. The reason for our choice is that we aim for the same NN architecture throughout this thesis. While a simple subtraction of the separate load and PV power generation point forecasts yields the prosumption point forecasts, a convolution[4] is necessary when considering probabilistic forecasts. A first analysis shows that this extra step can be time consuming, while leading to a negligible increase in forecast quality. Therefore, we directly forecast the prosumption.

Regarding the NN architecture, we use a fully connected three-layer NN, see Table 4.1. In both hidden layers, we use a ReLU [3] activation function, and in the input and output layer a linear activation function. Additionally, we use a batch size of 512 and the Adam optimiser [79].

As input features we consider the historical prosumption of the last seven days and calendar features, namely the month, the day of the week and a boolean feature indicating a holiday. Additionally, we incorporate actual weather data, namely the surface short-wave (solar) radiation downwards and two-metre temperature from the European Centre for Medium-Range Weather Forecasts (ECMWF) [64], as weather forecasts covering the Ausgrid dataset are not available. However, as the Ausgrid dataset does not specify the exact location of the buildings and the ECMWF grid point resolution of 0.25° is rather coarse, we use a broad approximation for the area covering the majority of the buildings, in particular Sydney and Newcastle. To achieve this, we average the values from several locations with the following longitude/latitude pairs: -34°/151°, -34°/151.25°, -33.75°/151°, -33.75°/151.25°, -33°/151.75°, -33°/151.5°, -32.75°/151.75°. These averaged values are used as weather features for all buildings. Furthermore, we scale the historical data and the weather data with SKLearn's min-max scaler [106] and encode the calendar features of the month and the holiday with sine-cosine encoding.

With respect to the data splitting, we split the three years of data from the Ausgrid dataset for training, validation, and testing as follows. We use the first year for training, the second year for validation to apply early stopping, and the last year for testing.

[4] Convolution is only adequate under the assumption of independence between the load and the PV power generation, which is typically not the case. To account for the correlation, copulas must be considered, which can be not straightforward to use, see [15].

Evaluation Metrics The point forecasts with different characteristics are evaluated with respect to both the forecast quality and the forecast value. As evaluation metric for the forecast quality, the MSE described in Subsection 2.1.3 is used. As the MSE measures the deviation of the forecast from the actual value, a lower MSE implies a higher forecast quality. To evaluate the forecast value for the DF, the cost resulting from the performance of the DF based on the forecast is used. We consider three average daily costs, namely the average daily DS cost, the average daily imbalance cost and the average daily total cost, with lower costs implying a higher forecast value. More precisely, the DS cost are the energy costs of the computed DS. We use the same DS cost for evaluation as during the computation of the DS, see Equation (2.17). Further, the imbalance cost result from the difference of the actual dispatch $p_g(k)$ and the DS $p_{g_{\text{DS}}}(k)$ and are calculated after the execution of the OP via

$$\begin{aligned} c_{\text{imb}}(p_{g_{DS}}(k), p_g(k)) = c^{\Delta}_{\text{quad}} \cdot ((p_{g_{DS}}(k) - p_g(k)) \cdot \Delta t)^2 + \\ c^{\Delta}_{\text{lin}} \cdot |(p_{g_{DS}}(k) - p_g(k)) \cdot \Delta t| \end{aligned} \tag{4.1}$$

with cost coefficients $c^{\Delta}_{\text{quad}}, c^{\Delta}_{\text{lin}} \in \mathbb{R}_{\geq 0}$. We set these coefficients equal to $c^{+}_{\text{quad}}, c^{+}_{\text{lin}}$ respectively. Finally, the total cost takes into account both of these costs and is defined as

$$\begin{aligned} c_{\text{total}}(p^{+}_{g_{DS}}(k), p^{-}_{g_{DS}}(k), p_g(k)) = c_{\text{DS}}(p^{+}_{g_{DS}}(k), p^{-}_{g_{DS}}(k)) + \\ \alpha \cdot c_{\text{imb}}(p_{g_{DS}}(k), p_g(k)) \end{aligned} \tag{4.2}$$

with imbalance cost factor $\alpha \in \mathbb{R}_{\geq 0}$. For the average daily costs of each of the introduced cost, we first calculate the daily cost by aggregating the hourly cost. Then, we average the daily cost over all considered days.

Additionally, for a better comparison between buildings with different prosumption scales, we calculate the wins of each forecast. More precisely, for each building, we calculate which forecast results in the minimal average daily cost. The corresponding forecasts then achieve a win. To measure the clarity of the win, we further consider the 5% win range. Specifically, for each building and each set of forecasts, we calculate the percentage difference $\frac{2 \cdot |c - c^{\min}|}{|c + c^{\min}|} \cdot 100$ between the resulting average daily cost c of the forecasts and the minimal average daily cost $c^{\min}$ of the forecasts that achieve the win for that building. If this percentage difference is less than 5%, then the corresponding forecasts achieve an occurrence within the 5% win range.

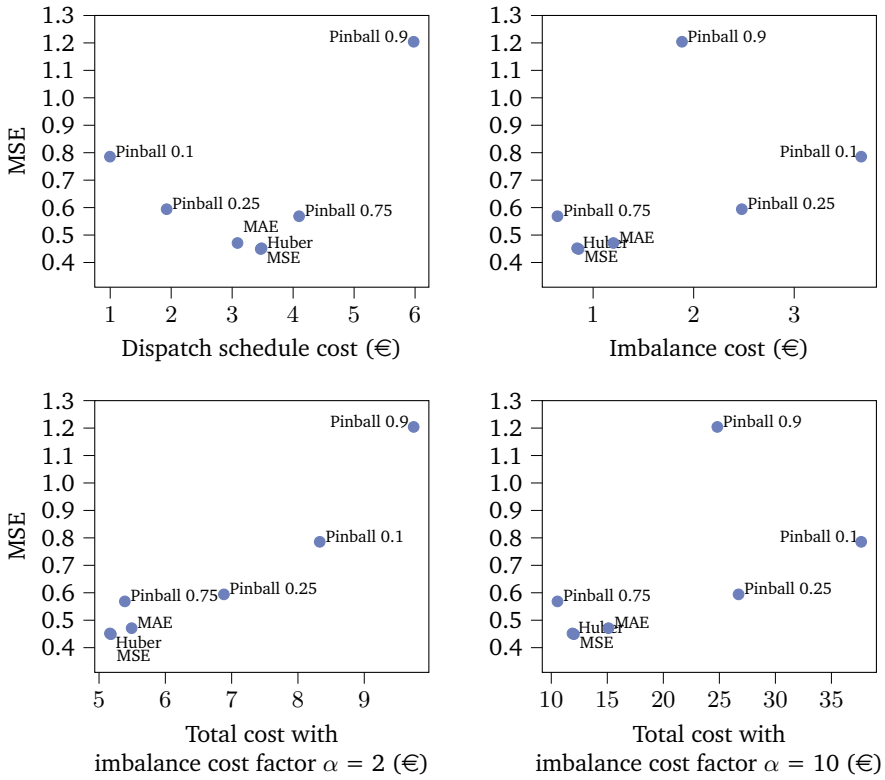

Fig. 4.3.: The MSE against the average daily dispatch schedule cost (upper left), the average daily imbalance cost (upper right), the average daily total cost with imbalance cost factor $\alpha = 2$ (lower left) and the average daily total cost with imbalance cost factor $\alpha = 10$ (lower right) for the considered loss functions. For this plot, we use the prosumption data original ($\beta_{\text{load}} = 1, \beta_{\text{PV}} = 1$) and the BESS energy capacity $e_s^{\max} = 19.5$ kWh. Note that for both the average daily costs and the MSE lower values are better.

4.2.2 Results

In this section, we evaluate point forecasts with different characteristics with respect to their forecast value for the two-level DF considering point forecasts. Since these different point forecasts are generated using NNs with different loss functions, we present the results according to the respective loss function's name. For this evaluation, we consider three aspects. First, we examine the relationship between forecast quality and forecast value. Second, we explore the forecast value for varying prosumption data. Lastly, we assess the forecast value for varying BESS energy capacities.

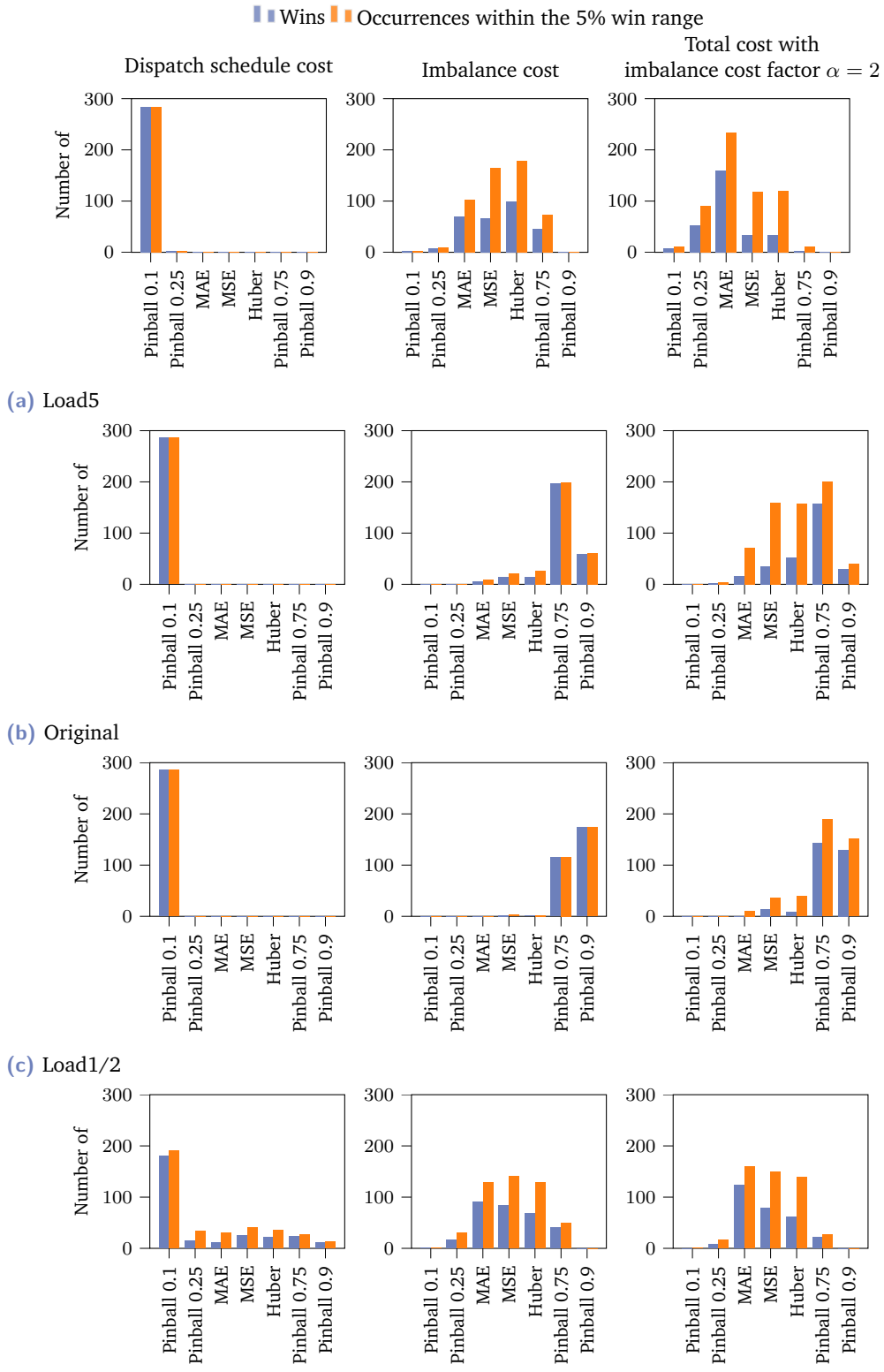

Fig. 4.4.: The wins and the occurrences within the 5% win range for the considered average daily cost, i.e. the dispatch schedule cost (left), the imbalance cost (middle), and the total cost with imbalance cost factor $\alpha = 2$ (right) and the prosumption data load5 ($\beta_{\text{load}} = 5, \beta_{\text{PV}} = 1$) (a), original ($\beta_{\text{load}} = 1, \beta_{\text{PV}} = 1$) (b), load1/2 ($\beta_{\text{load}} = 1/2, \beta_{\text{PV}} = 1$) (c), and PV5 ($\beta_{\text{load}} = 1, \beta_{\text{PV}} = 5$) (d) for the considered loss functions. Further, we consider the BESS energy capacity $e_{\text{s}}^{\max} = 19.5$ kWh. Note that more wins and more occurrences within the 5% win range are better.

Relation between Forecast Quality and Forecast Value

For this evaluation, we relate the MSE as forecast quality and the average daily costs as forecast value for the original data and the BESS energy capacity $e_s^{\max} = 19.5$ kWh in the scatter plots in Figure 4.3. In these plots, the forecast quality and the forecast value are averaged over all buildings considered.
For three average daily costs, we observe that the forecast resulting in the best forecast quality does not result in the best forecast value. Further, the relation between the forecast quality and value is not clearly deducible.
More precisely, for the DS cost, pinball 0.1 and pinball 0.25 achieve the best and second-best forecast value (1.00 and 1.93 respectively), but the sixth-best and fifth-best forecast quality (0.79 and 0.59 respectively).
For the imbalance cost, pinball 0.75 results in the best forecast value (0.65) and the fourth-best forecast quality (0.57).
For the total cost with imbalance cost factor $\alpha = 2$, Huber achieves the best forecast value (5.16) followed by MSE (5.18), which have the best forecast quality (0.45 both). For the total cost with imbalance cost factor $\alpha = 10$, the best forecast value is achieved with pinball 0.75 (10.55).

Comparison of different Loss Functions regarding varying Prosumption Data

In this subsection, we quantitatively and qualitatively compare the performance of different loss functions for varying prosumption data and the BESS energy capacity $e_s^{\max} = 19.5$ kWh. For the quantitative comparison, we consider the wins and the occurrences within the 5% win range for three average daily costs, namely the DS cost, the imbalance cost, and the total cost with imbalance cost factor $\alpha = 2$, for all buildings, as well as the prosumption data load5, original, load1/2, and PV5. For the qualitative comparison, we have a closer look on building 109. More precisely, we look at two average daily costs, namely the DS cost and the imbalance cost, for the prosumption data load5, original, load1/2, and PV5 and the results of the DF for an exemplary week and selected loss functions for the prosumption data original and PV5.

Quantitative Comparison Figure 4.4 shows the results of the quantitative comparison, which we describe for each average daily cost in the following. Starting with the DS cost, we observe that pinball 0.1 achieves almost all wins for load5, original, and load1/2. For PV5, pinball 0.1 achieves the most wins (181), but the remaining wins are spread over all considered loss functions. Regarding the clarity of the wins,

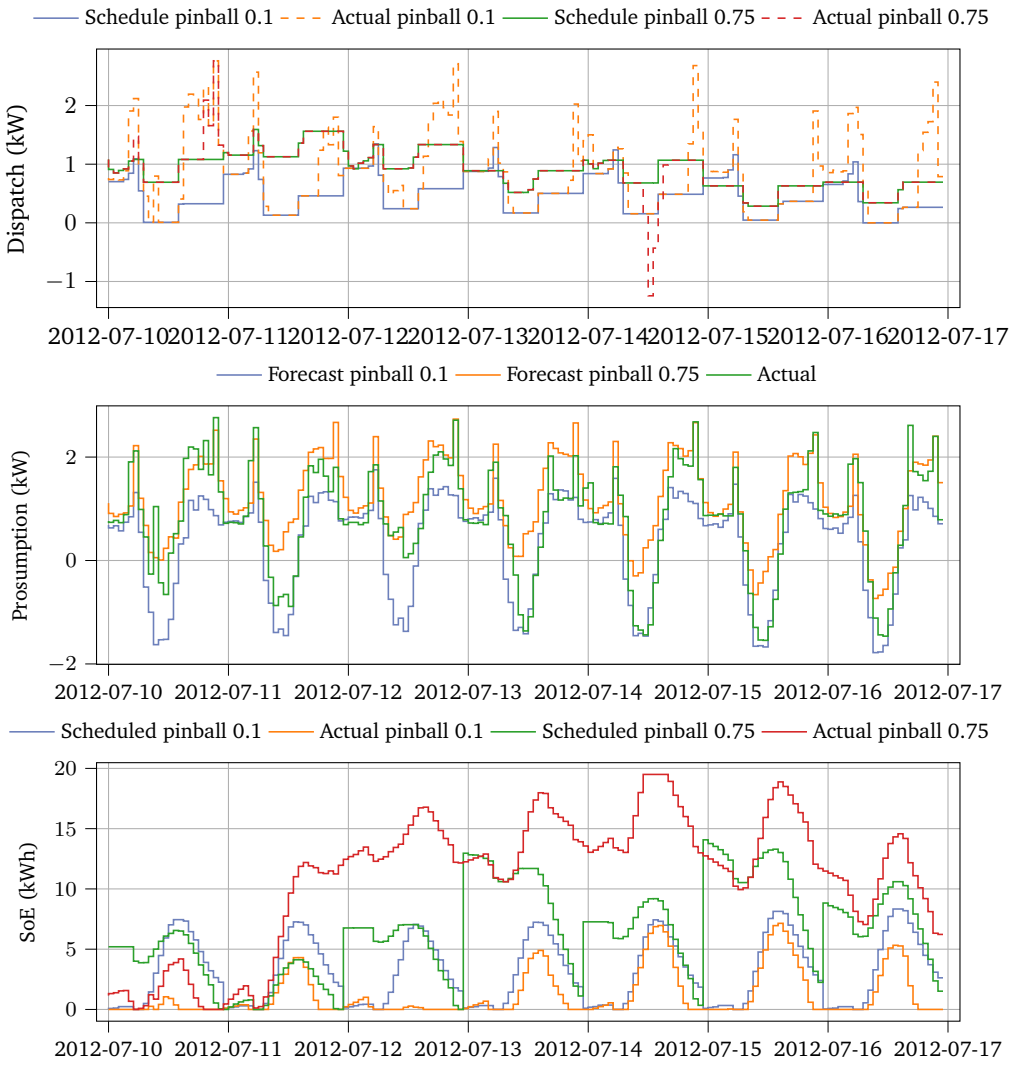

Fig. 4.5.: The dispatch schedule $p_{g_{DS}}$, the actual dispatch p_g, the prosumption forecast $\hat{\tilde{p}}_l$, the actual prosumption p_l, the scheduled BESS' SoE and the actual BESS' SoE resulting from the usage of pinball 0.1 and pinball 0.75 for the prosumption data original ($\beta_{\text{load}} = 1, \beta_{\text{PV}} = 1$) and the BESS energy capacity $e_s^{\max} = 19.5$ kWh for an exemplary week.

Tab. 4.2.: The considered average daily costs in €, i.e. the dispatch schedule cost and the imbalance cost, of building 109 and the prosumption data load5 ($\beta_{\text{load}} = 5, \beta_{\text{PV}} = 1$), original ($\beta_{\text{load}} = 1, \beta_{\text{PV}} = 1$), load1/2 ($\beta_{\text{load}} = 1/2, \beta_{\text{PV}} = 1$), and PV5 ($\beta_{\text{load}} = 1, \beta_{\text{PV}} = 5$) for all considered loss functions. Additionally, we use the BESS energy capacity $e_s^{\max} = 19.5$ kWh. Note that for the average daily costs lower values are better.

	Load5		Original		Load1/2		PV5	
	DS	Imbalance	DS	Imbalance	DS	Imbalance	DS	Imbalance
Pinball 0.1	**35.42**	34.92	**1.62**	4.17	**-0.30**	1.96	34.86	20.69
Pinball 0.25	50.47	22.32	2.51	2.78	-0.02	1.14	23.70	10.83
MAE	68.63	11.86	3.63	1.44	0.22	0.50	14.86	9.79
MSE	79.83	**10.28**	4.07	0.99	0.22	0.41	14.93	9.96
Huber	74.26	10.32	3.91	1.12	0.20	0.45	16.80	**8.87**
Pinball 0.75	93.21	12.44	4.95	**0.78**	0.37	**0.39**	8.69	15.03
Pinball 0.9	131.53	28.77	6.82	2.41	1.45	2.37	**4.67**	57.40

we observe that for load5, original, and load1/2 no other loss function achieves occurrences within the 5% win range except pinball 0.25 for load5 (3).

For the imbalance cost, we observe that a loss function's wins depend on the prosumption data. For original, the overestimating loss functions pinball 0.75 and pinball 0.9 achieve the most and second most wins (197 and 59 respectively). For load1/2, more wins are shifted to pinball 0.9, resulting in a dominance of wins (174), followed by pinball 0.75 (115). In contrast, for load5 and PV5, we observe that overestimation is less beneficial for the wins. More precisely, for load5, Huber achieves the most wins (99), while Pinball 0.75 achieves the fourth most wins (46). For PV5, MAE (91) achieves the most wins. Regarding the clarity of the wins, we observe for original and load1/2 that the occurrences within the 5% win range are almost equal to the number of wins for all loss functions indicating clear wins. On the other hand, for load5 and PV5, the number of occurrences within the 5% win range is higher than the number of wins, indicating that the average daily cost can be similar for different loss functions.

For the total cost with imbalance cost factor $\alpha = 2$, we observe for all prosumption data that the wins are more spread over the loss functions. More precisely, for load5, all loss functions except pinball 0.9 achieve wins with MAE achieving the most (159). For original, similar to the imbalance cost, pinball 0.75 (157) achieves the most wins. Also in consistency with the results of the imbalance cost, pinball 0.75 (143) and pinball 0.9 (130) achieve the most and second most wins for load1/2, while MAE (124) achieves the most wins for PV5. Regarding the clarity of the wins, the occurrences within the 5% win range are higher for all loss functions and prosumption data compared to the DS cost and imbalance cost.

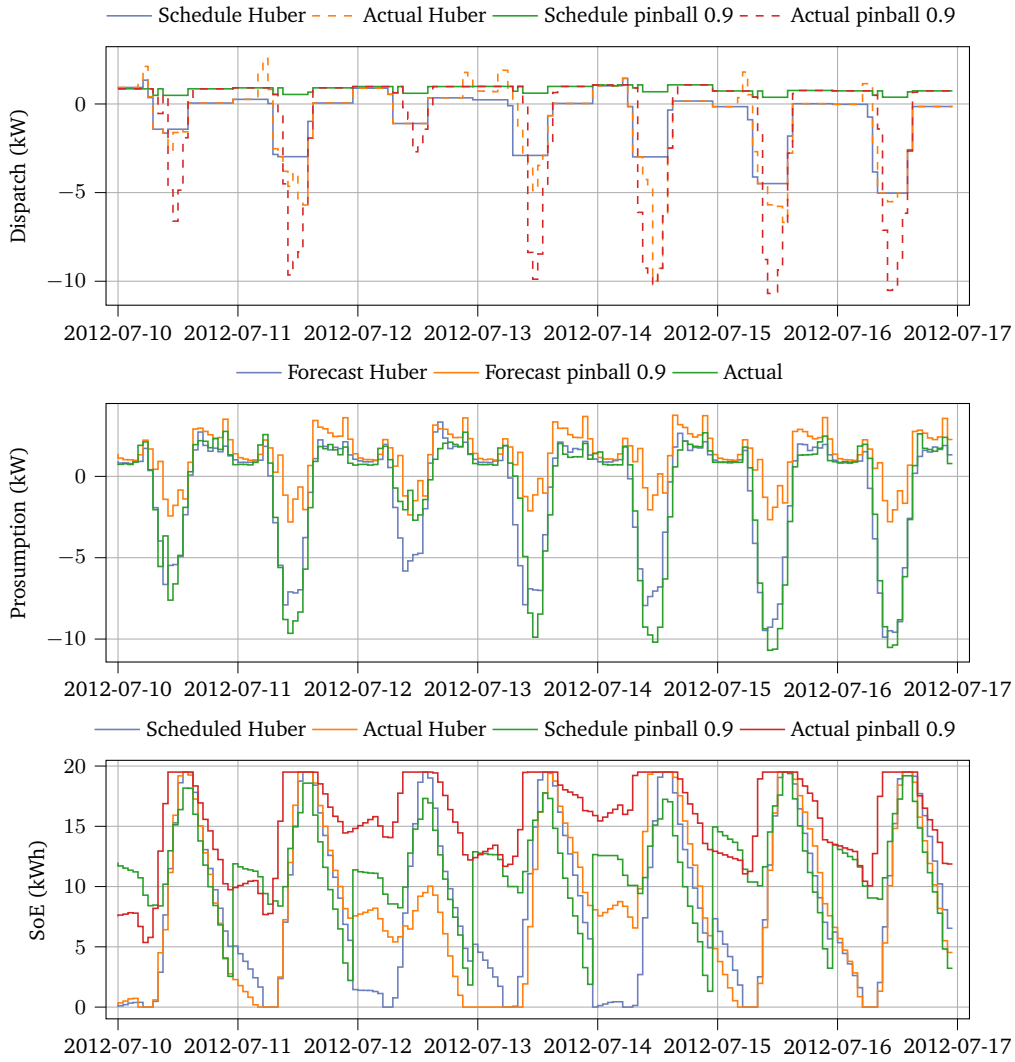

Fig. 4.6.: The dispatch schedule $p_{g_{DS}}$, the actual dispatch p_g, the prosumption forecast $\hat{\tilde{p}}_l$, the actual prosumption p_l, the scheduled BESS' SoE and the actual BESS' SoE resulting from the usage of Huber and pinball 0.9 for the prosumption data PV5 ($\beta_{\text{load}} = 1, \beta_{\text{PV}} = 5$) and the BESS energy capacity $e_s^{\max} = 19.5$ kWh for an exemplary week of building 109.

Qualitative Comparison Starting with the average daily costs, Table 4.2 shows the DS cost and the imbalance cost for building 109, where we make two observations. First, we observe that the DS cost and the imbalance cost can vary greatly depending on the loss function. Second, we observe that while there is one loss function that leads by far to the minimal DS cost, several loss functions can lead to imbalance costs similar to the minimal imbalance cost. More precisely, for the DS cost, consistent with the quantitative comparison, we observe that pinball 0.1 achieves by far the minimal DS cost for load5, original, and load1/2. For PV5, pinball 0.9 achieves clearly the minimal DS cost. In contrast, for the imbalance cost, we observe for load5 that MSE and Huber lead to similar imbalance costs. The same holds for original and load1/2 with pinball 0.75, MSE, and Huber. For PV5, Huber, MAE, and MSE lead to similar imbalance costs.
The results of the DF for an exemplary week are shown in Figure 4.5 for original and in Figure 4.6 for PV5. Both figures show the results of two loss functions, namely the loss functions leading to the minimal DS cost and the minimal imbalance cost, i.e. pinball 0.1 and pinball 0.75 for original and pinball 0.9 and Huber for PV5. Starting with original, we see that the DS with pinball 0.1 is smaller than the DS with pinball 0.75 for almost the whole week. However, while the DS and the actual dispatch with pinball 0.75 match at most hours, there are many imbalances with pinball 0.1. With respect to the SoE, we observe that the actual SoE with pinball 0.75 is higher than the actual SoE with pinball 0.1, which is at its lower BESS energy capacity $e_s^{\min} = 0$ kWh at the start and the end of the day. For PV5, we observe that the DS with Huber is during the PV power generation hours clearly negative and the absolute value of the DS is greater than the DS with pinball 0.9. Additionally, we observe that imbalances occur during the end of the PV power generation hours with Huber and pinball 0.9, while the imbalances occur earlier with pinball 0.9. During these hours, the actual SoE with Huber and pinball 0.9 is at its upper BESS energy capacity $e_s^{\max} = 19.5$ kWh.

Comparison of different Loss Functions regarding varying BESS Energy Capacities

For this comparison, we quantitatively and qualitatively compare the performance of different loss functions for varying BESS energy capacities and the prosumption data original. For the quantitative comparison, we consider the wins and the occurrences within the 5% win range for three average daily costs, namely the DS cost, the imbalance cost, and the total cost with imbalance cost factor $\alpha = 2$, the BESS energy capacities $e_s^{\max}$ of 3 kWh, 6 kWh, 13.5 kWh, and 19.5 kWh, and all buildings. For the qualitative comparison, we focus on building 109 and look at two average daily

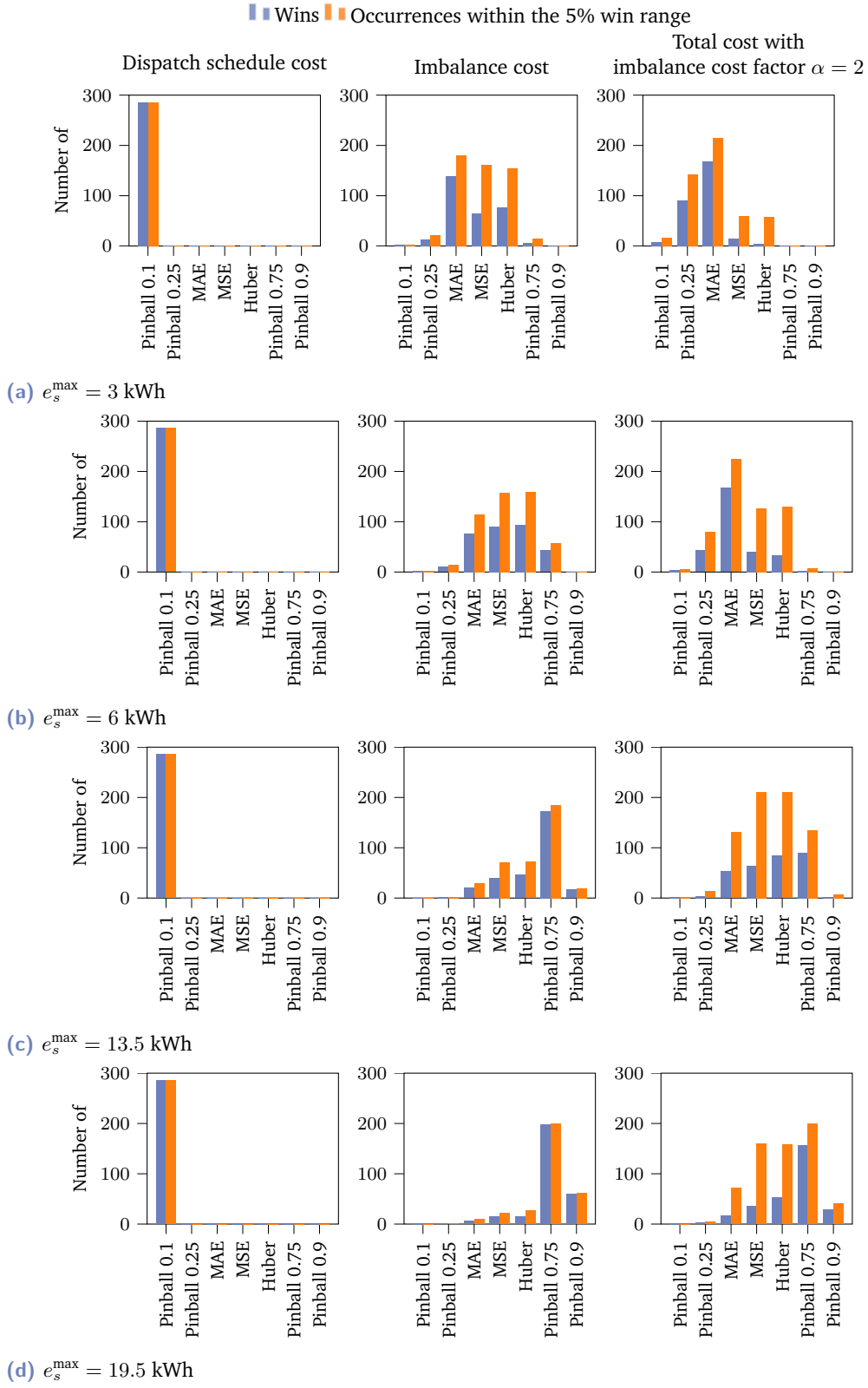

Fig. 4.7.: The wins and the occurrences within the 5% win range for the considered average daily costs, i.e. the dispatch schedule cost (left), the imbalance cost (middle), the total costs with imbalance cost factor $\alpha = 2$ (right) and the BESS energy capacities $e_s^{\max} = 3$ kWh (a), $e_s^{\max} = 6$ kWh (b), $e_s^{\max} = 13.5$ kWh (c), and $e_s^{\max} = 19.5$ kWh (d) for the considered loss functions. Further, we consider the prosumption data original ($\beta_{\text{load}} = 1, \beta_{\text{PV}} = 1$). Note that higher win values and higher occurrences within the 5% win range are better.

costs, namely the DS cost and the imbalance cost, for the BESS energy capacities $e_s^{\max}$ of 3 kWh, 6 kWh, 13.5 kWh, and 19.5 kWh. Further, we evaluate the results of the DF for an exemplary week and selected loss functions for the BESS energy capacity $e_s^{\max} = 13.5$ kWh.

Quantitative Comparison Figure 4.7 displays the results of the quantitative comparison for the considered average daily costs. Starting with the DS cost, we see a clear dominance of pinball 0.1, which achieves all wins for all BESS energy capacities and no other loss function achieves occurrences within the 5% win range.
For the imbalance cost, we observe that the smaller the BESS energy capacity, the more wins are shifted from the overestimating loss functions pinball 0.75 and pinball 0.9 to the loss functions MSE, Huber, and MAE. More precisely, for BESS energy capacity of 19.5 kWh, pinball 0.75 (197) achieves the most wins, followed by pinball 0.9 (59), and for BESS energy capacity of 13.5 kWh, pinball 0.75 (173) achieves the most wins. In contrast, for the BESS energy capacity of 6 kWh, Huber (94) achieves the most wins, while for the smallest considered BESS energy capacity of 3 kWh, MAE (139) achieves the most wins. Regarding the clarity of the wins, we observe especially for a BESS energy capacity of 3 kWh and 6 kWh that MSE, Huber, and MAE have more occurrences within the 5% win range than wins.
For the total cost with imbalance cost factor $\alpha = 2$, the difference between the occurrences within the 5% win range and the number of wins is big. More precisely, for a BESS energy capacity of 3 kWh and 6 kWh, MAE achieves the most wins (169 and 167 respectively) and occurrences within the 5% win range (214 and 224 respectively). For a BESS energy capacity of 13.5 kWh, pinball 0.75 (90) achieves the most wins. In contrast, MSE (211) and Huber (210) achieve more occurrences within the 5% win range than pinball 0.75 (135). For a BESS energy capacity of 19.5 kWh, pinball 0.75 (157) can increase his lead over Huber (53). This is also reflected in the occurrences within the 5% win range of pinball 0.75 (200) and Huber (158).

Qualitative Comparison The DS cost and the imbalance cost for building 109 are shown in Table 4.3 and lead to two observations. First, we observe that both average daily costs decrease as the BESS energy capacity increases. Second, we make the same observations as in the qualitative comparison with varying prosumption data, i.e. that both costs can vary greatly depending on the loss function, and that while pinball 0.1 leads to by far the minimal DS cost, several loss functions lead to similarly low imbalance costs.
Next, the results of the DF for an exemplary week are shown in Figure 4.8 for

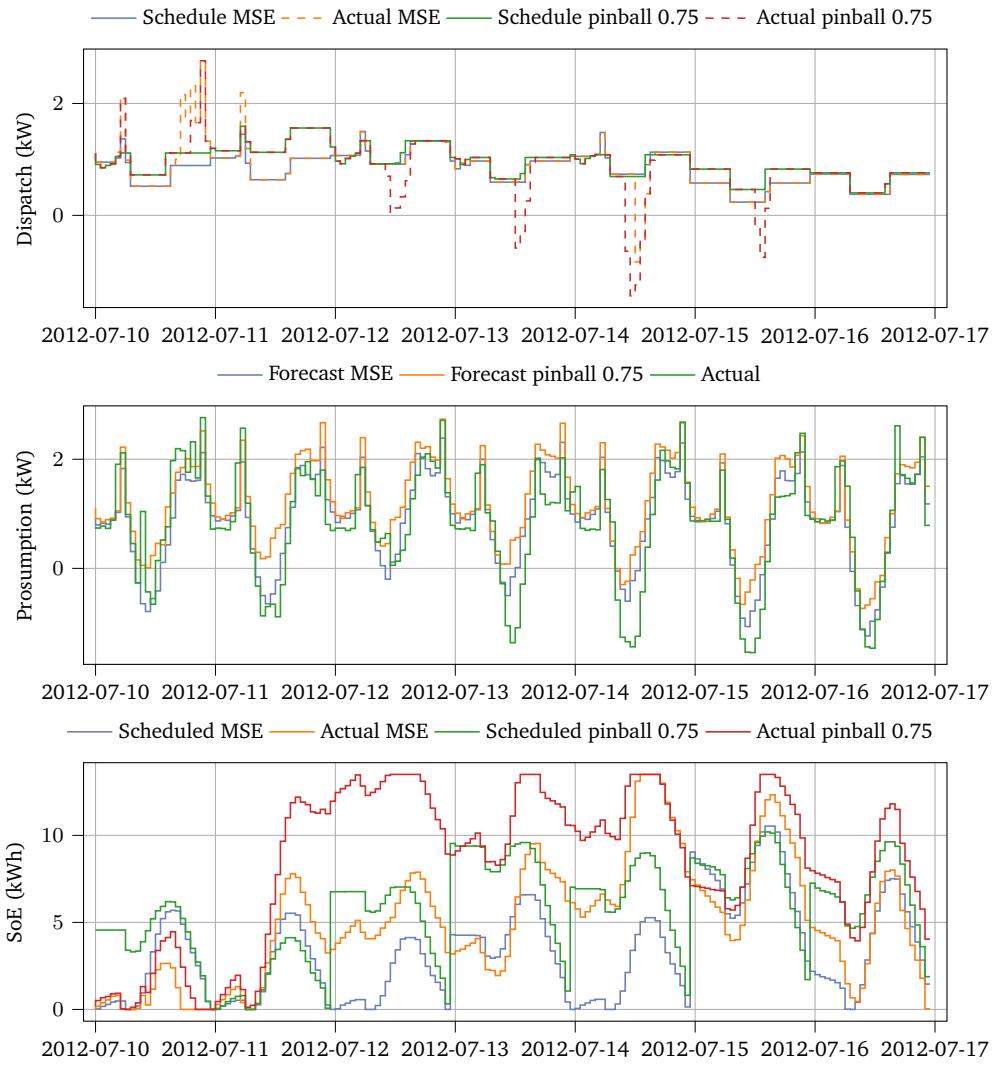

Fig. 4.8.: The dispatch schedule $p_{g_{DS}}$, the actual dispatch p_g, the prosumption forecast $\hat{\bar{p}}_l$, the actual prosumption p_l, the scheduled BESS' SoE and the actual BESS' SoE resulting from the usage of MSE and pinball 0.75 for the BESS energy capacity $e_s^{\max} = 13.5$ kWh and prosumption data original ($\beta_{\text{load}} = 1, \beta_{\text{PV}} = 1$) for an exemplary week of building 109.

Tab. 4.3.: The considered average daily costs in €, i.e. the dispatch schedule cost and the imbalance cost, of building 109 and the BESS energy capacities $e_s^{\max} = 3$ kWh, $e_s^{\max} = 6$ kWh, $e_s^{\max} = 13.5$ kWh, and $e_s^{\max} = 19.5$ kWh for all considered loss functions. Additionally, we use the prosumption data original ($\beta_{\text{load}} = 1, \beta_{\text{PV}} = 1$). Note that for the average daily costs lower values are better.

	3 kWh		6 kWh		13.5 kWh		19.5 kWh	
	DS	Imbalance	DS	Imbalance	DS	Imbalance	DS	Imbalance
Pinball 0.1	**2.30**	5.67	**1.88**	5.15	**1.61**	4.25	**1.62**	4.17
Pinball 0.25	3.26	4.22	2.87	3.72	2.53	2.90	2.51	2.78
MAE	4.97	2.50	4.34	2.28	3.73	1.63	3.63	1.44
MSE	5.65	2.49	5.10	2.19	4.25	**1.30**	4.07	0.99
Huber	5.43	**2.31**	4.79	**2.06**	4.08	1.36	3.91	1.12
Pinball 0.75	7.47	3.20	6.79	2.93	5.54	1.56	4.95	**0.78**
Pinball 0.9	10.67	6.23	9.69	5.58	8.05	3.80	6.82	2.41

the BESS energy capacity of 13.5 kWh and the loss functions MSE and pinball 0.75. These are the loss functions that lead to the minimal imbalance cost for this BESS energy capacity (MSE) and to the minimal imbalance cost for the next bigger BESS energy capacity (pinball 0.75), whose DF results are displayed in Figure 4.5. Comparing the DF results between MSE and pinball 0.75 shows that while the DS with pinball 0.75 is only slightly higher than the DS with MSE, the imbalances especially during the PV power generation hours are higher with pinball 0.75. In these hours, we observe that the actual SoE with pinball 0.75 is often at its upper BESS energy capacity $e_s^{\max} = 13.5$ kWh.

4.3 Discussion

This section discusses the findings of the evaluation, the limitations and further research.

4.3.1 Findings

The discussion of the findings focuses on three aspects. First, we discuss the relation between the forecast quality and the forecast value. Second, we discuss the influence of the forecast characteristics on the forecast value. Finally, we revisit the research question posed in this chapter and assess whether the findings provide a satisfactory answer.

First, regarding the relation between the forecast quality and forecast value, the results in Subsection 4.2.2 show that the relation between the considered forecast

quality, namely the MSE, and the considered forecast values for the DF, namely the average daily costs, is non-monotonic. This means that improving the forecast quality does not necessarily improve the forecast value for the DF and can even lead to higher average daily costs. This result indicates that it may be beneficial for the performance of the DF to consider not only the forecast quality but also the forecast value when generating the required point forecast.

Second, regarding the forecast characteristics' influence on the forecast value, the results demonstrate that the forecast characteristics affect highly the considered forecast value for the DF. When aiming for the best forecast value one might want to look beyond the usual forecast characteristics determined by standard loss functions. How the forecast characteristics affect the considered forecast value depends on the prosumption data and the BESS energy capacity. Furthermore, we observe that this impact varies for each forecast value. Thus, we further discuss this impact for each considered forecast value, namely the average daily costs, separately. For the DS cost, the results indicate that underestimating the prosumption leads by far to the minimal cost for all BESS energy capacities and prosumption data except for PV5. A possible reason why an underestimation of the prosumption is beneficial in most cases is that this leads to an underestimation of the load and an overestimation of the PV power generation. Thus, hardly any power is imported from the grid according to the resulting DS. As consequence, the cost associated with the DS are low. However, when the PV power generation is scaled with 5 a strong underestimation becomes disadvantageous. A possible reason, therefore, is that the building generates already so much PV power that an underestimation of the prosumption and thus an overestimation of the PV power generation can not be consumed by the building. Consequently, more PV power is fed into the grid which raises cost due to the specified cost coefficients taking into account self-consumption and peak shaving, see Appendix A.2. With respect to the imbalance cost, we observe that the preferred forecast characteristics depend on the prosumption data and the BESS energy capacity. We observe that overestimation becomes more beneficial the smaller the load factor and the bigger the BESS energy capacity indicating asymmetric imbalance cost. In the following, we aim to provide a possible explanation of this behaviour. If the prosumption is overestimated, the DS is calculated assuming that the building consumes more and generates less energy than it actually does. Thus, in the second level, the BESS then charges if possible to mitigate imbalances. As a result, the BESS has energy reserves for unexpected high prosumption. This behaviour is beneficial if the BESS is not fully charged and thus can still balance out unexpected low prosumption. For a higher load/PV power generation factor or a smaller BESS energy capacity, the BESS reaches its limit faster. As a result, imbalances become more likely. As the total cost is the

weighted sum of the DS cost and the imbalance cost, the performance of the forecast characteristics with respect to the two latter costs impacts the performance of the forecast characteristics with respect to the total cost. Thereby, the imbalance cost factor determines the impact of each cost. For both imbalance cost factors, we observe that an overestimation can be beneficial depending on the prosumption data and the BESS energy capacity. More specifically, for imbalance cost factor 10, the imbalance cost makes up the largest share of the total cost. As consequence, we observe the same results as for the imbalance cost, see Figure 4.3. On the other hand, for the imbalance cost factor $\alpha = 2$, the impact of the imbalance cost is less dominant. Therefore, the impact of the DS cost becomes more important and the results appear to be a combination of the results for both costs.
Finally, regarding the research question

RQ1: *How do different point forecast characteristics influence the forecast value for the dispatchable feeder, and how does this influence depend on problem-specific parameters?*

we can conclude that the forecast characteristics influence the forecast value for the two-level DF considering point forecasts and that this influence depends on the prosumption data and the BESS energy capacity.

4.3.2 Limitations and Further Research

The main limitations of this evaluation are the chosen specifications, including the forecast method used, the loss functions considered, and the DF specifications. Therefore, the potential for further research lies in extending these specifications. In particular, forecasts generated by different methods could be explored. Additionally, more complex loss functions resulting in diverse forecast characteristics could be examined, such as [57]. Regarding the DF specifications, further problem-specific parameters could be evaluated, such as the cost coefficients, and extending the DF to three levels could be of interest. Finally, other forecast values could be considered.

5 Value-Oriented Forecast Method Selection

As the evaluation of Chapter 4 shows, the forecast and its associated forecast method have a huge impact on the forecast value for the dispatchable feeder (DF). This impact depends on problem-specific parameters, namely the prosumption data and the BESS energy capacity. Based on this finding, this chapter presents a framework to select the best forecast method with respect to the forecast value[1]. While the forecast method may be found by a manual selection, the proposed framework aims to reduce the computational effort by using meta-learning. Therefore, the selection task is treated as a classification problem and a classifier is trained to select the forecast method leading to the forecast with the highest forecast value using a building's metadata as input. While the proposed framework is applicable to a variety of downstream applications, we evaluate it on the two-level DF considering point forecasts, illustrated in Figure 5.1. The research question addressed is:

RQ3: *How to automatically select the forecast method with respect to the forecast value with low computational effort using meta-learning?*

The remainder of this chapter is structured as follows. First, Section 5.1 presents the proposed framework. Then, Section 5.2 describes the experimental setup for evaluating the proposed framework on the two-level DF considering point forecasts in Subsection 5.2.1 and presents the results in Subsection 5.2.2. Afterwards, Section 5.3 discusses the results.

5.1 Proposed Framework

This section proposes a framework for selecting the forecast method leading to forecasts with a high forecast value. While this selection may be found by a computationally expensive manual search, the proposed framework aims to reduce this

[1]The content of this chapter is based on [143], licensed under a Creative Commons "Attribution 4.0 International" License (CC BY 4.0). While the concept is the same, the experimental setup differs, including the used classifiers, the forecasting specifications, the used prosumption data, and the used BESS energy capacity.

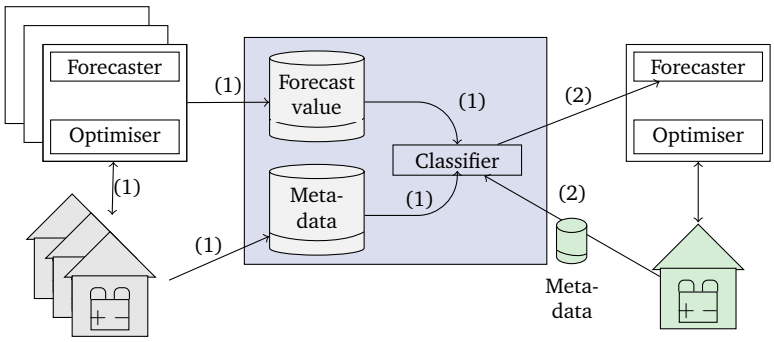

Fig. 5.1.: The schematic representation of the proposed framework with the novelty marked in blue, taken from [143] and licensed under CC BY 4.0. In step (1), a classifier is trained using the buildings' metadata and the buildings' label of the forecast method leading to the forecast with the highest forecast value. In step (2), the trained classifier can be operated to generate forecasts with a high forecast value for a new building utilising its metadata (marked in green). Then, the dispatchable feeder can be executed.

computational effort while achieving comparable results. Despite the evaluation on the DF in this thesis, the proposed framework is applicable to various downstream applications that require forecasts as input. Therefore, the following description is formulated for a general downstream application. Additionally, the consideration of buildings is generalised to instances.
Mathematically, the forecast method leading to the forecast with the highest forecast value for the downstream application a and for instance $i \in \mathcal{I}$ can be expressed as

$$m_i^\star = \underset{m \in \mathcal{M}}{\operatorname{argmax}} \operatorname{Value}\Big(a, D_i, m\Big) \tag{5.1}$$

with the set of forecast methods $\mathcal{M}$ and the instance's data D_i, which includes the relevant data for the forecast method and additional instance-specific data required for the downstream application such as the BESS energy capacity in the case of the DF. This data has a crucial impact on the forecast value. The forecast method m_i^* is hereafter referred to as the best forecast method and is the target of the selection task. The proposed framework treats this selection task as a classification problem. The following subsections describe the components of the proposed framework in Subsection 5.1.1 and the usage of the proposed framework in Subsection 5.1.2.

5.1.1 Components of the Proposed Framework

The proposed framework consists of a classifier that uses the instance's metadata to forecast the best forecast method for the considered downstream application. Therefore, the relevant components of the proposed framework are the set of forecasts

methods $\mathcal{M}$, the downstream application a, the metadata extraction component, and the classifier c. These components are described in the following:

- *Set of forecast methods* $\mathcal{M}$: This set contains all considered forecast methods. To handle the influence of the data D_i from different instances $i \in \mathcal{I}$ on which is the best forecast method, we need the set to be sufficiently diverse.

- *Downstream application* a: The downstream application must require a forecast as input for execution. The performance of the downstream application's execution determines the forecast value and must therefore be measurable.

- *Metadata extraction component*: This component extracts relevant metadata md_i from the data D_i that is used as input for the classifier. In general, metadata provides details and characteristics of data and can come in various types [118]. For the proposed framework, the metadata must contain information to classify the best forecast method for the considered downstream application.

- *Classifier* c: Since we interpret the selection task in Equation (5.1) as a classification problem, the classifier and its performance are crucial for the proposed framework. In general, classification involves the approximation of a parameterised function c to forecast either one class label, which represents a discrete outcome of a qualitative variable, or probabilities for each class, which represent the likelihood of each possible outcome, based on input features. As such, it is a type of supervised learning [60]. The approximation of the function c can be achieved by different classification algorithms based on different strategies. Examples are tree-based strategies (e.g. decision tree, XGBoost classifier [21]), distance-based strategies (e.g. k-nearest neighbour classifier [38]), support vector-based strategies (e.g. support vector classifier [113]), neural network-based strategies (e.g. multi-layer perceptron), and probabilistic strategies (e.g. naive Bayes classifier [151]). The choice of the classifier depends on the to be approximated function and the considered data. In the proposed framework, the classifier has to select the forecast method leading to the forecast with the highest forecast value in the considered downstream application. In doing so, each forecast method $m \in \mathcal{M}$ represents a distinct a class, into which each instance i is classified. The target variable of the classifier is then $m_i^\star$, and its output $\hat{m}_i^\star = c(md_i)$ can take one of two forms: either one forecast method, when forecasting a discrete outcome, or a vector of probabilities for each forecast method, when forecasting the likelihood of each possible outcome. Note that while the latter is a selection of the probabilities for each forecast method rather than a direct selection of the forecast method, we refer for simplicity to both forms as a selection of the forecast method.

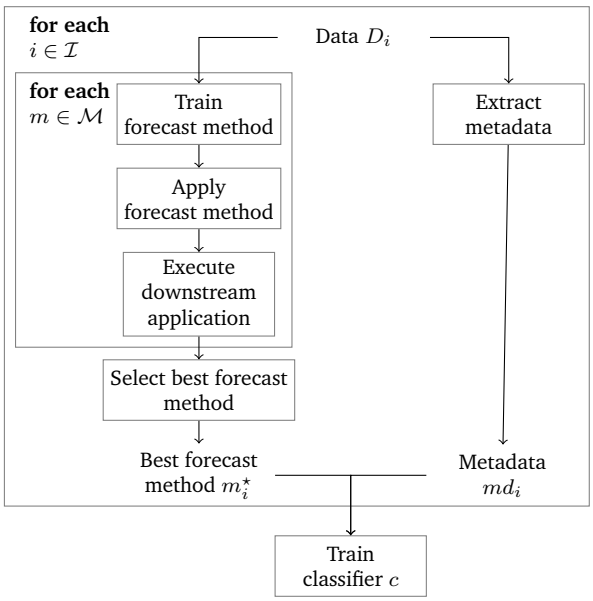

(a) To train the proposed framework, the training data needs to be created. Therefore, for each instance $i \in \mathcal{I}$ and its data D_i, the forecast value for each forecast method $m \in \mathcal{M}$ in the downstream application is calculated. Based on this information, the best forecast method $m_i^\star$ for this instance is determined. Afterwards, $m_i^\star$ is used as target variable together with the metadata md_i as input data to train the classifier c.

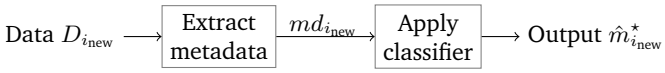

(b) To operate the proposed framework, the metadata $md_{i_{\text{new}}}$ from the data $D_{i_{\text{new}}}$ of the new instance i_{new} is extracted. Based on this information, the classifier outputs $\hat{m}^\star_{i_{\text{new}}}$, which is either a forecast method or probabilities for each forecast method. In the former case, the forecast method is trained, and its forecast is provided to the downstream application a. In the latter case, each forecast method is trained, and an ensemble forecast is generated as a weighted sum of the resulting forecasts, with the probabilities as weights, and this ensemble forecast is provided to the downstream application a.

Fig. 5.2.: The usage of the proposed framework, taken from [143] and licensed under CC BY 4.0. (a) In the first step, the framework needs to be trained. (b) Afterwards, the framework can be operated.

5.1.2 Usage of the Proposed Framework

To be able to use the proposed framework, two steps are necessary, as illustrated in Figure 5.2. First, the framework needs to be trained. Second, the framework can be operated to forecast either the forecast method leading to forecasts with a high forecast value or probabilities for each forecast method for a new instance. These two steps are described in more detail below.

Step 1: Training The training of the proposed framework consists of the training of the classifier, which requires the input features and the target variables. We first describe the creation of the input features and the target variables and then present the training of the classifier.
To create the input features and the target variables, the following steps are done for each instance $i \in \mathcal{I}$ of the training set. First, we extract the metadata md_i of the data D_i corresponding to the input features, which includes key information of the data D_i. In the case of the DF, this metadata could include the building size, BESS capacity, and statistical features such as the mean, variance, standard deviation, minimum, maximum, or quantiles of the prosumption, load, or PV power generation. To obtain the target variables, we first train each forecast method $m \in \mathcal{M}$ using the data D_i. Then, the forecasts generated by each forecast method are fed into the downstream application. After execution, the performance of the downstream application is evaluated and each forecast method is assigned its respective forecast value. Finally, the forecast method leading to the forecast with the highest forecast value is labelled with $m_i^\star$, which corresponds to the target variable.
The classifier c is then trained using the input features and the target variables over all instances $i \in \mathcal{I}$ of the training set.

Step 2: Operation After training, the proposed framework uses the metadata extracted from the data of a new instance $D_{i_{\text{new}}}$ and outputs $\hat{m}_{i_{\text{new}}}^\star$, which is either a forecast method or probabilities for each forecast method $m \in \mathcal{M}$. Based on this output, the forecasts can be generated. More precisely, if the output is one forecast method, this forecast method is trained and the forecast is generated. If the output is probabilities for each forecast method, each forecast method is trained, and their resulting forecasts are combined into an ensemble forecast, using the probabilities as weights in a weighted sum. Finally, the resulting forecasts can be used as input to the downstream application a.

5.2 Evaluation

In this section, we evaluate the proposed framework on the two-level DF considering point forecasts as downstream application. Therefore, Subsection 5.2.1 describes the experimental setup, while Subsection 5.2.2 presents the results.

5.2.1 Experimental Setup

The following describes the application of the proposed framework to the DF, the used data, the generation of the point forecasts, the considered benchmarks for comparing the performance, and the evaluation metrics.

Application to Dispatchable Feeder We apply the proposed framework to the two-level DF considering point forecasts as the downstream application a. The aim is to select for each building the forecast method for the prosumption point forecasts that leads to the highest forecast value. Therefore, an instance i is a building. In line with Chapter 4, we consider the average daily total cost in Equation (4.2) as the forecast value, with a lower average daily total cost indicating a higher forecast value. For the imbalance cost factor α we chose 2 and 10, which means that the proposed framework is trained and evaluated twice with identical component specifications, differing only in the target variable. In the following, the remaining components of the proposed framework are specified, namely the set of forecast methods $\mathcal{M}$, the metadata extraction component, and the classifier c.

As set of forecast methods $\mathcal{M}$, we consider the different prosumption point forecasts generated by a neural network (NN) with seven different loss functions described in Section 4.1 and Subsection 4.2.1. That is, we have seven classes associated with the mean squared error (MSE), the mean absolute error (MAE), the Huber metric, and the pinball loss with τ values of 0.1, 0.25, 0.75, and 0.9.

The metadata extraction component extracts relevant metadata md_i that captures relevant information of the building and its prosumption time series as input features for the classifier. Thus, as metadata md_i, we consider a set of statistical features of the prosumption time series as input features. More precisely, we first scale the prosumption time series with Scikit-learn's standard scaler and then calculate the mean, standard deviation, minimum, 0.25 quantile, median, 0.75 quantile, and maximum. We also include the mean, minimum, and maximum of each day[2].

Regarding the classifier c, we evaluate the proposed framework with six different classifiers[3] to cover a broad range of classification approaches including tree-,

[2] A cross-validation with five folds on the training buildings shows that these input features are sufficient to provide relevant information for the classifier to perform well, and thus, incorporating additional input features does not result in a noticeable increase in performance. The six additional input features considered are the average daily prosumption profile (i.e. the average over all considered days for each hour), the mean over all days of minimum and maximum for each day, the strength of seasonality and the strength of trend of the prosumption time series [70], the skewness and kurtosis of the prosumption time series, and the autocorrelation of the prosumption time series.

[3] To implement the classifiers, we use the implementations provided by SKLearn [106] except for XGBoost. For this classifier, we use the XGBoost library [33].

distance-, support vector-, and neural network-based classifiers. While five classifiers are used to forecast one class label, one classifier is used for both forecasting one class label and forecasting probabilities for each class. The different classifiers are briefly described in the following. The first classifier is the support vector classifier (**SVC**) [113], which is used for both forecasting one class label and forecasting probabilities for each class. The SVC determines the classes by dividing the input feature space with a line or hyperplane [133]. While SVC is typically used for binary classification, we apply it to our multi-class problem using the one-vs-one strategy. This strategy trains a classifier for each pair of classes. While the output probabilities are the percentages of votes received from all pairwise classifiers, the output class label is determined by the class that receives the most votes from all pairwise classifiers. To distinguish between the two classifiers, we refer to the SVC outputting probabilities as **ensemble SVC**. The second classifier is k-nearest neighbours (**kNN**) [38]. It determines the k nearest neighbours for each set of input features in the test data using a given distance metric. The output class label is then the class label of the majority of the k nearest neighbours. The third classifier is a decision tree (**DT**) [21]. The DT constructs a model by recursively splitting the input feature space based on the input feature values, creating a tree-like structure. Each internal node represents a check on an input feature, branches represent the outcome of the check, and leaf nodes represent the class labels. The output class label is then determined by traversing the tree from the root to a leaf, based on the input feature values. The fourth classifier is **XGBoost** [33]. XGBoost uses gradient tree boosting, where multiple decision trees, serving as weak learners, are trained iteratively. Each tree corrects the errors of its predecessor, and thus improving the performance. The fifth classifier is the multi-layer perceptron (**MLP**). The MLP is a NN consisting of one or more hidden layers of fully connected neurons with non-linear activation functions. In the output layer, where each neuron corresponds to one class, the softmax function is used as the activation function. The output is a probability for each class and the output class label is then the class with the highest probability. The sixth classifier is the naive Bayes (**NB**) [151]. NB is a probabilistic classifier based on Bayes' theorem, which assumes that the input features are conditionally independent given the class label. The classifier calculates the posterior probability of each class given the input features by combining the prior probability of each class with the conditional probabilities of the input features. The output class label is then the class with the highest posterior probability.

Data As prosumption data, we extend the original Ausgrid dataset by considering further ratios of load and PV power generation. More precisely, we use the same

prosumption data as in Section 4.1, i.e. we consider load5 with $\beta_{\text{load}} = 5, \beta_{\text{PV}} = 1$, original with $\beta_{\text{load}} = 1, \beta_{\text{PV}} = 1$, load1/2 with $\beta_{\text{load}} = \frac{1}{2}, \beta_{\text{PV}} = 1$, and PV5 with $\beta_{\text{load}} = 1, \beta_{\text{PV}} = 5$ in Equation (2.27). This results in a total of 1144 buildings. Of these, we use 764 buildings, i.e. for each ratio of load and PV power generation the buildings with IDs smaller than 200, to select the hyperparameters of the classifiers through cross-validation with five folds and to train the classifiers. To test the proposed framework, we use the remaining 380 buildings, i.e. for each ratio of load and PV power generation the buildings with IDs greater than or equal to 200. Additionally, for all buildings, we extract the metadata based on the first two years and consider the output labels based on the last year.
For the BESS, we use the BESS energy capacity $e_s^{\max}$ of 19.5 kWh.

Forecast Method As describes above, we use the same point forecasts generated for the evaluation in Chapter 4. Therefore, the reader is referred to Subsection 4.2.1 for the description of the forecast specifications, the input features, the splitting of the data in training, validation, and testing, and the neural network architecture. Here we recall that the testing data for the forecasting is the last year.

Benchmarks To evaluate the performance of our proposed framework, we compare it to two benchmarks. The first benchmark is the **one loss function** benchmark. As the name suggests, this benchmark applies one forecast method to all considered buildings. More precisely, we use the same loss function for all considered buildings for the last year of data. As second benchmark, we consider a **manually selected loss function** for each building. In this benchmark, we calculate which loss function is cost-minimal for each considered building based on the second year of data. We then apply this cost-minimal loss function for each considered building for the last year.

Evaluation Metrics For the evaluation, we use four metrics. The first metric is the F_1 score as an accuracy measure for the classification. The F_1 score is defined as

$$\mathrm{F}_1 = \frac{2 \cdot \mathrm{TP}}{2 \cdot \mathrm{TP} + \mathrm{FP} + \mathrm{FN}}, \tag{5.2}$$

with TP being the true positives, FP being the false positives, and FN being the false negatives. In our multi-class problem, we consider the micro-average F_1 score from SKLearn [106], which aggregates the total number of TP, FP, and FN across all classes. For each class, the TP consist then of the buildings for which the proposed

framework correctly selects the class if the class is cost-minimal. The FP consist of the buildings for which the proposed framework does not select the class even though it is the cost-minimal class and the FN consist of the buildings for which the proposed framework selects the class even though it is not the cost-minimal class. For the one loss function benchmark, the F_1 score corresponds to the percentage of buildings for which the loss function is cost-minimal. Additionally, since the F_1 is calculated on discrete class labels, the F_1 of the proposed framework with ensemble SVC is calculated using the class labels with the highest probabilities. As a result, it corresponds to the F_1 of the proposed framework with SVC. Second, to measure the forecast value of the forecast resulting from the selected forecast method, we calculate the forecast value of the selection task, i.e. the average daily total cost with imbalance cost factor either $\alpha = 2$ or $\alpha = 10$, averaged over the last year and all considered test buildings. Third, to measure the difference in average daily total cost averaged over last year between the proposed framework and the benchmarks for each building, we calculate the percentage difference

$$\%\mathrm{diff}_{\mathrm{benchmark}} = \frac{c^{\mathrm{benchmark}} - c^{\mathrm{framework}}}{c^{\mathrm{benchmark}}} \cdot 100. \tag{5.3}$$

A positive percentage difference indicates that the proposed framework achieves a lower average daily total cost compared to the benchmark. Fourth, we measure the computational effort by recording the average computation time of each component of the proposed framework and the benchmarks in seconds, and calculate based on this the average forecast method selection time in seconds. The latter consists of the time required to select the forecast method and to generate the forecast. The computational effort is calculated on Server 2 in Table 2.2.

5.2.2 Results

In this section, we evaluate the performance of the proposed framework. First, we compare the average daily total costs and the accuracy of the proposed framework with the two benchmarks. Then, we evaluate the impact of different classifiers on the performance of the forecast method selection, and, finally, we address the computational effort. Note that, we use the specification of the imbalance cost factor to distinguish between the results of the two forecast method selections.

Tab. 5.1.: The average daily total costs in € and the F_1 scores of the one loss function benchmark, the manually selected loss function benchmark, and the proposed framework for imbalance cost factor α of 2 and 10. The metrics are calculated for the testing data with the last year of data and for the buildings with IDs greater than or equal to 200. Note that for the average daily total costs lower values are better and for the F_1 scores higher values.

	$\alpha = 2$		$\alpha = 10$	
Approach	Total cost	F_1 score	Total cost	F_1 score
One loss function with				
Pinball 0.1	26.71	0.01	119.17	0.00
Pinball 0.25	22.01	0.06	84.61	0.03
MAE	19.70	0.26	57.63	0.18
MSE	20.85	0.14	56.25	0.15
Huber	20.87	0.13	56.42	0.14
Pinball 0.75	26.54	0.27	69.17	0.32
Pinball 0.9	54.36	0.13	158.18	0.18
Manually selected loss function	19.15	**0.76**	53.52	**0.74**
Proposed framework (ensemble SVC)	**18.95**	0.58	**53.10**	0.59

Benchmarking

For this evaluation, we compare the performance of the proposed framework and the two benchmarks in aggregate and in detail. For the aggregate comparison, we compare the average daily total costs averaged over the last year and the test buildings and the F_1 scores of our framework with the two benchmarks for imbalance cost factor α of 2 and 10. For the detailed comparison, we evaluate the percentage difference of the proposed framework and the two benchmarks for each building for imbalance cost factor α of 2 and 10.

Aggregate Comparison Table 5.1 shows the results of the aggregate comparison, which we describe below for each imbalance cost factor. Starting with imbalance cost factor $\alpha = 2$, we observe for the one loss function benchmark that the selected loss function has a noticeable impact on the average daily total cost and the accuracy. This benchmark achieves the lowest average daily cost (19.70) when MAE is used as loss function. However, similar average daily costs are obtained when using MSE (20.85) and Huber (20.87). The corresponding accuracy with MAE, MSE, and Huber is 0.26, 0.14, and 0.13 respectively. In contrast, pinball 0.75 results in an average daily cost of 26.54 despite being the cost-minimal forecast method for the most buildings (namely 27%). In comparison, the manually selected loss function benchmark has average daily total cost of 19.15 and an accuracy of 0.76. In contrast, the proposed framework with ensemble SVC reduces the average daily total cost of both the one loss function benchmark and the manually selected loss function

benchmark by at least 9.11% and by 1.04% respectively. However, the accuracy of the proposed framework with ensemble SVC is with 0.58 considerably lower than the accuracy of the manually selected loss function.
For imbalance cost factor $\alpha = 10$, the one loss function benchmark reaches its lowest average daily total cost (56.25) with MSE. Using Huber and MAE leads to similar average daily total costs of 56.42 and 57.63 respectively. The corresponding accuracy is 0.18 with MAE, 0.15 with MSE, and 0.14 with Huber. In contrast, pinball 0.9 leads to accuracy of 0.18 while resulting in average daily total cost of 158.18. The highest accuracy of 0.32 is achieved with pinball 0.75. In comparison, the manually selected loss function benchmark achieves an average daily total cost of 53.52 and an accuracy of 0.74. In contrast, the proposed framework with ensemble SVC, again, reduces the average daily total cost of both the one loss function benchmark and the manually selected loss function benchmark by at least 5.60% and by 0.78% respectively to 53.10. The accuracy of the proposed framework with ensemble SVC is with 0.59 again lower than the accuracy of the manually selected loss function benchmark.

Detailed Comparison Figure 5.3 shows the results of the detailed comparison, which we describe below for each benchmark. Note that for the one loss function benchmark, we consider the loss function that achieves the lowest average daily total cost, i.e. MAE for imbalance cost factor $\alpha = 2$ and MSE for imbalance cost factor $\alpha = 10$.
Compared to the one loss function benchmark, we observe for both imbalance cost factors that the percentage differences are positive for most buildings This positive skew is stronger for imbalance cost factor $\alpha = 10$.
Compared to the manually selected loss function benchmark, we observe a strong concentration of percentage differences around zero for both imbalance cost factors, with the majority of percentage differences falling within a range of 25% or 50%. However, there is a slight tendency towards positive percentage differences.

Impact of Classifier

To investigate the impact of the classifier, we compare the performance of the proposed framework with the seven classifiers. Based on the results for the imbalance cost factors α of 2 and 10 in Table 5.2, we present three observations.
First, starting with imbalance cost factor $\alpha = 2$, we observe that the proposed framework achieves the lowest average daily total cost of 18.95 with ensemble SVC. The second lowest average daily total cost of 19.43 is achieved with SVC, which is

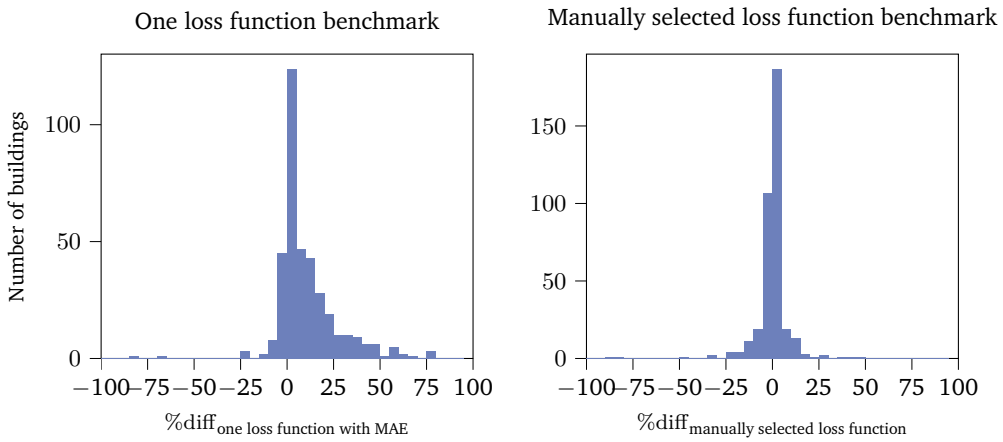

(a) $\alpha = 2$

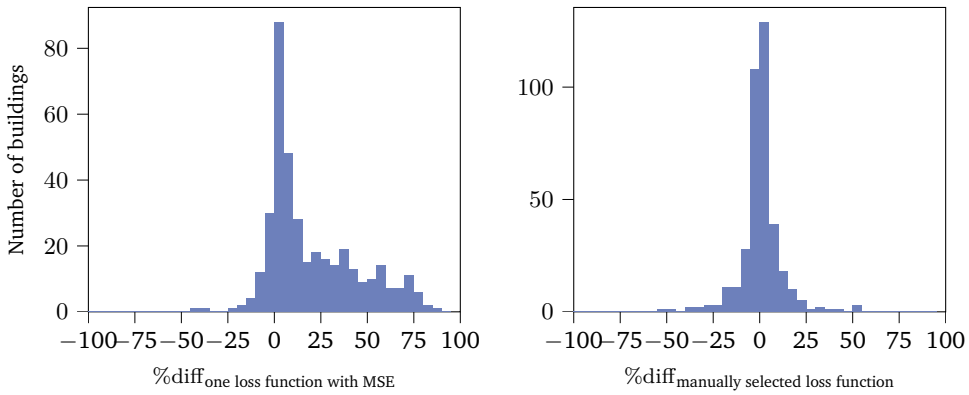

(b) $\alpha = 10$

Fig. 5.3.: The percentage differences in the average daily total cost with imbalance cost factor α of 2 (a) and 10 (b), are compared between the proposed framework with ensemble SVC and the two benchmarks: the one loss function benchmark with MAE (upper left), the one loss function benchmark with MSE (lower left) and the manually selected loss function benchmark (right), for each building. Note that positive percentage differences indicate that the proposed framework achieves a lower average daily total cost. Additionally, the plots show a range between -100 and 100.

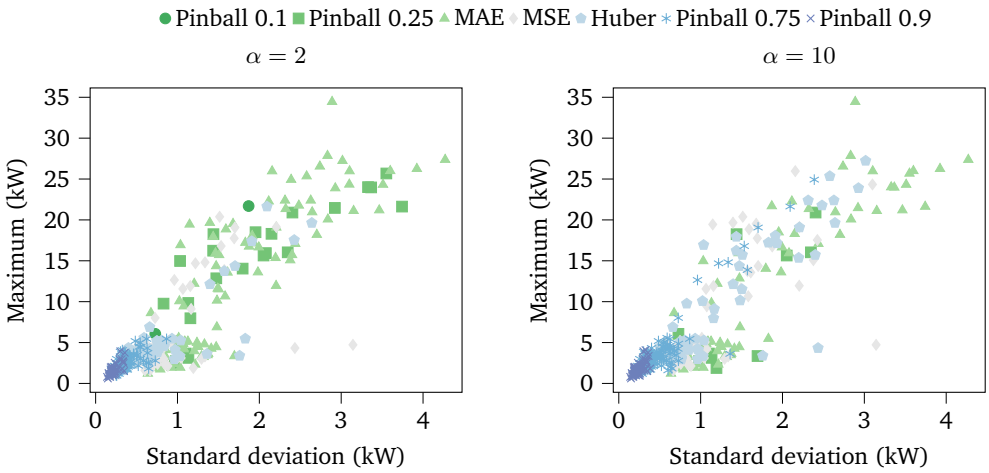

Fig. 5.4.: The standard deviation of the prosumption time series against the maximum of the prosumption time series with the colour indicating the loss function achieving the minimal average daily total cost with imbalance cost factor α of 2 (left) and the minimal average daily total cost with imbalance cost factor α of 10 (right) for each building.

2.47% higher than the lowest average daily total cost. The classifiers DT and kNN lead to average daily total cost of 19.45, and 19.50 respectively. With respect to the accuracy, the classifiers ensemble SVC, SVC, kNN, DT, and XGBoost have similar accuracies. In contrast, NB achieves the highest average daily total cost with 21.49 and the lowest accuracy with 0.38.

Second, for imbalance cost factor $\alpha = 10$, again, ensemble SVC achieves the lowest average daily total cost with 53.10, followed by SVC with 54.17 resulting in an increase of 1.98%. These classifiers achieve the highest accuracy with 0.59. The classifiers XGBoost, DT, and kNN follow with average daily total cost of 54.42, 54.52, and 54.64 respectively and accuracies of 0.56, 0.55, and 0.56 respectively. In consistency with the results for imbalance cost factor $\alpha = 2$, NB achieves the highest average daily total cost with 81.39 and the lowest accuracy with 0.41.

Finally, we provide a third observation based on Figure 5.4, which shows the values of the two most important input features for the tree-based classifiers, namely the standard deviation and the maximum of the prosumption time series, and the label of the target variable of the classification for imbalance cost factor $\alpha = 2$ and $\alpha = 10$ for each building. This figure shows that, while buildings with a high standard deviation and maximum do not show a clear relationship between input and target variables, a pattern emerges for buildings with a standard deviation below about 1 kW and a maximum below about 6 kW. More specifically, we observe that for standard deviations close to 1 kW, the target variables are primarily MAE, MSE, and Huber. As the standard deviation decreases further, the target variable for most

Tab. 5.2.: The average daily total costs in € and the F_1 scores of the proposed framework using different classifiers for imbalance cost factor α of 2 and 10. The metrics are calculated for the test data set with the last year of data and for the buildings with IDs greater than or equal to 200. Thereby, we calculate the mean over five runs with the values in the brackets being the minimum and maximum for the stochastic classifiers decision tree and multi-layer perceptron. Note that for the average daily total costs lower values are better and for the F_1 scores higher values.

	$\alpha = 2$		$\alpha = 10$	
Classifier	Total cost	F_1 score	Total cost	F_1 score
Ensemble SVC	**18.95**	0.58	**53.10**	**0.59**
SVC	19.43	0.58	54.17	**0.59**
kNN	19.50	**0.59**	54.64	0.56
DT	19.45 (19.44, 19.45)	**0.59** (0.58, 0.59)	54.52 (54.46, 54.57)	0.55 (0.54, 0.56)
XGBoost	19.60	**0.59**	54.42	0.56
MLP	19.74 (19.62, 19.82)	0.55 (0.54, 0.56)	56.67 (55.69, 59.50)	0.53 (0.51, 0.54)
NB	21.49	0.38	81.39	0.41

buildings first shifts to pinball 0.75, and at the smallest standard deviations, it is mostly pinball 0.9.

Computational Effort

To evaluate the computational effort, we first measure the computation time of each component of the proposed framework and the considered benchmarks. Afterwards, we calculate the forecast method selection time of the proposed framework and the benchmarks to select the forecast method for a new building.

For each component, Table 5.3a provides the average computation time in seconds per building. By far the most time-intensive component is the OP's run time on the second year of data, followed by the NN's training time. The other components require a negligible amount of time.

Based on the measured times of the components, we can estimate the forecast method selection time of the proposed framework and the two benchmarks for a new building. For the one loss function benchmark, the NN with the considered loss function must be trained on the first two years of the new building's data and the forecast must be generated. For the manually selected loss function benchmark, we need to train NNs for each loss function, generate forecasts with the trained NNs and solve the optimisation problem with the resulting forecasts for the second year. For the proposed framework, we must first extract the metadata based on the first two years, then run the classifier. For SVC, which outputs one forecast method, the NN with the selected loss function must be trained once. For ensemble SVC, we need to train NNs for each loss function, generate the forecasts, and then generate

Tab. 5.3.: The average computation time in seconds of each component and the average forecast method selection time in seconds of the one loss function benchmark, the manually selected loss function benchmark, the proposed framework with ensemble SVC, and the proposed framework with SVC for a new building. Note that the times do not depend on the considered imbalance cost factor and are measured on Server 2 in Table 2.2.

(a) Average computation time of the components

Component	Computation time
Classifier inference time	
Ensemble SVC	0.023
SVC	0.023
kNN	0.045
DT	0.001
XGBoost	0.003
MLP	0.004
NB	0.001
Metadata generation time	0.004
Ensemble generation time	0.028
Forecasting NN training time	0.431
Forecasting NN inference time	0.003
Optimisation problem run time	382.741

(b) Average forecast method selection time of the proposed framework and the considered benchmarks for a new building.

Approach	Forecast method selection time
One loss function	**0.434**
Manually selected loss function	2682.225
Proposed framework (ensemble SVC)	3.070
Proposed framework (SVC)	0.438

the ensemble forecast. Table 5.3b shows the resulting forecast method selection times. In this table, we make two observations. First, the manually selected loss function benchmark has, noticeably, the highest forecast method selection time with 2682.225 seconds. The one loss function benchmark and our proposed framework require notably less time. Second, we observe that despite using a meta-learning approach the forecast method selection time of the proposed framework with SVC is only slightly higher than that of the one loss function benchmark. The proposed framework with ensemble SVC has a higher forecast method selection time due to the training of the NNs for each loss function and the generation of the ensemble forecast.

5.3 Discussion

This section discusses the findings of the evaluation, the limitations and further research.

5.3.1 Findings

We discuss the findings with respect to five aspects. First, the results show that the classifier ensemble SVC clearly achieves the lowest average daily total costs over all considered classifiers, followed by the classifiers SVC, kNN, DT, and XGBoost, which achieve similar average daily total costs. In contrast, for this downstream application, the use of the MLP and the NB classifiers is not recommended. A possible explanation for the superior performance of the classifier ensemble SVC could be that the resulting ensemble forecast can exploit the strengths of each forecast with different characteristics, which is particularly advantageous given the limited number of loss functions considered. Consequently, the ensemble SVC may compensate for this limitation by generating a forecast with characteristics that are not fully captured by the individual loss functions [16].
Second, the results indicate that the proposed framework reduces the average daily total costs and improves the accuracy compared to the one loss function benchmark. Furthermore, the performance of the proposed framework with respect to the average daily total costs is comparable to the performance of the manually selected loss function benchmark. However, there is still potential for further improvement of our framework, especially with respect to the accuracy. For example, more advanced classification methods could be applied.
Third, we observe a non-monotonic, non-linear relation between the average daily total costs and the accuracy. More precisely, improving the accuracy does not necessarily lead to lower average daily total cost. For the one loss function benchmark, this means that the cost-minimal loss function for most buildings is not necessarily the cost-minimal loss function for the whole data set. This observation can be explained by largely high average daily total costs for the remaining buildings, and highlights the complexity of selecting the loss function with respect to the forecast value in the downstream application.
Fourth, the results show that the proposed framework reduces the computational effort compared to the manually selected loss function benchmark by 99%. That makes the proposed framework particularly interesting for downstream applications for which scalability is essential. For example, in the considered application of the

DF scalability and low computational effort could be important when multiple buildings are involved. Additionally, in contrast to the manually selected loss function benchmark, the computational effort of the proposed framework increases negligibly when the set of forecasting methods is expanded to include different forecasting methods. Finally, regarding the research question

RQ3: *How to automatically select the forecast method with respect to the forecast value with low computational effort using meta-learning?*

we can say that interpreting this selection task as a classification problem using a building's metadata as input results in a lower average daily total cost compared to using the same loss function for each building, and a lower computational effort compared to a manual selection. In particular, using the classifier to predict probabilities for each considered forecast method and generating an ensemble forecast based on these probabilities is more beneficial with respect to the average daily costs than using the classifier to select the forecast method with the highest forecasted probability.

5.3.2 Limitations and Further Research

With regard to the limitations of the proposed framework, we discuss three aspects. First, despite the encouraging results, it should be noted that the proposed framework has been evaluated on one downstream application only and that it adds a small computational effort to the forecasting task itself. However, the additional computational effort is small compared to the overall forecast method selection time.
Second, the proposed framework uses two years of historical data to generate the metadata input features. Further evaluation needs to consider whether using less data still leads to promising results. A first analysis shows a comparable performance when using one year of metadata.
Third, the proposed framework selects the forecast method once for each building. Further research could extend the framework to an online setting that continually re-classifies each building based on current information. This extension is especially motivated by the results of the manually selected loss function benchmark, which only achieves an accuracy of 0.76 or 0.74, suggesting that the forecast value of a forecast method may change over time. However, a first analysis of a daily re-classification shows no improvement in performance. A possible explanation is that we did not include weather forecasts as input features, which could influence the forecast quality in addition to the usage of different loss functions [50]. The

classifier could be learning the effect of missing weather forecasts rather than focusing on the effect of different loss functions. While this may average out in a one-time classification, it could persist in a daily re-classification. Therefore, we recommend considering weather forecasts as input features for the forecast methods when approaching a continuous re-classification.

Part III

Evaluations and Extensions for Dispatchable Feeder Considering Probabilistic Forecasts

6 Probabilistic Forecast Evaluation

This chapter evaluates probabilistic forecasts with respect to the forecast value for the two-level dispatchable feeder (DF) considering probabilistic forecasts. For this evaluation, different probabilistic forecasts with different characteristics are considered. More precisely, we modify the probabilistic forecasts to have a different dispersion or a different location, thus a bias. For these different forecasts, we analyse the relation between the considered forecast value and the considered forecast quality. Additionally, we evaluate the forecast value for the different forecasts depending on problem-specific parameters. Therefore, the addressed research question is:

RQ2: *How do different probabilistic forecast characteristics influence the forecast value for the dispatchable feeder, and how does this influence depend on problem-specific parameters?*

The structure of this chapter is as follows. First, Section 6.1 describes the approach, how forecasts with different characteristics are obtained, and how the probabilistic forecasts are generated. Second, Subsection 6.2.1 outlines the experimental setup. Then, Subsection 6.2.2 presents the results of the evaluation. Finally, Section 6.3 discusses the findings.

6.1 Approach

The evaluation conducted in this chapter is inspired by the concept of post-processing probabilistic forecasts via recalibration, as discussed in the literature, e.g. [84]. The idea of such a recalibration is to adjust probabilistic forecasts, which may suffer from biases [110] and inaccuracies depending on the forecast specifications, so that the forecasted probabilities align with the true outcomes. While such recalibration focuses on the forecast quality, our idea is to adjust the probabilistic forecasts with respect to the forecast value. Before we can proceed with such a value-oriented recalibration, we take a step back and start by evaluating the impact of different

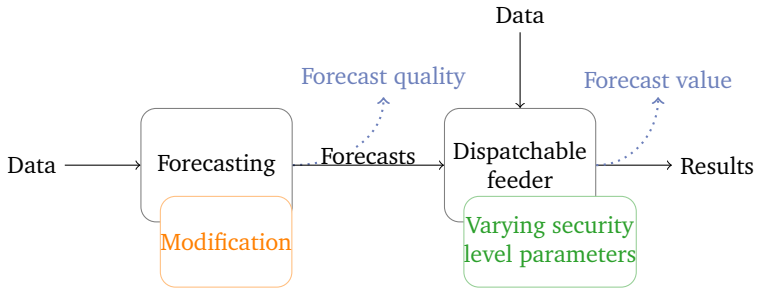

(a) The framework to evaluate probabilistic forecasts with different characteristics with respect to the forecast quality and the forecast value (marked in blue) for the two-level dispatchable feeder considering probabilistic forecasts. The probabilistic forecasts with different characteristics are generated via a nested neural network and modified to have different dispersions or biases (marked in orange). Additionally, varying problem-specific parameters, namely the security level parameters for the reformulated power and energy chance constraint, are considered (marked in green).

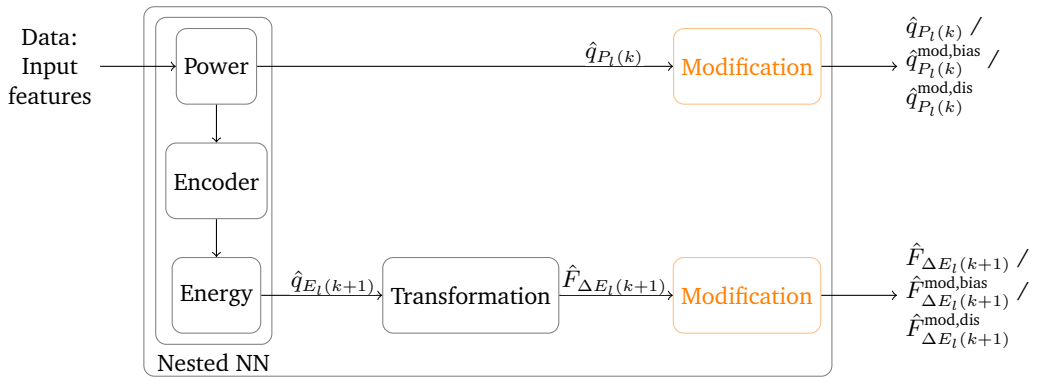

(b) The specification of the forecasting. The probabilistic forecasts are generated via a nested neural network. The resulting quantile energy forecasts $\hat{q}_{E_l(k+1)}$ are further transformed to obtain the required CDF forecasts $\hat{F}_{\Delta E_l(k+1)}$. Finally, the power or energy forecasts are modified to have different dispersions or biases (marked in orange).

Fig. 6.1.: The framework to evaluate probabilistic forecasts with different characteristics for the two-level dispatchable feeder considering probabilistic forecasts (a) and the specification of the forecasting to generate probabilistic forecasts with different characteristics (b).

probabilistic forecasts for the prosumption power quantiles $q_{P_l(k)}$ and the cumulative distribution function (CDF) of the deviation from the mean of the prosumption energy $F_{\Delta E_l(k+1)}$, which are used for the reformulated power and energy chance constraints in the computation of the dispatch schedule (DS). The evaluation of these forecasts focuses on the influence of different forecast characteristics on the forecast value for the two-level DF considering probabilistic forecasts as illustrated in Figure 6.1a. This evaluation follows the same steps as outlined in Section 4.1. More precisely, it involves generating the probabilistic forecasts, computing the day-ahead DS via the first-level optimisation problem (OP) based on these forecasts,

determining the actual dispatch by minimising the deviations from the DS in the second-level OP based on the actual prosumption values, and measuring the forecast value of the probabilistic forecasts.

To generate these probabilistic forecasts, we use in alignment with Chapter 4 a neural network (NN), see Figure 6.1b. More precisely, we use a nested NN that generates 99 quantile forecasts of $q_{P_l(k)}(p)$ and $q_{E_l(k+1)}(p)$ for $p = 0.01, ..., 0.99$ using the pinball loss in Equation (2.11) with τ values of $0.01, ...0.99$ as loss function. The nested NN operates in three stages: the first NN forecasts the power quantile forecasts of $q_{P_l(k)}(p)$ based on the input features. The second NN acts as an encoder of the power quantile forecasts. Finally, the third NN forecasts the energy quantiles of $q_{E_l(k+1)}(p)$ based on the encoded power quantile forecasts. The quantile forecasts of $q_{E_l(k+1)}(p)$ are then transformed to obtain the input of the DF, i.e. the CDF forecasts of $F_{\Delta E_l(k+1)}$, which is further described in Subsection 6.1.1. To obtain forecasts with different characteristics, we take a different approach compared to the evaluation of point forecasts in Chapter 4. While the different characteristics for the point forecasts are achieved by using different loss functions within the NN, we modify the probabilistic forecasts generated with the pinball loss[1]. The modification is such that the forecasted distribution has either a bias or a different degree of variability in the forecasted values, often referred to as dispersion[2]. While the motivation for different biases comes from the results presented in Chapter 4, the motivation for different dispersions is that it is an important characteristic influencing the performance of the DF considering probabilistic forecasts. More precisely, unlike the DF considering point forecasts, the DF considering probabilistic forecasts holds BESS reserves for the power and energy uncertainty of the prosumption via the reformulated power and energy chance constraints

$$\begin{aligned} p_{g_{DS}}(k) - p_s^{\max} &\leq \hat{q}_{P_l(k)}(0.5 - 0.5 \cdot (1 - \epsilon_P)) \\ p_{g_{DS}}(k) - p_s^{\min} &\geq \hat{q}_{P_l(k)}(0.5 + 0.5 \cdot (1 - \epsilon_P)) \end{aligned} \tag{6.1}$$

$$\begin{aligned} 1 - \epsilon_E - \epsilon_{\text{fix}}(k) - \epsilon_{\text{var}}(k) \leq \hat{F}_{\Delta E_l(k+1)} \left(\bar{e}_s(k+1) - e_s^{\min}\right) \\ - \hat{F}_{\Delta E_l(k+1)} \left(\bar{e}_s(k+1) - e_s^{\max}\right) \end{aligned} \tag{6.2}$$

in Equation (2.24). The extent of these reserves is thereby determined by the dispersion of the forecasts $\hat{q}_{P_l(k)}$ and $\hat{F}_{\Delta E_l(k+1)}$, the security level parameters ϵ_P and ϵ_E, and the BESS power and energy capacities $p_s^{\min}$, $p_s^{\max}$, $e_s^{\min}$, and $e_s^{\max}$. The importance of the dispersion is further underlined by the fact that both the forecast

[1] The modification of the generated probabilistic forecasts eliminates the need to generate new ones and thus reduces the computational effort.

[2] We use the term dispersion instead of sharpness to specifically refer to changes in the variability of the forecasted values, whereas sharpness typically describes the concentration around the centre-oriented forecast.

method[3] and its hyperparameters can influence the dispersion of the resulting probabilistic forecasts [96].
The modified probabilistic forecasts are used for the computation of the DS. Equally to Chapter 4, we use the unmodified median forecasts for the estimation of the SoE at 12 AM.
Additionally, we evaluate the performance of the DF considering probabilistic forecast by assessing the impact of further problem-specific parameters that may affect this performance. In addition to the technical parameters for the two-level DF considering point forecasts, the two-level DF considering probabilistic forecasts has operational parameters, namely the security level parameters ϵ_P and ϵ_E for the reformulated power and energy chance constraints described above. Therefore, in contrast to the problem-specific parameters of the prosumption data and the BESS energy capacity considered in Chapter 4, we evaluate the performance of the DF considering probabilistic forecasts based on the forecast value depending on the problem-specific parameters of the security level parameters ϵ_P and ϵ_E.
In this context, it is important to mention an effect that can occur in the computation of the DS depending on the security level parameter ϵ_P, the power forecasts, and the BESS capacities. Unlike the security level for the reformulated energy chance constraint, the security level for the reformulated power chance constraint can not be relaxed. As a consequence, the OP for the computation of the DS may be infeasible. A simple possible scenario where the OP is infeasible is when $p_s^{\max} - p_s^{\min} < q_{P_l(k)}(0.5 + 0.5 \cdot (1 - \epsilon_P)) - q_{P_l(k)}(0.5 - 0.5 \cdot (1 - \epsilon_P))$ for any k. In this scenario, the reformulated power chance constraint can not be satisfied for the security level $1 - \epsilon_P$. This effect is especially relevant for modified power forecasts with large dispersion. While this infeasibility is interesting but not critical for the evaluation performed in this chapter, it may be critical for a real-world implementation. To mitigate the infeasibility, the security level of the power chance constraint could be reduced, i.e. a higher security level parameter ϵ_P could be used, or a relaxation similar to the relaxation for the reformulated energy chance constraint could be included in the mathematical formulation for the computation of the DS. However, in this evaluation, we limit the consideration of this effect by reporting on the infeasible cases.
With these specifications, we aim to analyse whether the relationship between forecast quality and forecast value is monotone. Additionally, we seek to explore how the security level parameters and the characteristics of the probabilistic forecasts interact and influence the forecast value.

[3] We would like to highlight that probabilistic forecasts generated using NNs can have greater dispersion compared to those generated by other forecast methods due to the emphasis on good calibration [48].

In the following, we further describe how we transform the quantile forecasts $\hat{q}_{E_l(k+1)}$ to obtain the required CDF forecasts $\hat{F}_{\Delta E_l(k+1)}$ in Subsection 6.1.1 and how modify the probabilistic forecasts in Subsection 6.1.2.

6.1.1 Transformation of Energy Quantile Forecasts

The following describes the transformation of the energy quantile forecasts $\hat{q}_{E_l(k+1)}$ into the input for the DF using probabilistic forecasts, namely the CDF forecasts $\hat{F}_{\Delta E_l(k+1)}$. This transformation consists of two steps. First, the median forecast $\hat{q}_{E_l(k+1)}(0.5)$ is subtracted from all quantile forecasts to obtain the quantile forecasts $\hat{q}_{\Delta E_l(k+1)}$. Second, the quantile forecasts $\hat{q}_{\Delta E_l(k+1)}$ are transformed to obtain the CDF forecasts $\hat{F}_{\Delta E_l(k+1)}$. Since this CDF has to meet the requirements of Pyomo, it has to be described in closed form, as the piecewise implementation from Pyomo's piecewise function library does not give the expected results. Using a closed form turns the non-parametric quantile forecasts into a parametric CDF forecast. Therefore, the choice of the closed form affects the performance of the DF and thus the forecast value. In order to make a reasonable choice of this transformation, we evaluate different transformation approaches with respect to the forecast value for the two-level DF using probabilistic forecasts in a preliminary analysis. Therefore, we first describe the considered transformation approaches, and then present the results. Finally, we summarise the preliminary analysis.

Transformation Approaches

Following [8], we compare three transformation approaches, all based on the basic idea of using general logistic functions as closed form.
The first approach **one log** fits the quantile forecasts via least squares to a general logistic function, i.e.

$$\hat{F}_{\Delta E_l(k+1)}(q) = \frac{w_0}{1 + \exp(-w_1(q - w_2))}$$

with weights $w_0, w_1, w_2 \in \mathbb{R}$. This general logistic function is symmetric around w_2 and equivalent to a logistic distribution with mean w_2 and scale $\frac{1}{w_1}$. Consequently, the weights are mostly pre-defined with

$$\begin{aligned} w_0 &= 1 \\ w_1 &> 0 \\ w_2 &= \hat{q}_{\Delta E_l(k+1)}(0.5). \end{aligned}$$

In the second approach **two log**, two fittings via least squares are performed, namely to one general logistic function as in the one log approach and to the sum of two general logistic functions, i.e.

$$\hat{F}_{\Delta E_l(k+1)}(q) = \frac{w_0}{1+\exp(-w_1(q-w_2))} + \frac{w_3}{1+\exp(-w_4(q-w_5))}$$

with weights $w_0, w_1, w_2, w_3, w_4, w_5 \in \mathbb{R}$. The two log approach then selects the logistic function with the smallest MSE if the solver finds solutions for both least square fittings within the predefined error bounds. In contrast to one general logistic function, the sum of two general logistic functions does not have to be symmetric and can account for skewness. The weights are mostly free with

$$w_0 + w_3 = 1.$$

However, unlike the one log approach, additional constraints must be added to guarantee the properties of a CDF, namely that it is monotonically increasing, that it only takes values in $[0, 1]$, and that it has the limits

$$\lim_{q\to-\infty} \hat{F}_{\Delta E_l(k+1)}(q) = 0$$
$$\lim_{q\to\infty} \hat{F}_{\Delta E_l(k+1)}(q) = 1.$$

For the monotony, we add the constraints

$$\hat{F}'_{\Delta E_l(k+1)}(q) = \frac{w_0 \cdot w_1 \cdot \exp(-w_1 \cdot (q-w_2))}{(1+\exp(-w_1 \cdot (q-w_2)))^2} + \frac{w_3 \cdot w_4 \cdot \exp(-w_4 \cdot (q-w_5))}{(1+\exp(-w_4 \cdot (q-w_5)))^2} \geq 0$$

for $q \in \{-50, -49, ..., 49, 50\}$. Additionally, to achieve values large than or equal to zero, we add the constraints

$$\hat{F}_{\Delta E_l(k+1)}(q) = \frac{w_0}{1+\exp(-w_1(q-w_2))} + \frac{w_3}{1+\exp(-w_4(q-w_5))} \geq 0$$

for $q \in \{-50, -49, ..., 49, 50\}$. Regarding the limits, it is not straightforward to state constraints. Therefore, we adjust the least squares fitting by adding the tuples

$$(\hat{q}_{\Delta E_l(k+1)}(0.01) - i \cdot (\hat{q}_{\Delta E_l(k+1)}(0.1) - \hat{q}_{\Delta E_l(k+1)}(0.09)), 0) \text{ for } i = 1, ..., 50$$
$$(\hat{q}_{\Delta E_l(k+1)}(0.99) + i \cdot (\hat{q}_{\Delta E_l(k+1)}(0.1) - \hat{q}_{\Delta E_l(k+1)}(0.09)), 1) \text{ for } i = 1, ..., 50$$

to the data, see Figure 6.2. Additionally, as the used implementation of the ex-

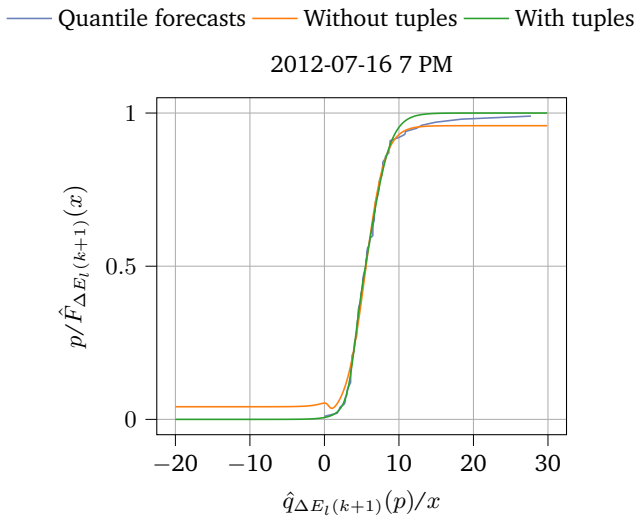

Fig. 6.2.: The quantile forecasts $\hat{q}_{E_l(k+1)}$ and the transformed CDF forecast $\hat{F}_{\Delta E_l(k+1)}$ via the two log without adding tuples and with adding tuples to achieve the limits of a CDF exemplarily for building 110 These forecasts are for 2012-07-16 at 7 PM and are generated on 2012-07-15 at 12 PM.

ponential function gets overflow issues for values bigger than 700, we add the constraints

$$
\begin{aligned}
-w_1 \cdot (\max_p \hat{q}_{\Delta E_l(k+1)}(p) - w_2) &\leq 700 \\
-w_1 \cdot (\min_p \hat{q}_{\Delta E_l(k+1)}(p) - w_2) &\leq 700 \\
-w_4 \cdot (\max_p \hat{q}_{\Delta E_l(k+1)}(p) - w_5) &\leq 700 \\
-w_4 \cdot (\min_p \hat{q}_{\Delta E_l(k+1)}(p) - w_5) &\leq 700.
\end{aligned}
$$

All these constraints can not formally guarantee the characteristics of the CDF. However, to be able to guarantee the characteristics of the CDF, conservative constraints would have to be added, which may restrict a proper fitting.
The third approach **weighted two log** is similar to the two log approach, but with a weighted least squares fitting for the fitting of the sum of two logistic functions. That is, the objective function is

$$
\sum_{i=1,\ldots,99} p_i \cdot (\hat{F}_{\Delta E_l(k+1)}(p_i) - \hat{q}_{E_l(k+1)}(p_i))^2
$$

for $p = (p_1, \ldots, p_{99}) = (0.01, \ldots, 0.99)$. The motivation for this weighting is the observation of a positive skewness of $\Delta E_l(k+1)$ in the quantile forecasts. The weights p_i emphasize the right tail, enabling the fitting to better capture the skewness.

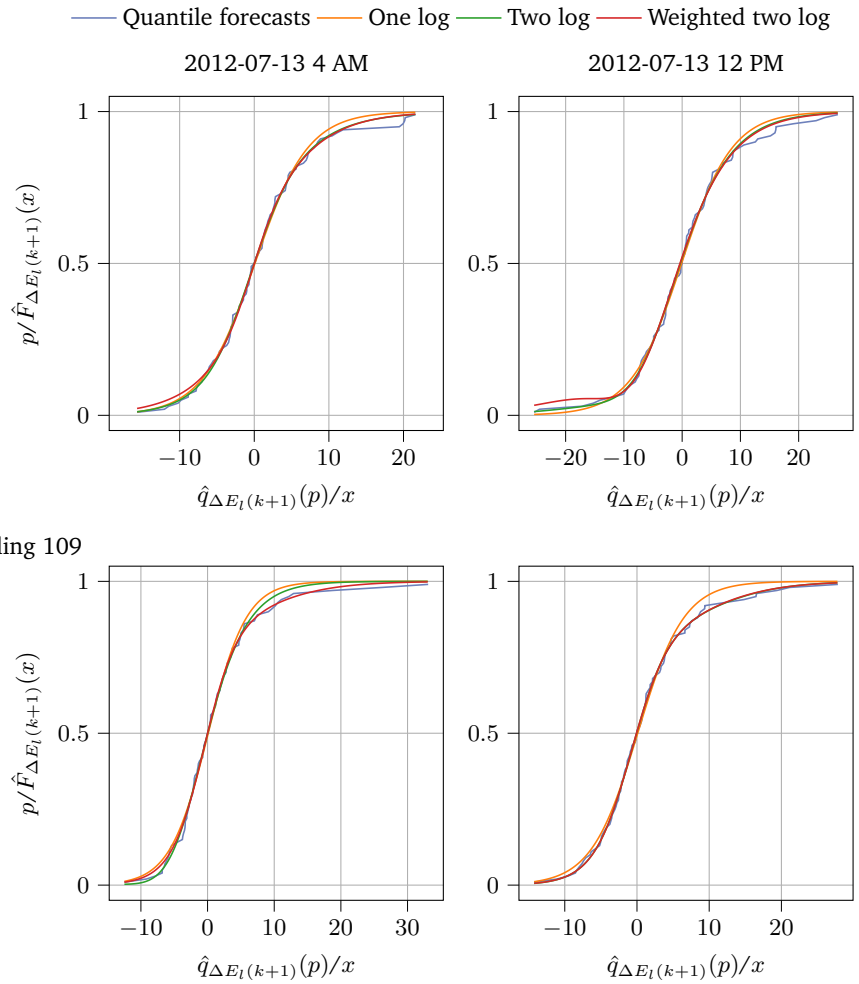

(a) Building 109

(b) Building 110

Fig. 6.3.: The quantile forecasts $\hat{q}_{E_l(k+1)}$ and the transformed CDF forecast $\hat{F}_{\Delta E_l(k+1)}$ via the one log, two log, and weighted two log approach for buildings 109 and 110. These forecasts are for 2012-07-13 at 4 AM (left) and 2012-07-12 at 12 PM (right) and are generated on 2012-07-12 at 12 PM.

Tab. 6.1.: The average time per transformation in seconds and the average daily costs in € for security level parameters $\epsilon_P = 0.1$ and $\epsilon_E = 0.3$ over the test data and buildings 109 and 110. Note that the average time per transformation is measured on Server 2 in Table 2.2.

Building		One log	Two log	Weighted two log
109	DS cost	**4.70**	4.71	4.71
	Imbalance cost	0.78	0.78	**0.77**
	Total cost $\alpha = 2$	**6.25**	6.26	**6.25**
	Total cost $\alpha = 10$	12.45	12.47	**12.39**
	Time	**0.07**	0.41	0.39
110	DS cost	**0.92**	0.94	0.94
	Imbalance cost	0.69	0.67	**0.66**
	Total cost $\alpha = 2$	2.29	2.27	**2.26**
	Total cost $\alpha = 10$	7.78	7.60	**7.54**
	Time	**0.07**	0.47	0.46

Results

In the following, we quantitatively compare the different transformation approaches described above with respect to the forecast value, i.e. the four average daily costs described in Subsection 4.2.1, and the average time per transformation exemplarily for the buildings 109 and 110. Additionally, we qualitatively compare the transformation approaches visually, exemplarily for two hours of buildings 109 and 110.
Starting with the quantitative comparison, Table 6.1 shows the average time per transformation and the average daily costs averaged over the last year for security level parameters $\epsilon_P = 0.1$ and $\epsilon_E = 0.3$. For both buildings we observe that almost all average daily costs are lowest with the weighted two log approach. However, the differences in the average daily costs are small. In contrast, the average time per transformation varies with the average time of the two log approach and the weighted two log approach being more than 5.5 times higher than the average time of the one log approach.
For the qualitative comparison, Figure 6.3 shows two hours of quantile forecasts $\hat{q}_{\Delta E_l(k+1)}$ generated at 12 PM on 2012-07-12 and the transformed CDF forecasts $\hat{F}_{\Delta E_l(k+1)}$ for the considered approaches of building 109 and 110 respectively. For building 109, we observe that the transformed CDFs of all considered approaches are almost equal. In contrast, for building 110, we observe differences in the transformed CDFs at the right tail. More specifically, for 4 AM, the weighted two log approach matches the quantile forecasts better than the one log and two log approaches, while for 12 PM, both the two log and the weighted two log approach match the quantile forecasts better than the one log approach.

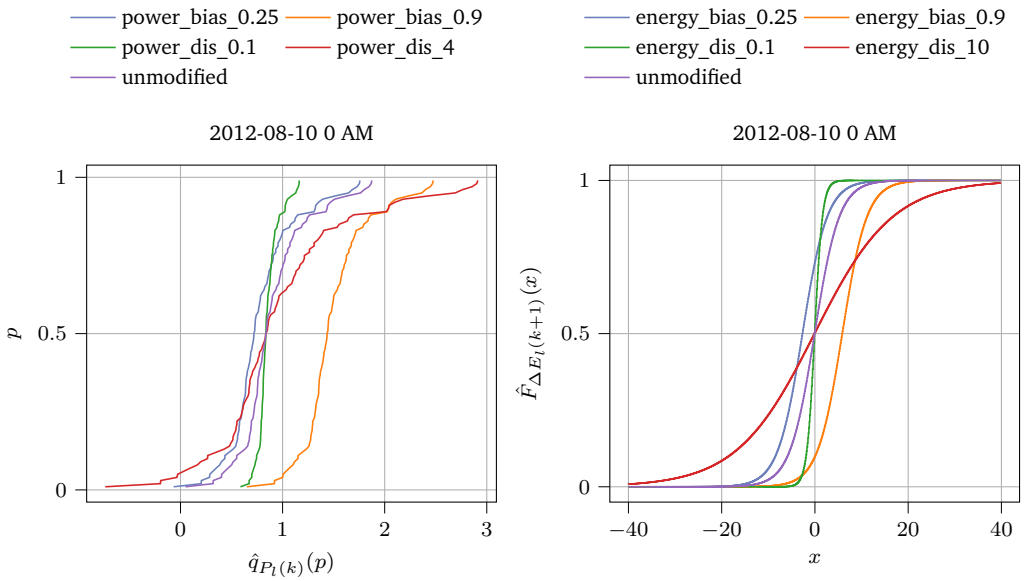

Fig. 6.4.: The probabilistic power forecasts $\hat{q}_{P_l(k)}$ (left) and energy forecasts $\hat{F}_{\Delta E_l(k+1)}$ (right) with different characteristics, generated with different biases and different dispersions, for building 109 and the exemplary hour 2012-08-10 0 AM.

Summary

The preliminary analysis shows that while the weighted two log approach results in the lowest average daily costs, the difference for the considered transformation approaches is small. This is true for both buildings, although the quantile forecasts for building 109 appear to follow the logistic distribution and the quantile forecasts for building 110 may be positively skewed. Furthermore, the average time per transformation is at least 5.5 times higher for the two log and the weighted two log approach than for the one log approach. The reason for this difference is that two transformations are performed for the two log and the weighted two log approach. As the subsequent evaluation of the probabilistic forecasts with respect to the average daily costs is carried out on 286 buildings with different problem-specific parameters, the two log and weighted two log approach would require an immense amount of computational effort and can be expected to improve the average daily costs only slightly. We therefore use the one log approach in the following evaluation.

6.1.2 Modification of Probabilistic Forecasts

In the following, we further describe the two types of modification, namely the modification for a bias and the modification of dispersion, and how we obtain the

corresponding probabilistic forecasts, see Figure 6.4. Note that we only modify either the forecasts $\hat{q}_{P_l(k)}$ or the forecasts $\hat{F}_{\Delta E_l(k+1)}$ in order to evaluate the impact of the modification on each forecast separately[4]. For simplicity, we refer to the forecasts $\hat{q}_{P_l(k)}$ as power forecasts and to the forecasts $\hat{F}_{\Delta E_l(k+1)}$ as energy forecasts[5]. Starting with the modification for a bias, we use

$$\hat{q}^{\text{mod,bias}}_{P_l(k)}(p) = \hat{q}_{P_l(k)}(p) + d^{\text{bias},P_l} \tag{6.3}$$

$$\hat{F}^{\text{mod,bias}}_{\Delta E_l(k+1)}(x) = \hat{F}_{\Delta E_l(k+1)}(x - d^{\text{bias},\Delta E_l}) \tag{6.4}$$

with $d^{\text{bias},P_l}, d^{\text{bias},\Delta E_l} \in \mathbb{R}$. These modifications[6] can be understood as modifying a random variable Z via

$$Z^{\text{mod,bias}} = Z + d^{\text{bias}} \tag{6.5}$$

resulting in

$$\mathbb{E}[Z^{\text{mod,bias}}] = \mathbb{E}[Z] + d^{\text{bias}} \tag{6.6}$$

$$\text{Var}[Z^{\text{mod,bias}}] = \text{Var}[Z] \tag{6.7}$$

with $d^{\text{bias}} = 0$ resulting in the unmodified random variable. To obtain modifications, which are comparable to Chapter 4, we set

$$d^{\text{bias},P_l} = \hat{q}_{P_l(k)}(\tau) - \hat{q}_{P_l(k)}(0.5) \tag{6.8}$$

$$d^{\text{bias},\Delta E_l} = \hat{q}_{\Delta E_l(k+1)}(\tau) \tag{6.9}$$

for $\tau \in (0, 1)$. In this way, the location of the power or energy[7] forecasts is shifted towards lower values, if τ is smaller than 0.5, similar to an underestimation in Section 4.1. If τ is greater than 0.5, the location of the power or energy forecasts is shifted towards higher values, similar to an overestimation in Section 4.1. Specifically, we consider the following modifications for a bias: **power_bias_0.1**, **power_bias_0.25**, **power_bias_0.75**, **power_bias_0.9** for the modification of the power forecasts in Equation (6.8) with τ of 0.1, 0.25, 0.75, and 0.9 respectively, and **energy_bias_0.1**, **energy_bias_0.25**, **energy_bias_0.75**, **energy_bias_0.9** for the modification of the energy forecasts in Equation (6.9) with τ of 0.1, 0.25, 0.75, and

[4] In this way we neglect the physical relation between the two forecasts.

[5] Note that while $E_l(k+1)$ is actually the prosumption energy, $\Delta E_l(k+1)$ is the deviation from the mean of $E_l(k+1)$.

[6] Note that d^{bias} corresponds to d^{bias,P_l} when modifying the power forecasts and to $d^{\text{bias},\Delta E_l}$ when modifying the energy forecasts.

[7] Note that $\Delta E_l(k+1)$, as the deviation from the mean, is a random variable with a mean of zero. Consequently, modifying for a bias of the energy forecasts $\hat{F}_{\Delta E_l(k+1)}$ effectively introduces an anticipated systematic offset.

0.9 respectively.
For the modification for a different dispersion, we consider

$$\hat{q}^{\text{mod,dis}}_{P_l(k)}(p) = \sqrt{d^{\text{dis},P_l}} \cdot \hat{q}_{P_l(k)}(p) + (1 - \sqrt{d^{\text{dis},P_l}}) \cdot \hat{q}_{P_l(k)}(0.5) \tag{6.10}$$

$$\hat{F}^{\text{mod,dis}}_{\Delta E_l(k+1)}(x) = \hat{F}_{\Delta E_l(k+1)}(\frac{x}{\sqrt{d^{\text{dis},\Delta E_l}}}) \tag{6.11}$$

with $d^{\text{dis},P_l}, d^{\text{dis},\Delta E_l} \in \mathbb{R}^+$. These modifications[8] can be understood as modifying a random variable Z via

$$Z^{\text{mod,dis}} = \sqrt{d^{\text{dis}}} \cdot Z + (1 - \sqrt{d^{\text{dis}}}) \cdot q_Z(0.5). \tag{6.12}$$

The modified random variable $Z^{\text{mod,dis}}$ has then the following mean and variance:

$$\mathbb{E}[Z^{\text{mod,dis}}] = \sqrt{d^{\text{dis}}} \cdot \mathbb{E}[Z] + (1 - \sqrt{d^{\text{dis}}}) \cdot q_Z(0.5) \tag{6.13}$$

$$\text{Var}[Z^{\text{mod,dis}}] = d^{\text{dis}} \cdot \text{Var}[Z] \tag{6.14}$$

with $d^{\text{dis}} = 1$ resulting in the unmodified random variable. In cases where the median[9] $q_Z(0.5)$ is close to the mean $\mathbb{E}[Z]$, it holds

$$\mathbb{E}[Z^{\text{mod,dis}}] \approx \mathbb{E}[Z]. \tag{6.15}$$

Specifically, we consider the following modifications of dispersion: **power_dis_0.1**, **power_dis_2**, **power_dis_4** for the modification of the power forecasts in Equation (6.10) with d^{dis,P_l} of 0.1, 2, 4 respectively, and **energy_dis_0.1**, **energy_dis_2**, **energy_dis_4**, **energy_dis_10**, **energy_dis_20** for the modification of the energy forecasts in Equation (6.11) with $d^{\text{dis},\Delta E_l}$ of 0.1, 2, 4, 10, 20 respectively.

6.2 Evaluation

In this section, we evaluate the different probabilistic forecasts with respect to the forecast value for the two-level DF considering probabilistic forecasts described in Subsection 2.4.1. Therefore, Subsection 6.2.1 describes the experimental setup and Subsection 6.2.2 presents the results of the evaluation.

[8] Note that d^{dis} corresponds to d^{dis,P_l} when modifying the power forecasts and to $d^{\text{dis},\Delta E_l}$ when modifying the energy forecasts.

[9] Note that instead of the median $q_Z(0.5)$, the mean $\mathbb{E}[Z]$ could be used. Then it holds $\mathbb{E}[Z^{\text{mod,dis}}] = \mathbb{E}[Z]$. However, since we generate the median forecast, we use the median instead of the mean.

Tab. 6.2.: The general and detailed neural network architectures to generate the probabilistic forecasts. Note that the forecast horizon is 42 hours and the number of quantile forecasts for each hour is 99.

(a) The general architecture of the used neural networks.

Input features	Architecture	Output
historical data,[10] calendar features, weather features[10]	three nested three-layer NN Power - Encoder - Energy	Quantiles $\hat{q}_{P_l(k)}(p)$ and $\hat{q}_{E_l(k+1)}(p)$, $k = k_0, ..., k_0 + 41; p = 0.01, ..., 0.99$

(b) The detailed architecture of the used three-layer neural networks. Note that the layer size of the input layer is 267 for the power NN, 42·99 for the encoder NN, and 50 for the energy NN, and the layer size of the output layer is 42·99 for the power NN, 50 for the encoder NN, and 42·99 for the energy NN.

Layer	Activation function	Layer size
Input	Linear	267/42·99/50
Hidden	ReLU	20
	ReLU	50
Output	Linear	42·99/50

6.2.1 Experimental Setup

In the following, we describe the used data, how we generate the necessary probabilistic forecasts and present the evaluation metrics used for the forecast quality and the forecast value.

Data We use the prosumption data original with $\beta_{\text{load}} = 1$ and $\beta_{\text{PV}} = 1$ in Equation (2.27) and a BESS energy capacity $e_s^{\max}$ of 19.5 kWh. As problem-specific parameters, we consider the combinations of the security levels (ϵ_P, ϵ_E) of $(0.1, 0.1)$, $(0.1, 0.3)$, $(0.3, 0.3)$, and $(0.1, 0.7)$.

Forecast Method While the forecast specifications, input features, and the splitting of the data in training, validation, and testing to generate the probabilistic forecasts are identical to the generation of the point forecasts described in Subsection 4.2.1, the NN architecture differs. More precisely, we use three nested NNs as displayed in Figure 6.1b. The further architecture specifications are specified in Table 6.2. All three NNs are fully connected with three layers with a ReLU [3] activation function in both hidden layers and a linear activation function in the input and output layer. The nested NN is trained end-to-end by using a weighted sum of the power NN and

[10] This input feature is scaled with SKLearn's min-max scaler [106].

energy NN losses as the overall training loss, which is backpropagated through all preceding NNs. Furthermore, training is performed using a batch size of 512 and the Adam optimizer [79]. Finally, to ensure that the quantile forecasts are strictly monotonically increasing, we sort them in ascending order for each forecasted hour.

Evaluation Metrics The probabilistic forecasts with different characteristics are evaluated both with respect to the forecast quality and the forecast value. We use the same forecast values as in Subsection 4.2.1, i.e. the four average daily costs, namely the average daily DS cost, the average daily imbalance cost, the average daily total cost with imbalance cost factor $\alpha = 2$, and the average daily total cost with imbalance cost factor $\alpha = 10$. For these costs, lower values imply a higher forecast value. Additionally, for a better comparison between the buildings with different prosumption scales, we calculate the wins and the occurrences within the 5% win range for each forecast described in Subsection 4.2.1. For the wins and the occurrences within the 5% win range, we set each average daily cost for the building, forecast, and security level parameters to infinity if the OP is infeasible. This way, the forecast can not achieve a win and an occurrence within the 5% win range for that combination of building and security level parameters.
To measure the forecast quality, we use an evaluation metric specifically designed for probabilistic forecasts, namely the continuous ranked probability score (CRPS) described in Equation (2.10) with lower values implying a higher forecast quality.
Furthermore, to report the infeasible OPs, we consider the percentage of infeasible cases

$$\%\text{IC} = \frac{|\mathcal{C}_{\text{infeasible}}|}{|\mathcal{C}|} \cdot 100 \tag{6.16}$$

with $\mathcal{C}$ referring to the set of all considered cases, namely the energy security level parameters ϵ_E and the buildings, for a specific security level parameter ϵ_P and a specified subset of forecasts, and $\mathcal{C}_{\text{infeasible}}$ referring to the subset of $\mathcal{C}$ with infeasible OPs. Additionally, we consider the percentage of infeasible buildings

$$\%\text{IB} = \frac{\sum_{b \in \mathcal{B}} \mathbb{1}_{\exists c \in \mathcal{C}_{\text{infeasible}}: \text{building}(c)=b}}{|\mathcal{B}|} \cdot 100 \tag{6.17}$$

with $\mathcal{B}$ referring to the set of all considered buildings and the indicator function $\mathbb{1}$.

Tab. 6.3.: The percentage of infeasible cases %IC and the percentage of infeasible buildings %IB for the power security level parameter ϵ_P of 0.1 and 0.3 and several forecast conditions. For $\epsilon_P = 0.1$, the set of cases consist of all considered buildings and the energy security level parameters ϵ_E of 0.1, 0.3, 0.5, and 0.7, while for $\epsilon_P = 0.3$ the set of cases consists of all considered buildings and the energy security level parameter $\epsilon_E = 0.3$. Note that higher percentages indicate more infeasible optimisation problems.

Forecast condition	$\epsilon_P = 0.1$		$\epsilon_P = 0.3$	
	%IC	%IB	%IC	%IB
Overall	11.58	75.52	2.55	29.02
Unmodified	7.78	**10.14**	0.70	**0.70**
Power forecasts modified	17.00	64.34	5.04	25.52
Energy forecasts modified	7.80	29.02	0.82	4.55
Bias	8.14	30.42	0.83	3.85
Underestimation	7.63	15.38	**0.61**	1.40
Overestimation	8.10	32.17	0.82	4.29
Modification dispersion	15.50	67.83	4.50	26.57
Smaller dispersion	**4.90**	17.13	1.75	3.50
Greater dispersion	19.04	63.99	5.42	23.78

6.2.2 Results

In this section, we evaluate probabilistic forecasts with different characteristics with respect to their forecast value for the two-level DF considering probabilistic forecasts. Since these different probabilistic forecasts are obtained via modifying the dispersion or introducing bias, we present the results according to the respective modification's name. For this evaluation, we consider five aspects. First, we analyse the number of infeasible OPs. Second, we investigate the relationship between the forecast quality and the forecast value. Third, we examine the forecast value for varying security level parameters of the reformulated power and energy chance constraints for forecasts with different biases. Fourth, we evaluate the forecast value for varying security level parameters of the reformulated power and energy chance constraints for forecasts with different dispersions. Finally, we compare the overall performance of the DF considering probabilistic forecasts over several forecasts and security level parameters.

Analysis of Infeasible Optimisation Problems

For the analysis of the infeasible OPs, we calculate the percentage of infeasible cases and the percentage of infeasible buildings for $\epsilon_P = 0.1$ and $\epsilon_P = 0.3$ depending on multiple forecast conditions in Table 6.3. In this table, we make three observations. First, we see that the percentage of infeasible cases and the percentage of infeasible buildings are higher for $\epsilon_P = 0.1$ compared to $\epsilon_P = 0.3$.

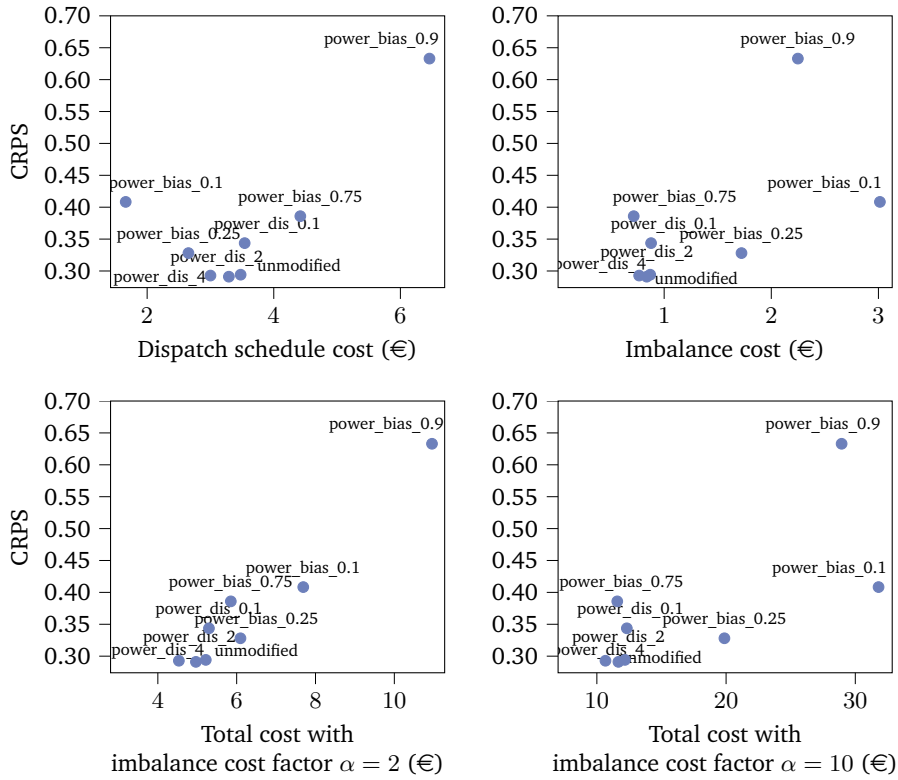

Fig. 6.5.: The CRPS against the average daily costs, namely the DS cost (upper left), the imbalance cost (upper right), the total cost with imbalance cost factor $\alpha = 2$ (lower left) and the total cost with imbalance cost factor $\alpha = 10$ (lower right) for the considered power forecasts. For this plot, we use the security level parameters $\epsilon_P = 0.3$, $\epsilon_E = 0.3$ and exclude the combination of forecast and building resulting in an infeasible optimisation problem. Note that for both the average daily costs and the CRPS lower values are better.

Second, the percentage of infeasible cases and the percentage of infeasible buildings are higher for modified forecasts. In particular, the modification of the dispersion and the modification of the power forecasts results in a higher percentage of infeasible cases and percentage of infeasible buildings than the modification for a bias and the modification of the energy forecasts. Furthermore, we observe that while the differences in the percentage of infeasible cases and the percentage of infeasible buildings are only slightly higher for overestimation than for underestimation, we observe that a greater dispersion leads to higher percentages than a smaller dispersion.

Finally, we see that the percentage of infeasible cases is lower than the percentage of infeasible buildings for all considered conditions.

Relation between Forecast Quality and Forecast Value

For this evaluation, we relate the CRPS as forecast quality and the average daily costs as forecast values for the different power forecasts $\hat{q}_{P_l(k)}$ for security level parameters $\epsilon_P = 0.3$, $\epsilon_E = 0.3$ in Figure 6.5. In these plots, the forecast quality and the forecast value is averaged over all buildings considered. Note that this evaluation is not carried out for the energy forecasts $\hat{F}_{\Delta E_l(k+1)}$, as it is not possible to calculate the CRPS, since $\Delta E_l(k+1)$ corresponds to the deviation from the mean.
For all costs, we can not deduce a clear relation between the forecast quality and the forecast value. However, we observe for the total costs that the forecast resulting in the best forecast quality does result in the best forecast value. More precisely, power_bias_0.1 achieves the best forecast value (1.66) and the seventh-best forecast quality (0.41) for the DS cost. For the imbalance cost, power_bias_0.75 results in the best forecast value (0.72) and the six-best forecast quality (0.39). For both total cost, the best forecast value is achieved with power_dis_4 (4.53 for for $\alpha = 2$ and 10.67 for $\alpha = 10$), which results together with power_dis_2 and the unmodified forecasts in the best forecast quality (0.29).

Comparison of Biases regarding varying Security Levels

We quantitatively and qualitatively compare the performance of different biases for varying security level parameters ϵ_P and ϵ_E. For the quantitative comparison, we report the wins and the occurrences within the 5% win range for three average daily costs, namely the DS cost, the imbalance cost, and the total cost with imbalance cost factor $\alpha = 2$ for all buildings and the security level parameter combinations (ϵ_P, ϵ_E) of $(0.1, 0.1)$, $(0.3, 0.3)$, and $(0.1, 0.7)$. For the qualitative comparison, we have a closer look at building 109. More precisely, we look at two average daily costs, namely the DS cost and the imbalance cost, for the security level parameter combinations (ϵ_P, ϵ_E) of $(0.1, 0.1)$, $(0.3, 0.3)$, and $(0.1, 0.7)$. Additionally, we look at the results of the DF for an exemplary week, selected forecasts, and selected security level parameters.

Quantitative Comparison Figure 6.6 shows the results for different biases for each considered average daily cost. Starting with the DS cost, the results show that power_bias_0.1 achieves the most wins for all security level parameters. While this dominance is clear for the combinations of security level parameters $(0.3, 0.3)$ and $(0.1, 0.7)$, we observe for $(0.1, 0.1)$ that energy_bias_0.1 achieves more than the half of the wins of power_bias_0.1. Additionally, we observe that for $\epsilon_P = 0.1$ each

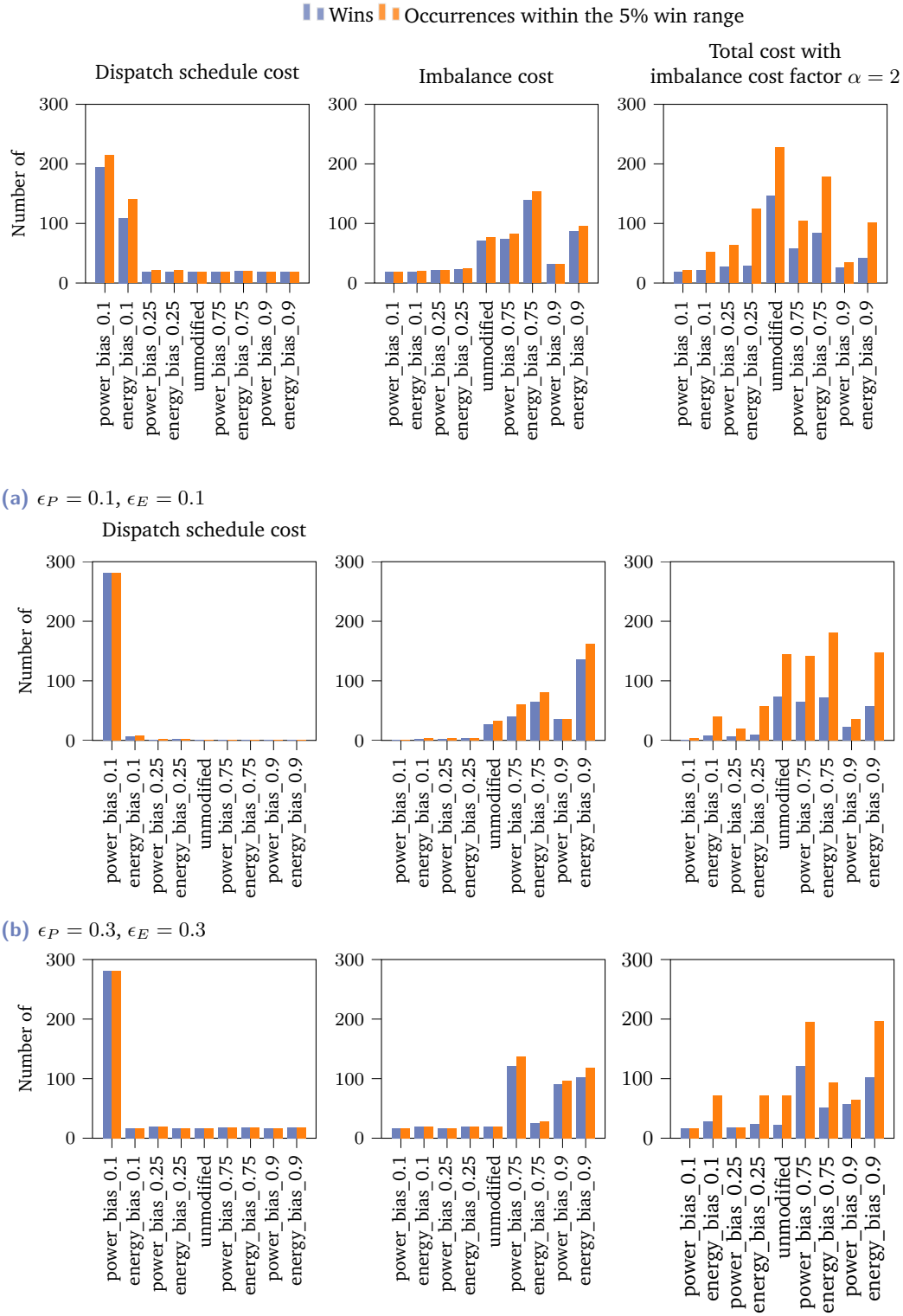

(a) $\epsilon_P = 0.1$, $\epsilon_E = 0.1$

(b) $\epsilon_P = 0.3$, $\epsilon_E = 0.3$

(c) $\epsilon_P = 0.1$, $\epsilon_E = 0.7$

Fig. 6.6.: The wins and the occurrences within the 5% win range for the considered average daily cost, i.e. the dispatch schedule cost (left), the imbalance cost (middle), and the total cost with imbalance cost factor $\alpha = 2$ (right) and the security level parameter combinations (ϵ_P, ϵ_E) of $(0.1, 0.1)$ (a), $(0.3, 0.3)$ (b), and $(0.1, 0.7)$ (c) for the considered biases. Note that more wins and more occurrences within the 5% win range are better.

Tab. 6.4.: The considered average daily costs in €, i.e. the dispatch schedule cost and the imbalance cost, of building 109 for all considered biases and the combinations of security level parameters (ϵ_P, ϵ_E) of $(0.1, 0.1)$, $(0.3, 0.3)$, and $(0.1, 0.7)$. Note that for the average daily costs lower values are better.

	$(0.1, 0.1)$		$(0.3, 0.3)$		$(0.1, 0.7)$	
	DS	Imbalance	DS	Imbalance	DS	Imbalance
power_bias_0.1	**5.41**	4.27	**2.29**	4.20	**0.70**	5.78
energy_bias_0.1	5.62	1.40	4.11	1.37	3.84	1.21
power_bias_0.25	6.51	1.38	3.76	1.51	2.25	2.95
energy_bias_0.25	6.02	0.90	3.98	1.12	3.84	1.21
unmodified	6.06	**0.53**	4.70	**0.78**	3.84	1.21
power_bias_0.75	6.71	1.03	6.06	1.48	5.14	1.00
energy_bias_0.75	6.55	0.57	5.33	0.90	4.08	1.05
power_bias_0.9	10.16	4.25	9.13	4.52	7.48	3.09
energy_bias_0.9	6.73	0.98	5.76	1.04	4.81	**0.81**

modification achieves at least 17 wins. In contrast, for $\epsilon_P = 0.3$, the wins are mostly concentrated on power_bias_0.1 and energy_bias_0.1.
For the imbalance cost, we observe that the overestimating modifications achieve the most wins. While overestimating the energy forecasts with energy_bias_0.75 and energy_bias_0.9 achieves the most and second most wins for the security level parameters $(0.1, 0.1)$ and $(0.3, 0.3)$, the overestimation of the power forecasts with power_bias_0.75 achieves the most wins for $(0.1, 0.7)$. Similar to the DS cost, we observe for $\epsilon_P = 0.1$ that each modification achieves at least 17 wins.
For the total cost, the results show that for the security level parameters $(0.1, 0.1)$ and $(0.3, 0.3)$ the most wins are achieved for the unmodified forecasts, followed by energy_bias_0.9. For the security level parameters $(0.1, 0.7)$, power_bias_0.75 achieves the most wins. Regarding the clarity of the wins, we observe that the occurrences within the 5% win range are noticeable higher than the wins for the unmodified forecasts and the overestimating modifications.

Qualitative Comparison Starting with the average daily costs, Table 6.4 shows the DS cost and the imbalance cost for building 109, where we make three observations. First, we observe that the greater the location of the forecast, the higher the DS cost. This is true for both the power and energy forecasts, although the increase in DS cost for the energy forecasts is not as large as for the power forecasts. Second, we observe that the imbalance cost is lowest for a specific forecast and increases in both directions of under- and overestimation, with a stronger increase for underestimation. More precisely, for the security level parameters $(0.1, 0.1)$ and $(0.3, 0.3)$, the lowest imbalance cost is achieved with the unmodified forecasts, and for $(0.1, 0.7)$ with energy_bias_0.9. Third, while the DS cost is higher for a smaller ϵ_E for all forecasts,

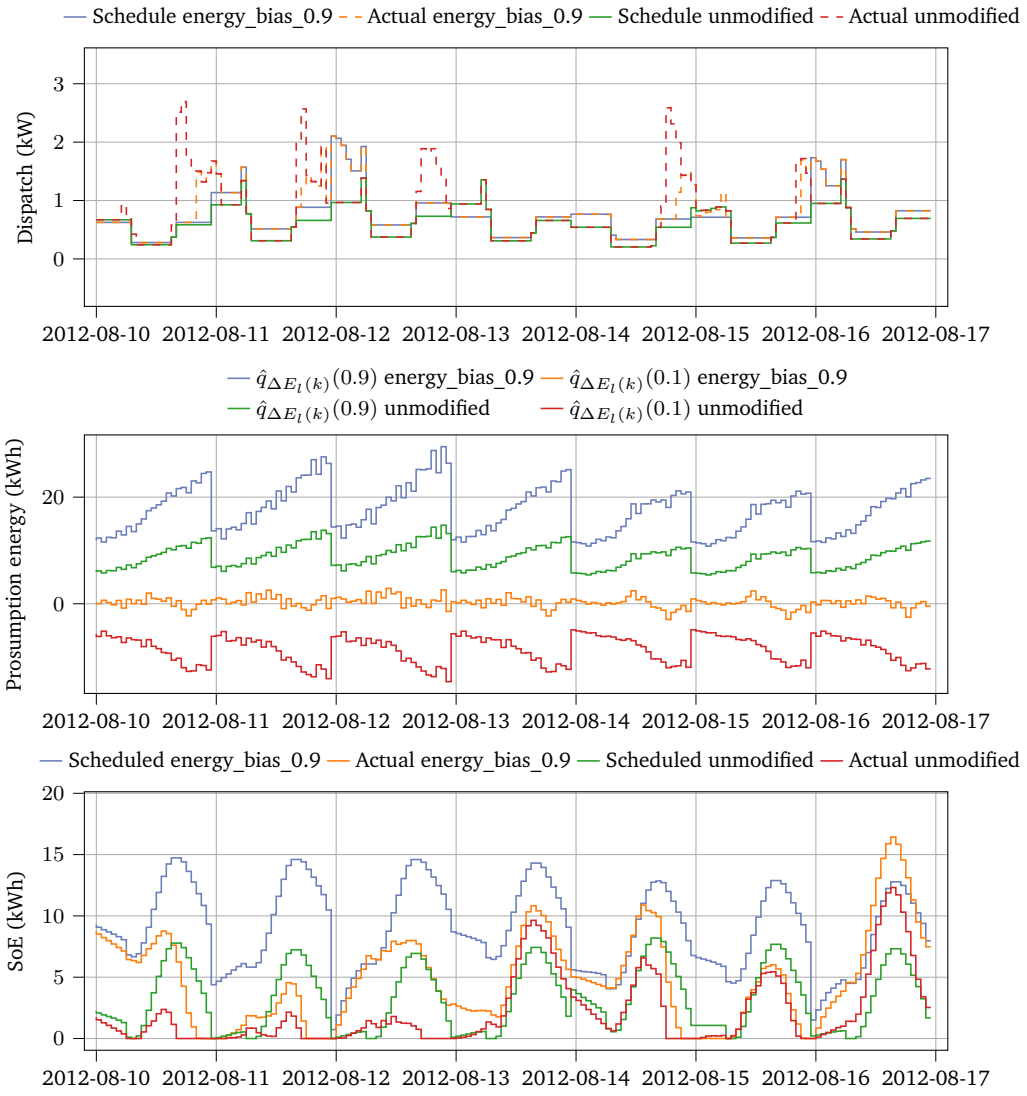

Fig. 6.7.: The dispatch schedule $p_{g_{DS}}$, the actual dispatch p_g, the prosumption power forecast $\hat{\bar{p}}_l$ as $\hat{q}_{P_l(k)}(0.5)$, the actual prosumption p_l, the scheduled BESS' SoE and the actual BESS' SoE resulting from the usage of power_bias_0.9 and the unmodified forecasts for the security level parameters $\epsilon_P = 0.1$, $\epsilon_E = 0.7$ for an exemplary week of building 109.

the relation between ϵ_E and the imbalance cost is not directly deducible and depends on the forecasts.
The results of the DF for an exemplary week are shown in Figure 6.7 for $\epsilon_P = 0.1$, $\epsilon_E = 0.7$. This figure shows the results of two forecasts, namely the forecasts leading to the minimal imbalance cost, i.e. energy_bias_0.9, and the unmodified forecasts. Comparing the DS, we observe that the DS with unmodified forecasts is slightly lower than the DS with energy_bias_0.9 at most hours. The consideration of different forecasts also leads to different actual dispatches and imbalances. More precisely, while the imbalances with both forecasts occur mainly in the evening hours with higher load values, the imbalances with unmodified forecasts occur earlier. During these hours, we observe that the actual SoE with the unmodified forecasts is at its lower BESS energy capacity $e_s^{\min} = 0$ kWh.

Comparison of Dispersions regarding varying Security Levels

In this subsection, we quantitatively and qualitatively compare the performance of different modifications of the dispersion for varying security level parameters ϵ_P and ϵ_E. For the quantitative comparison, we report the wins and the occurrences within the 5% win range for three average daily costs, namely the DS cost, the imbalance cost, and the total cost with imbalance cost factor $\alpha = 2$ for all buildings and the security level parameter combinations (ϵ_P, ϵ_E) of $(0.1, 0.1)$, $(0.3, 0.3)$, and $(0.1, 0.7)$. For the qualitative comparison, we focus on building 109 and look at two average daily costs, namely the DS cost and the imbalance cost, for the security level parameter combinations (ϵ_P, ϵ_E) of $(0.1, 0.1)$, $(0.3, 0.3)$, and $(0.1, 0.7)$. Further, we evaluate the results of the DF for an exemplary week, selected modifications of the dispersion, and selected security level parameters.

Quantitative Comparison Figure 6.8 displays the results for the different dispersions for each considered average daily cost. Starting with the DS cost, we observe that for the combination of the security level parameters $(0.1, 0.1)$ and $(0.3, 0.3)$, energy_dis_0.1 achieves by far the most wins. In contrast, for $(0.1, 0.7)$, many modifications achieve many wins. The most wins are achieved with power_dis_0.1 and energy_dis_0.1 and the unmodified forecasts.
For the imbalance cost, the results show that the modifications leading to greater dispersion of the energy forecasts achieve the most wins. More precisely, while the most wins are achieved with energy_dis_4 for the combination of security level parameters $(0.1, 0.1)$, energy_dis_10 achieves the most wins for $(0.3, 0.3)$. For $(0.1, 0.7)$,

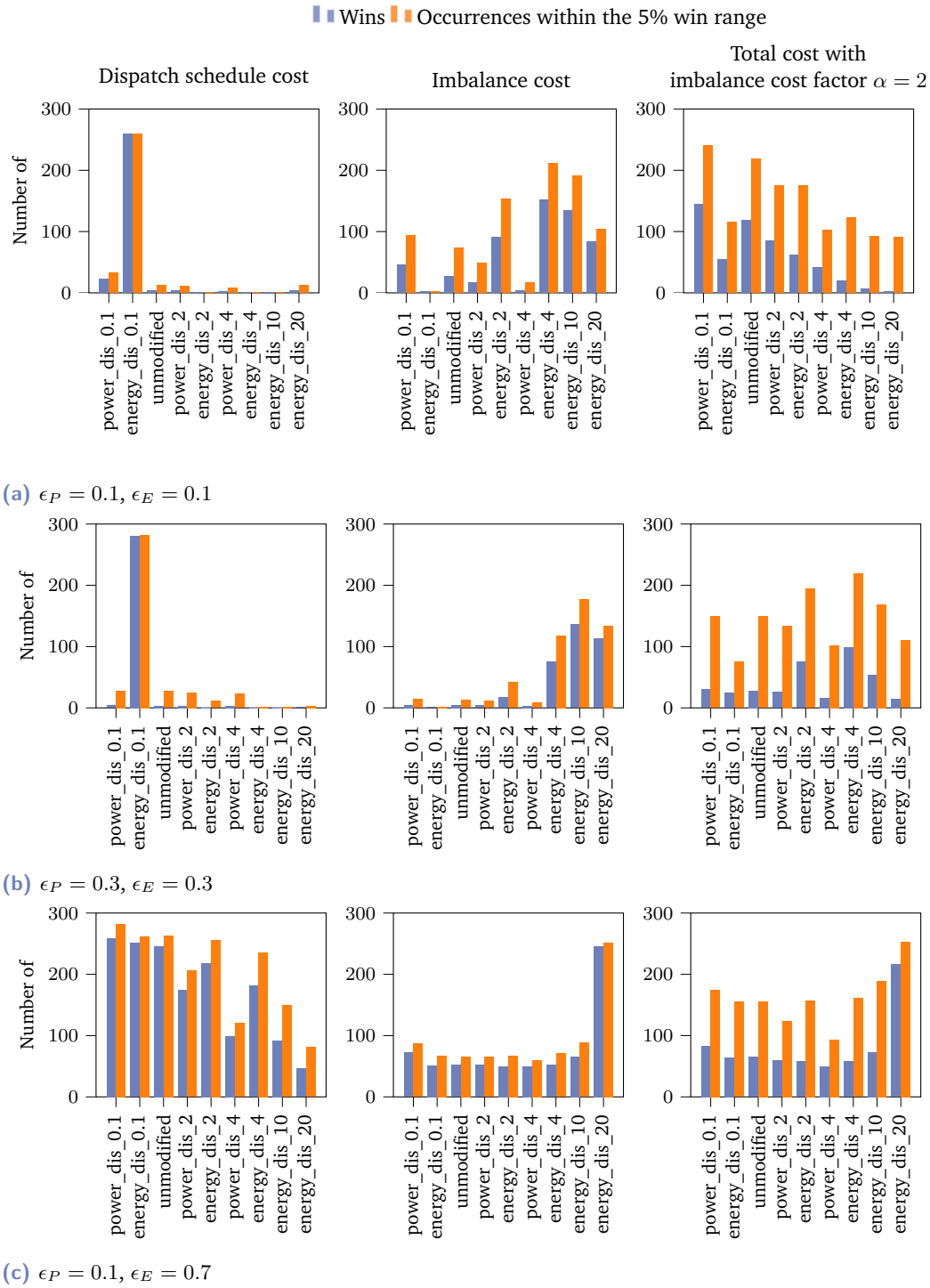

(a) $\epsilon_P = 0.1$, $\epsilon_E = 0.1$

(b) $\epsilon_P = 0.3$, $\epsilon_E = 0.3$

(c) $\epsilon_P = 0.1$, $\epsilon_E = 0.7$

Fig. 6.8.: The wins and the occurrences within the 5% win range for the considered average daily cost, i.e. the dispatch schedule cost (left), the imbalance cost (middle), and the total cost with imbalance cost factor $\alpha = 2$ (right) and the security level parameter combinations (ϵ_P, ϵ_E) of $(0.1, 0.1)$ (a), $(0.3, 0.3)$ (b), and $(0.1, 0.7)$ (c) for the considered modifications of the dispersion. Note that more wins and more occurrences within the 5% win range are better.

Tab. 6.5.: The considered average daily costs in €, i.e. the dispatch schedule cost and the imbalance cost, of building 109 for all considered modifications of dispersion and the combinations of security level parameters (ϵ_P, ϵ_E) of $(0.1, 0.1)$, $(0.3, 0.3)$, and $(0.1, 0.7)$. Note that for the average daily costs lower values are better.

	$(0.1, 0.1)$		$(0.3, 0.3)$		$(0.1, 0.7)$	
	DS	Imbalance	DS	Imbalance	DS	Imbalance
power_dis_0.1	6.06	0.53	4.70	0.78	3.84	1.21
energy_dis_0.1	**4.35**	0.91	**4.04**	1.07	3.84	1.21
unmodified	6.06	0.53	4.70	0.78	3.84	1.21
power_dis_2	6.06	0.53	4.70	0.78	3.84	1.21
energy_dis_2	6.68	0.50	5.22	0.60	3.84	1.21
power_dis_4	5.52	**0.45**	4.70	0.78	**3.28**	1.17
energy_dis_4	6.61	0.51	6.16	**0.53**	3.86	1.19
energy_dis_10	6.06	0.57	6.06	0.57	4.46	0.84
energy_dis_20	5.49	0.73	5.49	0.73	4.57	**0.82**

energy_dis_20 achieves the most wins, and all other modifications achieve comparable wins.

For the total cost, we observe for the combination of security level parameters $(0.1, 0.1)$ that the most wins are achieved with power_dis_0.1, followed by the unmodified forecasts. For $(0.3, 0.3)$, the modifications leading to greater dispersion achieve the most wins, with energy_dis_4 achieving the most. For $(0.1, 0.7)$ we observe similar results as for the imbalance cost, i.e. energy_dis_20 clearly achieves the most wins, while all other modifications achieve similar wins. With regard to the clarity of the wins, we see that the many modifications achieve occurrences within the 5% win range clearly above 100 for all security level parameters.

Qualitative Comparison The DS cost and the imbalance costs for building 109 are shown in Table 6.5, which leads to three observations. First, modifying the dispersion of the power forecasts has little or no impact on the DS and imbalance costs for all security level parameters except for the security level parameters $(0.1, 0.1)$. For these security level parameters we observe the lowest imbalance cost with power_dis_4. In contrast, modifying the dispersion of the energy forecasts has an impact on both costs. Second, for the DS cost, we see that for almost all modifications, the lower the dispersion of the energy forecasts, the lower the cost. In contrast, similar to the results for the bias, the imbalance cost is lowest for a specific energy forecast and increases in both directions of higher and lower dispersion. In this context we make a third observation, namely that the higher ϵ_E, the higher the dispersion of the forecast that leads to the lowest imbalance cost.

The results of the DF for an exemplary week are shown in Figure 6.9 for $\epsilon_P = 0.1$, $\epsilon_E = 0.7$. This figure shows the results of the modification leading to the minimal

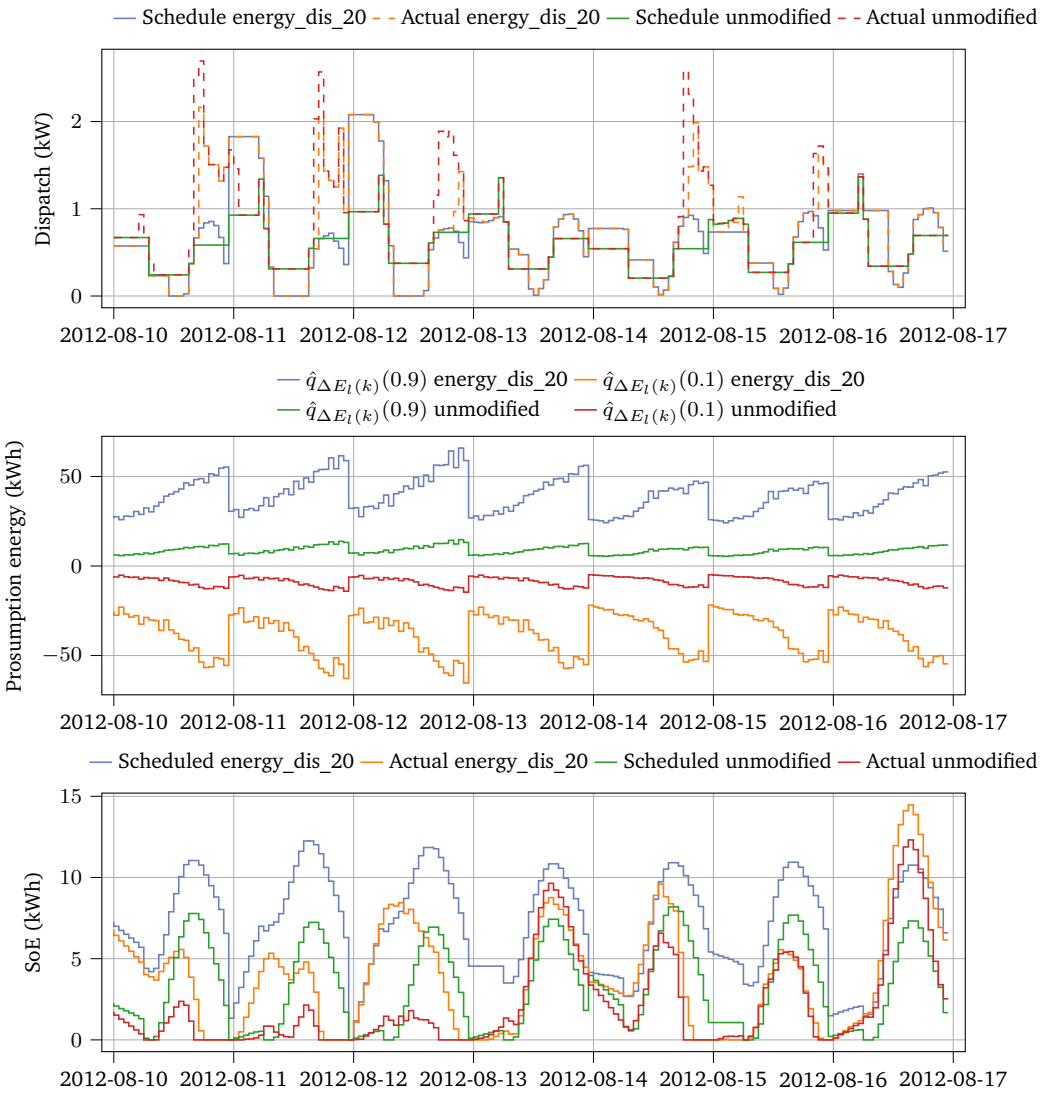

Fig. 6.9.: The dispatch schedule $p_{g_{DS}}$, the actual dispatch p_g, the prosumption energy forecasts $\hat{q}_{\Delta E_l(k+1)}$ for $p = 0.1$ and $p = 0.9$, the scheduled BESS' SoE and the actual BESS' SoE resulting from the usage of energy_dis_20 and the unmodified forecasts for the security level parameters $\epsilon_P = 0.1$, $\epsilon_E = 0.7$ for an exemplary week of building 109.

imbalance cost, i.e. energy_dis_20, and the unmodified forecasts. In this figure we can see that the DS with the unmodified forecasts is smoother than the DS with energy_dis_20. The corresponding scheduled SoE with the unmodified forecasts is lower than the SoE with energy_dis_20. As for the imbalances, we observe higher and more imbalances with the unmodified forecasts, while the imbalances of energy_dis_20 often occur during hours of imbalances with the unmodified forecasts.

Overall Comparison

For the overall comparison, we quantitatively compare the performance of different combinations of security level parameters and modifications. As combinations, we choose those that lead to the most wins in Figure 6.6 and Figure 6.8, resulting in a total of eighteen combinations. For this comparison, we look at the wins and the occurrences within the 5% win range for the four average daily costs, namely the DS cost, the imbalance cost, the total cost with imbalance cost factor $\alpha = 2$, and the total cost with imbalance cost factor $\alpha = 10$ for all buildings. The results are displayed in Figure 6.10, which we describe below for each average daily cost.

Starting with the DS cost, the combination of the highest energy security level parameter $\epsilon_E = 0.7$ and the modification power_bias_0.1 achieves by far the most wins (264). No other combination achieves wins and occurrences within the 5% win range, except the combination of $\epsilon_P = 0.3$, $\epsilon_E = 0.3$ and power_bias_0.1 (21 both).

For the imbalance cost, we observe that either modifications overestimating the energy forecasts or energy forecasts with a greater dispersion achieve the most wins. More precisely, the combination $\epsilon_P = 0.1$, $\epsilon_E = 0.1$ and energy_dis_4 achieves the most wins (130), followed by the combination $\epsilon_P = 0.1$, $\epsilon_E = 0.1$ and energy_bias_0.75 (103).

For the total cost with imbalance cost factor $\alpha = 2$, the wins are spread across the combinations, with more wins achieved by overestimating modifications and modifications with a greater dispersion. In addition, we observe a high number of occurrences within the 5% win range for the combinations achieving wins, with eight combinations achieving around or more than 150 occurrences within the 5% win range.

Finally, for the total cost with imbalance cost factor $\alpha = 10$, we observe similar results to those for the imbalance cost. More precisely, almost the same combinations achieve wins as the combination that achieve wins for the imbalance cost. However, the clarity of the wins is reduced as the occurrences within the 5% win range are clearly higher than the wins.

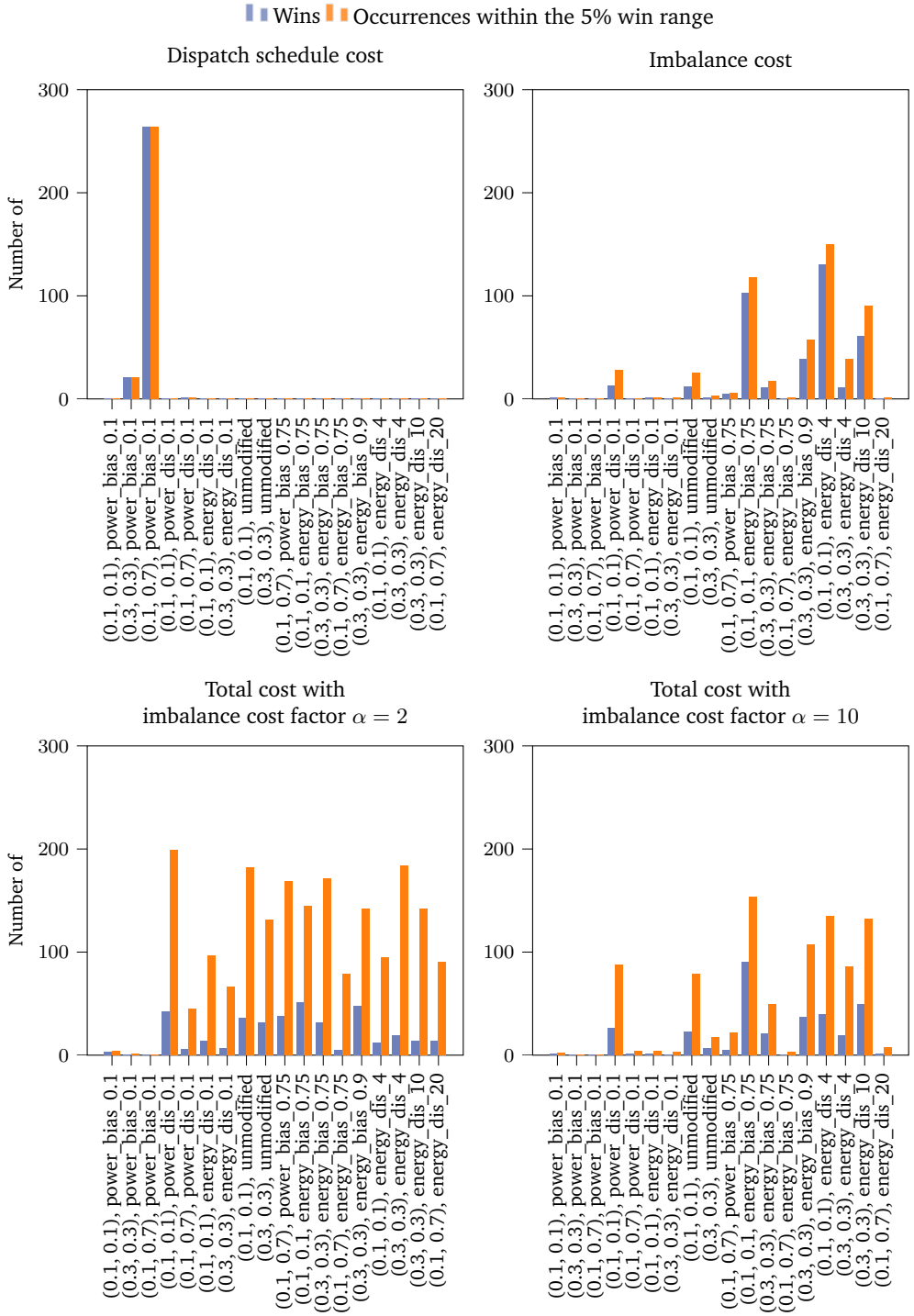

Fig. 6.10.: The wins and the occurrences within the 5% win range for the considered average daily cost, i.e. the dispatch schedule cost (upper left), the imbalance cost (upper right), the total cost with imbalance cost factor $\alpha = 2$ (lower left), and the total cost with imbalance cost factor $\alpha = 10$ (lower right) for different security level parameters and modifications written as „(ϵ_P, ϵ_E), *name of modification*“. Note that more wins and more occurrences within the 5% win range are better.

6.3 Discussion

In this section, we discuss the findings of the evaluation and identify limitations and further research.

6.3.1 Findings

The discussion of the findings focuses on four aspects. First, we discuss the issue of infeasible OPs for the DF considering probabilistic forecasts. Second, we discuss the relation between the forecast quality and the forecast value for the power forecasts. Third, we discuss the influence of the forecast characteristics on the forecast value. Finally, we address whether the findings provide a sufficient answer to the addressed research question.

First, regarding the infeasibility of the OPs for the DF considering probabilistic forecasts, the results show that the infeasibility depends on the security level parameter of the reformulated power chance constraint ϵ_P and the probabilistic forecasts, given fixed BESS capacities. This infeasibility is evident for several buildings, suggesting that it may be a critical effect for a real-world DF implementation. To address this, a coordination of the security level parameter ϵ_P, the forecasts, and available BESS capacities may be required. Alternatively, introducing a relaxation of the power chance constraint in the mathematical formulation of the OP could mitigate the infeasibility.

Second, regarding the relation between the forecast quality and the forecast value, the results show that for the power forecasts the relation between the considered forecast quality, namely the CRPS, and the considered forecast value, namely the average daily costs, is non-monotonic. Similar to the evaluation of the point forecasts in Chapter 4, this indicates that improving the forecast quality does not necessarily lead to a higher forecast value for the DF. However, two aspects should be noted. First, for both total costs, the forecast with the highest forecast quality results in the highest forecast value. Second, the performance of the DF considering probabilistic forecasts depends not only on the power forecasts but also on the energy forecasts, which limits the interpretation of the relation between the forecast quality and forecast value.

Third, regarding the influence of the forecast characteristics on the forecast value for the DF, the results show that the forecast characteristics affect the forecast value for the DF and that this influence depends on the security level parameter ϵ_E. In contrast, the security level parameter ϵ_P has only a small effect, see Appendix A.4. In the following, we discuss the findings for each conducted comparison, i.e. the

modification for a bias, the modification of the dispersion, and the overall comparison, in more detail.

Starting with the modification for a bias, the results are comparable to the results in Chapter 4 for each average daily cost. More precisely, for the DS cost, the results indicate that underestimating the power forecasts leads to lower cost for all security level parameters. A possible explanation for the lower DS cost when power forecasts are underestimated is equivalent to the finding in Section 4.3: an underestimation of load and an overestimation of PV power generation leads to lower grid imports and thus lower DS cost. For the imbalance cost, the results indicate that overestimation is beneficial, although which forecast should be overestimated depends on the security level parameter ϵ_E. While overestimating energy forecasts leads to lower imbalance cost for smaller ϵ_E, overestimating power forecasts is more advantageous for $\epsilon_E = 0.7$. A possible explanation for the former could be that these energy forecasts are shifted to be centred around a positive value, rather than being centred around zero. As a result, the BESS is scheduled to keep a higher reserve for these higher energy forecasts, and thus has more energy reserves for unexpectedly high prosumption values. This effect may not be as strong for $\epsilon_E = 0.7$. For this security level, the DF considering probabilistic forecasts behaves more like the DF considering point forecasts in the way that the BESS energy reserve for the prosumption energy uncertainty is reduced. As a consequence, it may be beneficial to increase the BESS energy reserve operationally imposed by the energy chance constraint by overestimating the power forecasts as follows: since the DS is calculated assuming that the building consumes more and generates less PV power, the BESS charges in the second level if possible to mitigate imbalances, resulting in a higher energy reserve for unexpectedly high prosumption values. Finally, the results of the total cost indicate that the combined effects of both DS and imbalance costs tend to cancel each other out. Consequently, the unmodified forecasts give the lowest total cost when ϵ_E is small and the imbalance cost factor is set to $\alpha = 2$.

For the modification of the dispersion, the results reflect the strong relation between the dispersion of the forecasts and the security level parameters via the reformulated power and energy chance constraints in Equation (6.1) and Equation (6.2). More precisely, for the DS cost, a smaller dispersion, especially for the energy forecasts, is associated with lower costs, especially for a lower energy security level parameter ϵ_E. For $\epsilon_E = 0.7$ several forecasts lead to similar costs. A possible explanation for the former could be that due to the lower dispersion of the energy forecasts, the BESS energy reserve held for the prosumption energy uncertainty is reduced, allowing more BESS reserve to be allocated to minimise the DS cost. This effect can also be achieved by increasing the energy security level parameter ϵ_E, which may explain the similar performance of several forecast characteristics for $\epsilon_E = 0.7$. For the

imbalance cost, the results indicate that a greater dispersion of the energy forecasts reduces the cost, with a greater dispersion being more beneficial for a higher ϵ_E. Both a greater dispersion of the energy forecasts and a higher ϵ_E result in more BESS energy reserves for the prosumption energy uncertainty and thus potentially to smaller imbalances. Thus, if the security level parameter ϵ_E is reduced, a greater dispersion of the energy forecasts may counteract the reduction of the BESS energy reserves and provide a similar level of security against imbalances.
For the overall comparison, the results show that the underestimation of the power forecasts in combination with the security level parameter, which results in the lowest BESS energy reserve for the prosumption energy uncertainty, results in the lowest DS cost for almost all buildings. In contrast, for the imbalance cost, the modification of the energy forecasts, namely an overestimation or the increase of the dispersion, results in lower costs for most buildings. This suggests that the cause of imbalances is more likely to be the uncertainty of the prosumption energy than the uncertainty of the prosumption power. Furthermore, while for the total cost with imbalance cost factor $\alpha = 2$ several combinations of forecasts and security level parameters perform similarly, the results for the total cost with imbalance cost factor $\alpha = 10$ are similar to the results for the imbalance cost, highlighting the strong influence of the imbalance cost.
Finally, regarding the research question

RQ2: *How do different probabilistic forecast characteristics influence the forecast value for the dispatchable feeder, and how does this influence depend on problem-specific parameters?*

we can conclude that the forecast characteristics can influence the forecast value for the two-level DF considering probabilistic forecasts and that this influence depends on the security level of the reformulated chance constraints. In particular, with respect to the dispersion of the probabilistic forecast, it is beneficial to coordinate the dispersion and the security level parameters for the reformulated power and energy chance constraints.

6.3.2 Limitations and Further Research

The main limitations of this evaluation are related to the chosen specifications. These include the considered problem-specific parameters and the modifications used. In particular, for a broader scope of the evaluation, the prosumption data and the BESS energy capacity could be considered as further problem-specific parameters motivated by the results of Chapter 4. Additionally, as we do not approach the

infeasibility of the OPs due to the reformulated power chance constraint introduced in Section 6.1, a forecast evaluation including the relaxation of the reformulated power chance constraint in the mathematical formulation for the computation of the DS could be interesting. Finally, with the results of the conducted forecast evaluation, a value-oriented recalibration of the probabilistic forecasts for the DF could be approached.

7 Comparison of Dispatchable Feeder Considering Point and Probabilistic Forecasts

This chapter compares the performance between the two-level dispatchable feeder (DF) considering point forecasts and the two-level dispatchable feeder considering probabilistic forecasts. For this comparison, we evaluate both value-oriented forecasts and standard forecasts. In doing so, we examine how the forecast characteristics and the integration of the prosumption uncertainty affect the performance of the DF. Additionally, we analyse whether value-oriented point forecasts can compensate for the lack of integration of the prosumption uncertainty. The research question addressed is:

RQ4: *How does the performance of the dispatchable feeder considering point forecasts compare to the performance of the dispatchable feeder considering probabilistic forecasts for difference forecast characteristics?*

The remainder of this chapter is structured as follows. First, Section 7.1 describes the approach. Second, Section 7.2 presents the evaluation with Subsection 7.2.1 describing the experimental setup and Subsection 7.2.2 presenting the results of the evaluation. Finally, Section 7.3 discusses the results.

7.1 Approach

This section provides an overview of the comparison between the performance of the two-level DF considering point forecasts and the performance of the two-level DF considering probabilistic forecasts. For this comparison, we use forecasts with a high forecast value and standard forecasts. This means that instead of only comparing the performance of both DFs for a single building, as done in [7], and only comparing different forecast characteristics with respect to the forecast value for each DF separately, as done in Chapter 4 and Chapter 6, this chapter evaluates the effect of both the integration of the prosumption uncertainty and the forecast characteristics on the performance of the DF. Although such an evaluation can be

Tab. 7.1.: The selected value-oriented forecasts (a) and the considered dispatchable feeder specifications (b).

(a) The selected value-oriented point and probabilistic forecasts from Chapter 4 and Chapter 6 respectively, for the dispatchable feeder considering point forecasts and the dispatchable feeder considering probabilistic forecasts respectively, and the security level parameters ϵ_P and ϵ_E for the dispatchable feeder considering probabilistic forecasts. The considered forecast value is the average daily total cost with either imbalance cost factor $\alpha = 2$ or imbalance cost factor $\alpha = 10$.

Forecast value	Point forecast	Probabilistic forecast	Security level parameters
Total cost $\alpha = 2$	Pinball 0.75	energy_bias_0.9	$\epsilon_P = 0.3$, $\epsilon_E = 0.3$
Total cost $\alpha = 10$	Pinball 0.75	energy_bias_0.75	$\epsilon_P = 0.1$, $\epsilon_E = 0.1$

(b) The used point forecasts for the different dispatchable feeders considering point forecasts, i.e. the $DF_{\text{v-o point}}$ and the $DF_{\text{MSE point}}$, and the used probabilistic forecasts and security level parameters ϵ_P and ϵ_E for the different dispatchable feeder considering probabilistic forecasts, i.e. the $DF_{\text{v-o prob,total 2}}$, the $DF_{\text{v-o prob,total 10}}$, the $DF_{\text{unmod prob,total 2}}$, and the $DF_{\text{unmod prob,total 10}}$.

DF	Forecast	Security level parameters
$DF_{\text{v-o point}}$	Pinball 0.75	–
$DF_{\text{v-o prob,total 2}}$	energy_bias_0.9	$\epsilon_P = 0.3$, $\epsilon_E = 0.3$
$DF_{\text{v-o prob,total 10}}$	energy_bias_0.75	$\epsilon_P = 0.1$, $\epsilon_E = 0.1$
$DF_{\text{MSE point}}$	MSE	–
$DF_{\text{unmod prob,total 2}}$	unmodified	$\epsilon_P = 0.3$, $\epsilon_E = 0.3$
$DF_{\text{unmod prob,total 10}}$	unmodified	$\epsilon_P = 0.1$, $\epsilon_E = 0.1$

seen as a forecast evaluation with respect to the forecast value for the DF, similar to Chapter 4 and Chapter 6, we present it here as a performance comparison of different DFs. In this way, we highlight both the differences in the mathematical formulations of the DFs to consider the prosumption uncertainty and the differences in the parameter specifications for the DF considering probabilistic forecasts, in particular the security level parameters ϵ_P and ϵ_E for the reformulated power and energy chance constraints.

In order to select the value-oriented forecasts for this evaluation, we could ideally apply the value-oriented forecast method selection described in Chapter 5, which would result in a forecast with a high forecast value for each building and each considered forecast value. However, as we have not yet applied the value-oriented forecast method selection to the DF considering probabilistic forecasts, we proceed as follows. For each forecast value and each DF, we evaluate which forecast characteristic achieves the highest wins, described in Subsection 4.2.1, among the buildings[1] with IDs smaller than or equal to 200. This forecast is then used for the remaining buildings for the corresponding forecast value and DF. As set of potential forecast characteristics we use those considered in Chapter 4 and Chapter 6. More precisely, the set of potential point forecasts consists of the seven point forecasts

[1]We exclude building 109, as we use this building for the qualitative comparisons.

obtained by using different loss functions in the neural network. As set of potential probabilistic forecasts, we use the eighteen combinations of security level parameters ϵ_P and ϵ_E and the probabilistic forecasts obtained by introducing a bias or modifying the dispersion in Subsection 6.2.2. In doing so, not only the probabilistic forecast but also the problem-specific parameters of the security level, which are not given by technical constraints, are selected in a value-oriented manner. The resulting forecasts are displayed in Table 7.1a with the average daily total costs with imbalance cost factor $\alpha = 2$ or $\alpha = 10$ from Equation (4.2) as the forecast value. In the following, we refer to the DFs with these value-oriented forecasts as follows, see Table 7.1b. Since the value-oriented point forecasts are identical for both considered forecast values, we use the term DF using value-oriented point forecasts, or $\mathbf{DF}_{\textbf{v-o point}}$ for short. For the probabilistic forecasts, we distinguish between the DF considering value-oriented probabilistic forecasts based on the total cost with imbalance cost factor $\alpha = 2$ and $\alpha = 10$. These are referred to as $\mathbf{DF}_{\textbf{v-o prob,total 2}}$ and $\mathbf{DF}_{\textbf{v-o prob,total 10}}$, respectively.

In addition to the three DFs considering value-oriented forecasts, we use three other DFs considering standard forecasts, namely the DF considering MSE point forecasts, or $\mathbf{DF}_{\textbf{MSE point}}$ for short, the DF considering unmodified probabilistic forecasts with security level parameters based on the total cost with imbalance cost factor $\alpha = 2$, or $\mathbf{DF}_{\textbf{unmod prob,total 2}}$ for short, the DF considering unmodified probabilistic forecasts with security level parameters based on the total cost with imbalance cost factor $\alpha = 10$, or $\mathbf{DF}_{\textbf{unmod prob,total 10}}$ for short, see Table 7.1b. As the name implies, the DF considering MSE point forecasts uses the point forecasts generated with the mean squared error (MSE) described in Equation (2.7) as loss function and thus corresponding to a standard loss function used when generating point forecasts. Similarly, the DF considering unmodified probabilistic forecasts uses the probabilistic forecasts generated from the nested NN described in Subsection 6.2.1 without modification. The security level parameters ϵ_P and ϵ_E are those resulting from the value-oriented selection reported in Table 7.1a, i.e. $\epsilon_P = 0.3$, $\epsilon_E = 0.3$ for the total cost with imbalance cost factor $\alpha = 2$ and $\epsilon_P = 0.1$, $\epsilon_E = 0.1$ for the total cost with imbalance cost factor $\alpha = 10$. In this way, it is possible to compare the sole effect of the probabilistic forecast on the performance of the DF.

The aim of this evaluation is to compare, for several buildings, how forecasts with different characteristics and the integration of the prosumption uncertainty affect the performance of the DF, and whether value-oriented point forecasts can compensate for the lack of integration of the prosumption uncertainty.

7.2 Evaluation

In this section, we compare the performance of the different DFs. Therefore, Subsection 7.2.1 presents the experimental setup and Subsection 7.2.2 reports the results.

7.2.1 Experimental Setup

In the following, we describe the used data, the used forecast methods to generate the point and probabilistic forecasts, and the used evaluation metrics.

Data As the evaluation in Chapter 6 is done for the problem-specific parameters of the prosumption data original with $\beta_{\text{load}} = 1$ and $\beta_{\text{PV}} = 1$ in Equation (2.27) and the BESS energy capacity $e_s^{\max}$ of 19.5 kWh, we restrict this evaluation to these problem-specific parameters.
In addition, the evaluation is carried out on buildings with IDs greater than 200, from which ten buildings are excluded for which the OPs of the DFs considering probabilistic forecasts are infeasible.

Forecast Method We use the same point forecasts and probabilistic forecasts generated for the evaluations in Chapter 4 and Chapter 6 respectively. Therefore, the reader is referred to Subsection 4.2.1 and Subsection 6.2.1 for the description of the forecast specifications, the input features, the splitting of the data in training, validation, and testing, and the neural network architecture.

Evaluation Metrics We use the two average daily total costs with imbalance cost factor $\alpha = 2$ and $\alpha = 10$, explained in Equation (4.2), averaged over the last year, as evaluation metrics. For these costs, lower values are better. In addition, to measure the difference in average daily cost between the DF considering point forecasts and the DF considering probabilistic forecasts for each building, we calculate the percentage difference of a given total cost

$$\%\text{diff} = \frac{c^{\text{DF}_{\text{point}}} - c^{\text{DF}_{\text{prob}}}}{c^{\text{DF}_{\text{point}}}} \cdot 100 \tag{7.1}$$

with $c^{\text{DF}_{\text{point}}}$ and $c^{\text{DF}_{\text{prob}}}$ being the total cost for the DF considering point forecasts and the DF considering probabilistic forecasts respectively. A positive percentage

Tab. 7.2.: The average daily total costs in € for the $DF_{\text{v-o point}}$, the $DF_{\text{v-o prob,total 2}}$, the $DF_{\text{v-o prob,total 10}}$, the $DF_{\text{MSE point}}$, the $DF_{\text{unmod prob,total 2}}$, and the $DF_{\text{unmod prob,total 10}}$. The average daily costs are averaged over the last year and over all buildings with IDs greater than 200. For the average daily total costs, lower values are better. Further average daily costs are displayed in Appendix A.5.

Approach	Total cost $\alpha = 2$	Total cost $\alpha = 10$
$DF_{\text{v-o point}}$	5.04	9.73
$DF_{\text{v-o prob,total 2}}$	5.26	9.51
$DF_{\text{v-o prob,total 10}}$	5.14	**8.81**
$DF_{\text{MSE point}}$	**4.89**	11.31
$DF_{\text{unmod prob,total 2}}$	4.96	11.37
$DF_{\text{unmod prob,total 10}}$	4.90	9.16

difference indicates that the DF considering probabilistic forecasts achieves a lower average daily cost compared to the DF considering point forecasts.

7.2.2 Results

To present the results of the comparison, we first quantitatively compare the performances of the DFs over all buildings with IDs greater than 200 and the last year of data. Afterwards, we qualitatively compare the performances for building 109.

Quantitative Comparison over all Buildings For this evaluation, we compare the performance of the DFs on the buildings with IDs greater than 200. Therefore, we first aggregate each average daily cost over the last year and over all buildings, and then look at the differences in each total cost in more detail by looking at the percentage differences of both total costs for selected DFs.
Starting with the aggregated average daily costs, the results are presented in Table 7.2. In this table, we make three observations. First, we observe that the total cost with imbalance cost factor $\alpha = 2$ is lowest for the $DF_{\text{MSE point}}$. However, the difference in total cost between the different DFs is small. For the cost with imbalance cost factor $\alpha = 10$, $DF_{\text{v-o prob,total 10}}$ achieves the lowest cost, while $DF_{\text{MSE point}}$ and $DF_{\text{unmod prob,total 2}}$ achieve the second highest and highest cost. Second, when comparing the value-oriented forecasts with the standard forecasts, we observe lower total cost with imbalance cost factor $\alpha = 10$ for the $DF_{\text{v-o point}}$ compared to the $DF_{\text{MSE point}}$. With a smaller difference in cost, this is also true when comparing the $DF_{\text{v-o prob,total 10}}$ and the $DF_{\text{unmod prob,total 10}}$. In contrast, for the total cost with imbalance cost factor $\alpha = 2$, we observe higher cost for the $DF_{\text{v-o point}}$ compared to the $DF_{\text{MSE point}}$ as well as when comparing the $DF_{\text{v-o prob,total 2}}$ and the $DF_{\text{unmod prob,total 2}}$.

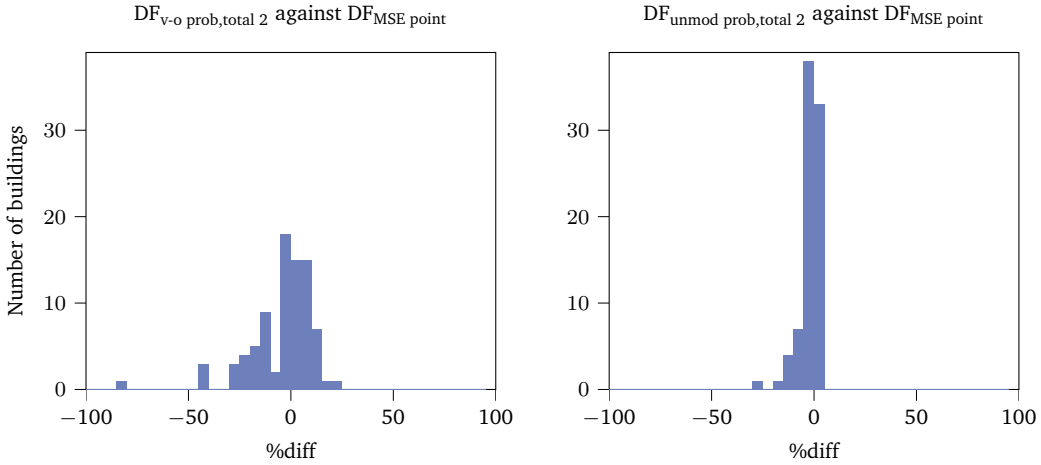

(a) Total cost with imbalance cost factor $\alpha = 2$

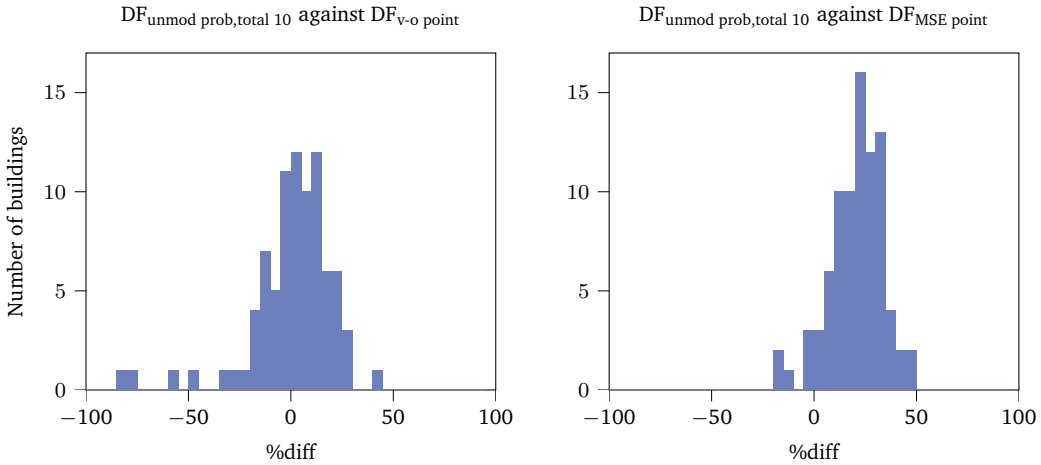

(b) Total cost with imbalance cost factor $\alpha = 10$

Fig. 7.1.: The percentage differences of the total cost with imbalance cost factor $\alpha = 2$ (a) between the $DF_{\text{MSE point}}$ and the $DF_{\text{v-o prob,total 2}}$ (left) and between the $DF_{\text{MSE point}}$ and the $DF_{\text{unmod prob,total 2}}$ (right) and the percentage differences of the total cost with imbalance cost factor $\alpha = 10$ (b) between the $DF_{\text{v-o point}}$ and the $DF_{\text{unmod prob,total 10}}$ (left) and between the $DF_{\text{MSE point}}$ and the $DF_{\text{unmod prob,total 10}}$ (right). Note that positive percentage differences indicate lower cost for the dispatchable feeder considering probabilistic forecasts. Additionally, the plots show a range between -100 and 100.

Tab. 7.3.: The average daily total costs in € for the $DF_{\text{v-o point}}$, the $DF_{\text{v-o prob,total 2}}$, the $DF_{\text{v-o prob,total 10}}$, the $DF_{\text{MSE point}}$, the $DF_{\text{unmod prob,total 2}}$, and the $DF_{\text{unmod prob,total 10}}$. The average daily costs are averaged over the last year of building 109. For the average daily total costs, lower values are better.

Approach	Total cost $\alpha = 2$	Total cost $\alpha = 10$
$DF_{\text{v-o point}}$	6.51	12.77
$DF_{\text{v-o prob,total 2}}$	7.84	16.20
$DF_{\text{v-o prob,total 10}}$	7.70	12.29
$DF_{\text{MSE point}}$	**6.04**	13.92
$DF_{\text{unmod prob,total 2}}$	6.25	12.45
$DF_{\text{unmod prob,total 10}}$	7.12	**11.35**

Third, if we compare the $DF_{\text{v-o point}}$ with $DF_{\text{unmod prob,total 10}}$, we observe that the difference in total cost with imbalance cost factor $\alpha = 10$ is smaller than the difference in this cost between $DF_{\text{MSE point}}$ and $DF_{\text{unmod prob,total 10}}$.
The results of the more detailed percentage differences are shown in Figure 7.1 for both total costs. Specifically, we consider for the percentage differences of the total cost with imbalance cost factor $\alpha = 2$ the $DF_{\text{MSE point}}$ and the $DF_{\text{v-o prob,total 2}}$ as well as the $DF_{\text{MSE point}}$ and the $DF_{\text{unmod prob,total 2}}$ to evaluate the difference between the best performing point forecasts and both probabilistic forecasts. For the percentage differences of the total cost with imbalance cost factor $\alpha = 10$, we compare the $DF_{\text{v-o point}}$ and the $DF_{\text{unmod prob,total 10}}$ as well as the $DF_{\text{MSE point}}$ and the $DF_{\text{unmod prob,total 10}}$ to evaluate whether value-oriented point forecasts can compensate for the lack of this integration. Based on the percentage differences of the total cost with imbalance cost factor $\alpha = 2$ between the $DF_{\text{MSE point}}$ and the $DF_{\text{v-o prob,total 2}}$, we observe that the percentage differences are centred around zero with more spreads for values less than zero. For the percentage differences of the total cost with imbalance cost factor $\alpha = 2$ between the $DF_{\text{MSE point}}$ and the $DF_{\text{unmod prob,total 2}}$, we observe that the percentage differences are strongly centred around zero, with more percentage differences being negative. Regarding the percentage differences of the total cost with imbalance cost factor $\alpha = 10$ between the $DF_{\text{MSE point}}$ and the $DF_{\text{unmod prob,total 10}}$, we observe that the majority of the percentage differences are positive. Additionally, while the percentage differences of the total cost with imbalance cost factor $\alpha = 10$ between the $DF_{\text{v-o point}}$ and the $DF_{\text{unmod prob,total 10}}$ are also positive for most buildings, we observe that they are more symmetrical around zero with a greater spread towards negative values.

Qualitative Comparison on Building 109 For this evaluation, we compare the performance of the DFs on building 109. Therefore, we first look at the average daily cost and, then present the results for an exemplarily week of the $DF_{\text{v-o point}}$ and the

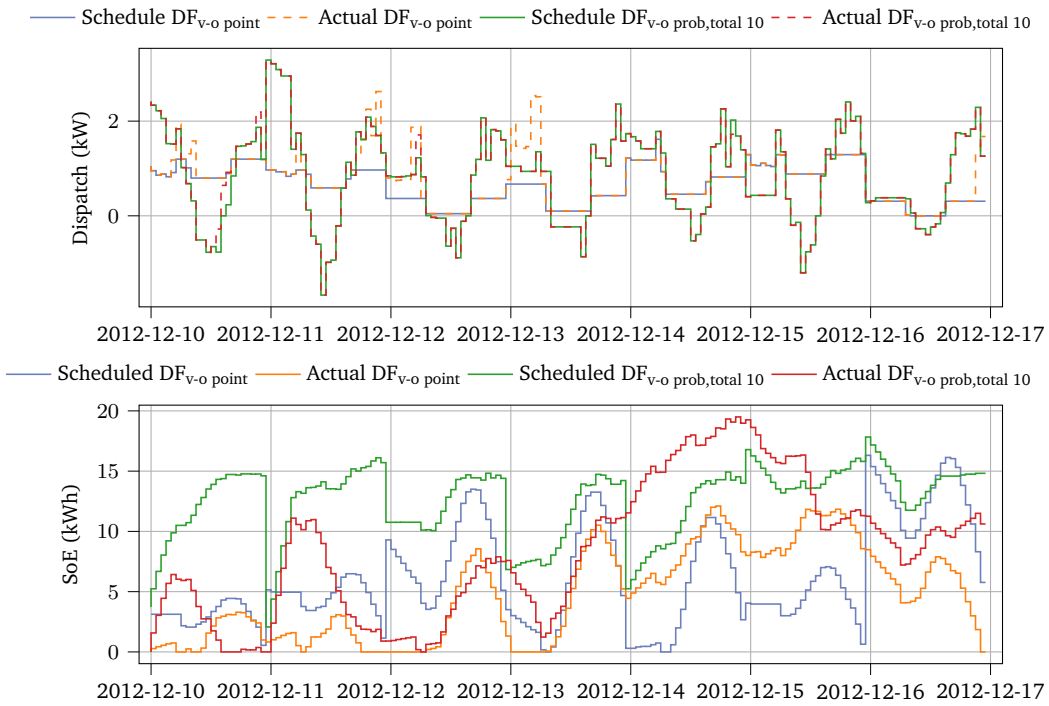

Fig. 7.2.: The dispatch schedule $p_{g_{DS}}$, the actual dispatch p_g, the scheduled BESS' SoE and the actual BESS' SoE of the DF$_{\text{v-o point}}$ and the DF$_{\text{v-o prob,total 10}}$, for an exemplary week of building 109.

DF$_{\text{v-o prob,total 10}}$.

Starting with the average daily costs, Table 7.3 shows the results, where we make two observations. First, we observe that the total cost with imbalance cost factor $\alpha = 2$ is lowest for the DF$_{\text{MSE point}}$. While similar costs are obtained with DF$_{\text{unmod prob,total 2}}$ and DF$_{\text{v-o point}}$, the DF$_{\text{v-o prob,total 2}}$ results in the highest cost. For the cost with imbalance cost factor $\alpha = 10$, DF$_{\text{unmod prob,total 10}}$ has the lowest cost, followed by DF$_{\text{v-o prob,total 10}}$, DF$_{\text{unmod prob,total 2}}$, and DF$_{\text{v-o point}}$, which have comparable costs. Second, when comparing the value-oriented forecasts with the standard forecasts, we observe that the DF$_{\text{v-o point}}$ results in lower total cost with imbalance cost factor $\alpha = 10$ compared to the DF$_{\text{MSE point}}$, while the DF$_{\text{MSE point}}$ achieves lower total cost with imbalance cost factor $\alpha = 2$. Similarly, for the probabilistic forecasts, we observe that the total cost with imbalance cost factor $\alpha = 2$ is lower for DF$_{\text{unmod prob,total 2}}$. Additionally, the total cost with imbalance cost factor $\alpha = 10$ is lower for the DF$_{\text{unmod prob,total 10}}$ compared to DF$_{\text{v-o prob,total 10}}$.

The results of an example week are shown in Figure 7.2. This figure shows that the DS of the DF$_{\text{v-o point}}$ is much smoother than the DS of the DF$_{\text{v-o prob,total 10}}$, whose SoE is scheduled to be higher. This results in fewer imbalances for the DF$_{\text{v-o prob,total 10}}$, especially in the first four days, where the DF$_{\text{v-o point}}$ causes imbalances.

7.3 Discussion

In the following, we discuss the results presented above by reporting the findings and specifying limitations and further research.

7.3.1 Findings

In discussing the results, we focus on four aspects. First, we compare the performance of all considered DFs and discuss whether the integration of the prosumption uncertainty is beneficial. Second, we discuss the impact of the value-oriented forecasts. Third, we discuss whether the consideration of value-oriented point forecasts can compensate for the lack of integration of prosumption uncertainty. Finally, we review the stated research question and address whether the findings provide a satisfactory answer to it.

First, the results show that the $\text{DF}_{\text{v-o prob,total 10}}$ achieves the lowest total cost with imbalance cost factor $\alpha = 10$ averaged over all buildings, followed by $\text{DF}_{\text{unmod prob,total 10}}$ and $\text{DF}_{\text{v-o prob,total 2}}$. This result indicates that it is beneficial to consider the prosumption uncertainty to avoid imbalances. In contrast, for the total cost with imbalance cost factor $\alpha = 2$, $\text{DF}_{\text{MSE point}}$ has the lowest cost both averaged over all buildings and for building 109 specifically. However, the costs of the other DFs are comparable. For this total cost, the proportions of the DS cost and the imbalance cost are similar, so the trade-off between reducing the DS cost and reducing the imbalance cost is not clear. As a result, the integration of the prosumption uncertainty to reduce the imbalance cost is less beneficial, leading to similar performances of the different DFs.

Second, regarding the impact of value-oriented forecasts, the results show that these forecasts can reduce the total costs when the imbalance cost factor is $\alpha = 10$, especially for point forecasts. However, the results for building 109 show that the benefit of value-oriented forecasts for this cost is building-dependent. Additionally, for $\alpha = 2$, standard forecasts are more beneficial averaged over all buildings. The results in Appendix A.5 show that DFs considering value-oriented forecasts tend to achieve lower imbalance costs but incur higher DS costs compared to DFs considering standard forecasts averaged over all buildings. This suggests that the value-oriented forecasts may over-prioritise the reduction of the imbalance cost, resulting in a conservative BESS operation, and thus higher DS costs. This implies that the choice of the value-oriented forecast based on the total cost with imbalance cost factor $\alpha = 2$ may be suboptimal. As the results in Chapter 4 and Chapter 6 show, it is not clear which point and probabilistic forecast leads to the lowest total cost

with imbalance cost factor $\alpha = 2$ and that it may be building-dependent. Therefore, the value-oriented selection approach used, which results in the same choice of value-oriented forecasts for each building, may not take this variability into account. Third, regarding the compensation for the lack of integration of prosumption uncertainty by using value-oriented point forecasts, the results show that the differences in the total cost with imbalance cost factor $\alpha = 10$ between the $\mathrm{DF}_{\text{v-o point}}$ and the $\mathrm{DF}_{\text{unmod prob,total 10}}$ are noticeably smaller than the differences between the $\mathrm{DF}_{\text{MSE point}}$ and the $\mathrm{DF}_{\text{unmod prob,total 10}}$. This suggests that a value-oriented selection of the point forecasts can compensate to some extent, if not completely, for the lack of integration of prosumption uncertainty for this total cost, for which the imbalance cost has a high impact.
Finally, regarding the research question

RQ4: *How does the performance of the dispatchable feeder considering point forecasts compare to the performance of the dispatchable feeder considering probabilistic forecasts for difference forecast characteristics?*

we can conclude that the consideration of probabilistic forecasts, in particular value-oriented forecasts, performs best with respect to the total cost that heavily weights imbalances, i.e. with an imbalance cost factor $\alpha = 10$. For this total cost, the use of value-oriented forecasts is more beneficial than standard forecasts. In particular, the consideration of value-oriented point forecasts can compensate to some extent, if not completely, for the lack of integration of prosumption uncertainty. In contrast, for the total cost with imbalance cost factor $\alpha = 2$, the DFs with different forecasts perform comparably when averaged over all buildings, and the best performing DF may depend on the specific building.

7.3.2 Limitations and Further Research

With regard to the limitations of the conducted comparison, we discuss two aspects. First, the approach used to select the value-oriented forecasts could be improved. One possible improvement would be to make the data splitting cleaner. In particular, instead of calculating the performance of the DF on the testing data of the forecasting, i.e. the last year of data, and selecting the value-oriented forecasts based on these results, the selection could be based on the performance of the DF on the training and validation data of the forecasting, i.e. the first two years of data. A further improvement could be to apply the value-oriented forecast method selection introduced in Chapter 5 for an improved value-oriented forecast selection for each building individually. This refinement could improve the performance of both the DF

using value-oriented point forecasts and the DF using value-oriented probabilistic forecasts.

Second, the scope of the comparison could be broadened. This includes incorporating additional forecast characteristics for both point and probabilistic forecasts, and introducing problem-specific parameters, such as prosumption data and BESS energy capacity, to increase the robustness and generalisability of the results.

8 Line-Restricted Dispatchable Feeder

This chapter introduces the technical power flow restriction on the line connecting the dispatchable feeder (DF) to the grid into the mathematical formulation of the three-level DF considering probabilistic forecasts[1] described in Subsection 2.4.1, which we refer to as the line-restricted dispatchable feeder (LRDF). Furthermore, we evaluate the ability of the LRDF to mitigate line overloadings. In doing so, we compare the performance of the LRDF with five benchmarks. The research question addressed is:

RQ5: *How to consider the line restriction and mitigate line overloadings for the dispatchable feeder considering probabilistic forecasts?*

The remainder of this chapter is structured as follows. First, Section 8.1 introduces the line restriction. Then, Section 8.2 describes the experimental setup to evaluate the LRDF in Subsection 8.2.1 and presents the results in Subsection 8.2.2. Finally, Section 8.3 discusses the results.

8.1 Introduction Line Restriction

In order to mitigate the line overloadings in the low-voltage distribution grid coming from the rising electrical energy demand and the massive integration of distributed renewable energy sources, we propose to model each building as a three-level line-restricted dispatchable feeder considering probabilistic forecasts (LRDF). The LRDF differs from the three-level dispatchable feeder (DF) considering probabilistic forecasts by adding the technical restriction of the line in the mathematical formulation of the optimisation problem (OP). In contrast to market-based mechanisms that aim to comply with line restrictions through price signals, e.g. [47], we implement the line restriction as a fixed, time-independent technical restriction within the OP. As we stay in the single-building scenario, the line restriction corresponds to a

[1]The content of this chapter is based on [145]. While the concept is the same, the experimental setup differs, including the forecasting specification, the used prosumption data, and the used BESS energy capacity.

single building's share on the street line. As a result, the line restriction reflects the individual building's contribution to potential line overloadings without considering potential load-shifting or balancing effects between neighbouring buildings. This line restriction is added in all considered levels, i.e.

$$\begin{aligned} \underline{p}_{g_{DS}} \leq & p_{g_{DS}}(k) \leq \overline{p}_{g_{DS}} && \text{(1. Level)} \\ \underline{p}_{g_{reDS}} \leq & p_{g_{reDS}}(k) \leq \overline{p}_{g_{reDS}} && \text{(2. Level)} \\ \underline{p}_{g} \leq & p_{g}(k) \leq \overline{p}_{g} && \text{(3. Level)} \end{aligned} \tag{8.1}$$

with lower and upper limits $\underline{p}_{g_{DS}} \leq \overline{p}_{g_{DS}} \in \mathbb{R}$, $\underline{p}_{g_{reDS}} \leq \overline{p}_{g_{reDS}} \in \mathbb{R}$, and $\underline{p}_{g} \leq \overline{p}_{g} \in \mathbb{R}$. In this thesis, we use the same lower and upper limits in all levels, i.e. $\underline{p}_{g_{DS}} = \underline{p}_{g_{reDS}} = \underline{p}_{g}$ and $\overline{p}_{g_{DS}} = \overline{p}_{g_{reDS}} = \overline{p}_{g}$, and set $-\underline{p}_{g} = \overline{p}_{g} =: p^{*}$.

The consequences of the line restriction are twofold: First, the power exchange between the LRDF and the grid is limited, which, together with the technical power capacity $p_s^{\max}$ and energy capacity $e_s^{\max}$ of the battery energy storage system (BESS), results in a potentially infeasible OP. As the LRDF holds power and energy reserves for the uncertainty of the prosumption via the reformulated power and energy chance constraints in the computation of the dispatch schedule (DS) in Equation (2.24), the BESS' effective power and energy capacity are further reduced. While this reduction is fixed by the security level parameter ϵ_P for the power chance constraint, the security level of the energy chance constraint can be relaxed by the relaxation parameters $\epsilon_{\text{fix}}(k)$ and $\epsilon_{\text{var}}(k)$. This leads to the second consequence, namely that the line restriction in the first level OP for the computation of the DS can lead to relaxed security levels of the reformulated energy chance constraint via the relaxation parameters $\epsilon_{\text{fix}}(k)$ and $\epsilon_{\text{var}}(k)$ and thus to a lower reserve of the BESS for the energy uncertainty of the prosumption. As a consequence, more imbalances may occur.

These consequences show that it is important to coordinate the line restriction p^{*}, the technical BESS' power capacity $p_s^{\max}$ and energy capacity $e_s^{\max}$, and the power and energy reserves held for the uncertainty of the prosumption via the security level parameters ϵ_P and ϵ_E. In cases where this coordination is not possible, additional flexibility providing measures, such as demand-side management, could be considered to overcome the infeasibility of the OP.

With the inclusion of the line restriction, we aim to analyse the feasibility of the OP for the LRDF with different line restrictions and thus the ability to mitigate line overloadings. Additionally, we evaluate how the problem-specific parameters of the BESS energy capacity $e_s^{\max}$ and the security level parameters ϵ_P and ϵ_E for the reformulated power and energy chance constraints influence the feasibility.

8.2 Evaluation

This section evaluates the line-restricted dispatchable feeder (LRDF). Consequently, Subsection 8.2.1 presents the experimental setup, whereas Subsection 8.2.2 shows the results.

8.2.1 Experimental Setup

The following describes the used data, how the probabilistic forecasts are generated, the benchmarks for comparison of the LRDF, and the considered evaluation metrics.

Data To address the efficiency increase and the broader expansion of PV panels since 2013, we scale the PV power generation with a factor of three, i.e. we use $\beta_{\text{PV}} = 3$ in Equation (2.27). Due to the computational effort[2] to generate the results for the LRDF and the comparison with several benchmarks, we limit the evaluation to building 109. In addition, we choose twelve weeks, namely the days from the 9th to the 15th for the months from July 2012 to June 2013.
For the BESS, we use the BESS energy capacity $e_s^{\max}$ of 19.5 kWh. When analysing the influence of the BESS energy capacity, we further consider $e_s^{\max}$ of 13.5, 16.5, and 22.5 kWh.
For the security level parameters ϵ_P and ϵ_E for the reformulated power and energy chance constraint, we perform the evaluation for multiple parameters, namely for ϵ_P of 0.25, 0.40, 0.55, 0.70, 0.85 and ϵ_E of 0.10, 0.25, 0.40, 0.55, 0.70, 0.85. Then, we chose two combinations of security level parameters. First, we chose for each week the combination that results in the best performance of the LRDF. The specific security level parameters chosen each week are given in Appendix A.6. These weekly selections represent optimal parameters, which could potentially be predicted in practice based on calendar features, the optimal parameters from the previous week, or forecasted weather uncertainty. Second, we identify a single set of security level parameters that performs well across the initial three weeks and apply this fixed combination to all subsequent weeks. For this fixed parameter approach, we use

[2] To generate the results of the LRDF for one week, one building, and one combination of security level parameters ϵ_P and ϵ_E, the required forecasts must be generated and the OP must be calculated. For the generation of the forecasts, the transformation of the energy forecasts is the most time consuming task, see Subsection 6.1.1. The approximate time needed for the total of 252 transformations for one week is 98.28 seconds. Additionally, the OP runtime for one week and one combination of security level parameters ϵ_P and ϵ_E is approximately 107.44 seconds.

$\epsilon_P = 0.55$ and $\epsilon_E = 0.7$. To differentiate the results from these two approaches, we refer to the LRDF with weekly optimal security level parameters as **LRDF$^{\text{opt}}$** and to the LRDF with fixed security level parameters $\epsilon_P = 0.55$ and $\epsilon_E = 0.7$ as **LRDF$^{\text{fix}}$**.

Forecast Method The LRDF requires the probabilistic forecasts of $q_{P_l(k)}$ and $F_{\Delta E_l(k+1)}$ generated at 12 PM for the computation of the DS and the point forecasts of $\overline{p}_l(k)$ for each hour for the rescheduling via MPC. Therefore, we train 24 NNs, one for each hour of the day. While the NN generating the forecasts at 12 PM has the same specifications as described in Subsection 6.2.1, the NNs for all other hours only output the quantile forecasts of $q_{P_l(k)}$ and $q_{E_l(k)}$ for the next eight hours, using the median forecast of $q_{P_l(k)}$ as the point forecast of $\overline{p}_l(k)$. The reason for shortening the forecast horizon is to improve the forecast quality of the forecasts for these hours, while still covering the necessary hours for the rescheduling via MPC. For a detailed description of the forecast specifications, the input features, the splitting of the data in training, validation, and testing, and the neural network architecture, the reader is referred to Subsection 4.2.1 and Subsection 6.2.1. Additionally, as described in Subsection 6.1.1, the quantile forecasts of $q_{E_l(k+1)}$ have to be transformed into the input for the LRDF, namely the CDF forecasts of $F_{\Delta E_l(k+1)}$. This involves transforming the quantile forecasts into a closed-form CDF. While in Subsection 6.2.2 this transformation is done via the one log approach, we use the weighted two log approach described in Subsection 6.1.1 to account for the skewness of the CDF forecasts of $F_{\Delta E_l(k+1)}$. This approach is computationally affordable in the subsequent evaluation due to the limitation to building 109.
Finally, as NNs are inherently stochastic forecast methods, meaning their forecasts can vary with each training run, we generate five sets of forecasts for each hour. While we present the results of one set of forecasts in this chapter, a summary of the results across all sets of forecasts is provided in Appendix A.7 to give a more comprehensive view of the overall performance and variability.

Benchmarks We compare the LRDF against five benchmarks evaluating three aspects. First, to evaluate the LRDF's hierarchical operation, we use two benchmarks, namely **no BESS** and **simple BESS operation**. In the benchmark no BESS, no BESS exists. Hence, the prosumption is not shaved and the actual prosumption equals the actual dispatch. Thus, the maximum absolute value of the actual prosumption is crucial for respecting the line restriction. In the benchmark simple BESS operation, we use the simple BESS operation from the PowerFactory library [51]. More precisely, the BESS charges as much power as possible if the PV power generation exceeds the load. The other way around, if the load exceeds the PV power generation, the BESS

discharges as much power as possible.
Second, to evaluate the impact of considering the line restriction in the mathematical formulation, we compare the LRDF with the three-level DF considering probabilistic forecasts without the line restriction, which we refer to as **no LR**.
Finally, to evaluate the sensitivity of the considered uncertainty, we use the LRDF considering perfect forecasts **LRDF$_{\text{perf}}$** and considering point forecasts **LRDF$_{\text{point}}$**. For the LRDF considering perfect forecasts, perfect knowledge of future prosumption eliminates the need for forecasts, reducing the hierarchical OP to the first level. The solution of this benchmark equals the best possible solution for the LRDF. For the LRDF considering point forecasts, the line restriction is added to the three-level DF considering point forecasts described in Subsection 2.4.1. For better comparability, we use the median forecasts $\hat{q}_{P_l(k)}(0.5)$ as point forecasts.

Evaluation Metrics As we consider the single-building scenario, the line restriction corresponds to a single building's share on the street line. Therefore, the lower the line restriction can be set, the lower the chance of line overloadings and the more buildings can be served via the same street line. Thus, for evaluation of the LRDF, we consider the minimum possible line restriction (MPLR). It corresponds to the minimum value of p^*, for which the OP is still feasible. To obtain the MPLR for the LRDF, we first calculate the maximum absolute value of the actual dispatch within the considered week of the three-level DF considering probabilistic forecasts without the line restriction, i.e. the benchmark no LR. Then, we successively reduce p^* by 0.1 kW and solve the OP until it is infeasible. The same procedure is done for the benchmarks LRDF$_{\text{perf}}$ and LRDF$_{\text{point}}$. For the benchmark no BESS, the MPLR corresponds to the maximum absolute value of the actual prosumption and for the benchmark simple BESS operation the MPLR corresponds to the maximum absolute value of the actual dispatch.
Furthermore, we consider six further evaluation metrics. First, to assess the ability to shave the peaks of the maximum absolute value of the actual prosumption, i.e. the MPLR of the benchmark no BESS, we consider the percentage of peak shaving

$$\%\text{PS}_{\text{no BESS}} = \frac{\text{MPLR}_{\text{no BESS}} - \text{MPLR}_{\text{approach}}}{\text{MPLR}_{\text{no BESS}}} \cdot 100. \tag{8.2}$$

Second, to assess the impact of adding the line restriction in the mathematical formulation, we consider the percentage of differences in MPLR relative to the benchmark no LR

$$\%\text{diff}_{\text{no LR}} = \frac{1}{|\mathcal{C}|} \sum_{i \in \mathcal{C}} \mathbb{1}_{\{\text{MPLR}_{\text{no LR}}(i) > \text{MPLR}_{\text{LRDF}}(i)\}} \tag{8.3}$$

with $\mathcal{C}$ referring to the set of all considered cases, namely the weeks and the security level parameters ϵ_P, for a specific energy security level parameter ϵ_E, and indicator function $\mathbb{1}$. This metric considers only the number of differences and not the height of the differences in MPLR. To assess the height of the differences in MPLR relative to the benchmark no LR, we calculate the minimum, average, and maximum of the differences over all cases, in which we observe a difference, i.e.

$$\min\{\text{diff}\}_{\text{no LR}} = \min_{i \in \mathcal{C}}\{\text{diff}_i\}, \tag{8.4}$$

$$\text{average}\{\text{diff}\}_{\text{no LR}} = \frac{\sum_{i \in \mathcal{C}} \text{diff}_i}{\sum_{i \in \mathcal{C}} \mathbb{1}_{\{\text{MPLR}_{\text{no LR}}(i) > \text{MPLR}_{\text{LRDF}}(i)\}}}, \tag{8.5}$$

$$\max\{\text{diff}\}_{\text{no LR}} = \max_{i \in \mathcal{C}}\{\text{diff}_i\} \tag{8.6}$$

with $\text{diff}_i = (\text{MPLR}_{\text{no LR}}(i) - \text{MPLR}_{\text{LRDF}}(i)) \cdot \mathbb{1}_{\{\text{MPLR}_{\text{no LR}}(i) > \text{MPLR}_{\text{LRDF}}(i)\}}$. Finally, to assess the sensitivity of the considered uncertainty, we compare the percentage share of the MPLR relative to the MPLR using the benchmark $\text{LRDF}_{\text{perf}}$, i.e.

$$\%\text{share}_{\text{perf}} = \frac{\text{MPLR}_{\text{LRDF}_{\text{perf}}}}{\text{MPLR}_{\text{approach}}} \cdot 100. \tag{8.7}$$

The higher the percentage of MPLR relative to the MPLR using the benchmark $\text{LRDF}_{\text{perf}}$, the closer the MPLR to the best possible solution.

8.2.2 Results

We evaluate the line-restricted dispatchable feeder (LRDF) with respect to four aspects. First, we assess the hierarchical operation of the LRDF. Second, we analyse the impact of adding the line restriction in the mathematical formulation of the three-level DF considering probabilistic forecasts. Third, we investigate the sensitivity of the considered uncertainty of the prosumption. Finally, we evaluate the impact of problem-specific parameters, namely the BESS energy capacity $e_s^{\max}$ and the security level parameters ϵ_P and ϵ_E.

Benchmarking the BESS Operation

In this subsection, we qualitatively and quantitatively compare the hierarchical operation of the LRDF with the benchmark no BESS and the benchmark simple BESS operation. For the qualitative comparison, we examine the actual dispatch and the corresponding SoE of the BESS for week 2. For the quantitative comparison, we

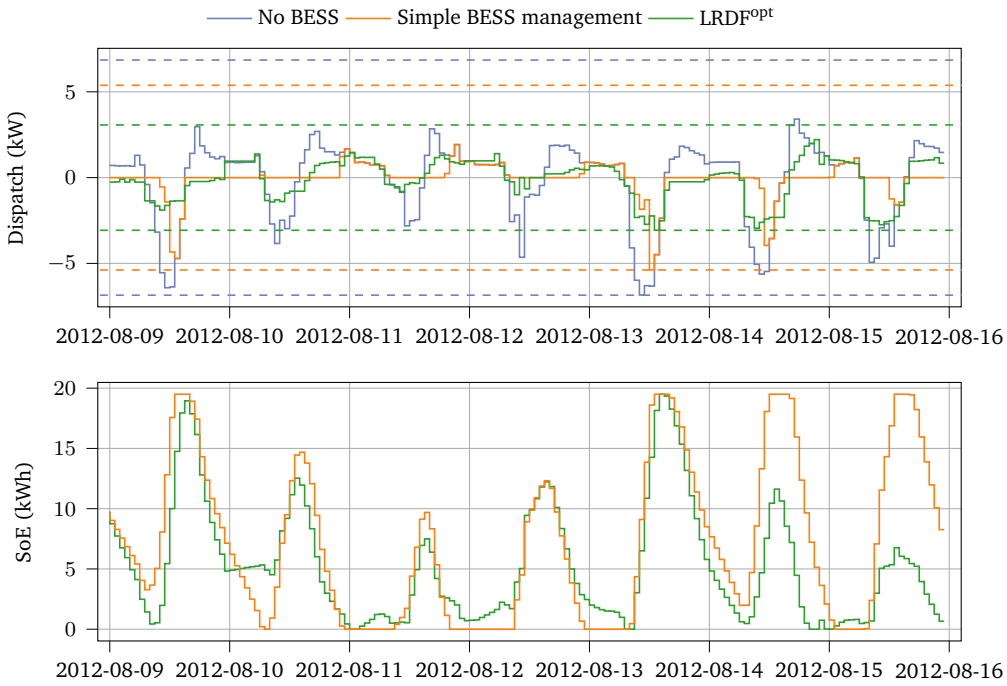

Fig. 8.1.: The actual dispatch and the corresponding BESS' state of energy of the benchmark no BESS, the benchmark simple BESS operation, and the LRDF^{opt} for week 2 with the minimum possible line restriction of the benchmark no BESS in dashed blue (6.85 kW), of the benchmark simple BESS operation in dashed orange (5.38 kW), and of the LRDF^{opt} in dashed green (3.07 kW)

compare the MPLR and the percentage of peak shaving relative to the benchmark no BESS for all weeks.

Qualitative Comparison Figure 8.1 shows the actual dispatch and the corresponding BESS' SoE for both benchmarks and the LRDF^{opt} exemplary for week 2. For the LRDF^{opt}, we set the line restriction to the MPLR of week 2, i.e. 3.07 kW. In this figure, we make two observations. First, we see that while the benchmark no BESS does not shave the actual prosumption, the benchmark simple BESS operation achieves some improvement. In contrast, the LRDF^{opt} noticeably reduces the negative peaks. This difference in peak shaving is reflected in the MPLRs. The MPLR of the benchmark no BESS is 6.85 kW and of the benchmark simple BESS operation is 5.38 kW. In correspondence to the first observation, we, secondly, observe differences in the BESS' SoE for the LRDF^{opt} and the benchmark simple BESS operation. The benchmark simple BESS operation charges the BESS in the first hours of PV power overgeneration to its full capacity at the first and the fifth day. In contrast, the LRDF^{opt} operates the BESS leaving reserves for the whole period of PV power overgeneration.

Tab. 8.1.: The minimum possible line restriction in kW of the benchmark no BESS, the benchmark simple BESS operation, the LRDF$^{\text{fix}}$, and the LRDF$^{\text{opt}}$, and the percentage of peak shaving relative to the benchmark no BESS in % of the benchmark simple BESS operation, the LRDF$^{\text{fix}}$, and the LRDF$^{\text{opt}}$ for all considered weeks.

Week	No BESS	Simple BESS operation		LRDF$^{\text{fix}}$		LRDF$^{\text{opt}}$	
	MPLR	MPLR	$\%\text{PS}_{\text{no BESS}}$	MPLR	$\%\text{PS}_{\text{no BESS}}$	MPLR	$\%\text{PS}_{\text{no BESS}}$
1	6.11	4.69	23.24	3.63	40.59	**3.37**	**44.84**
2	6.85	5.38	21.46	**3.07**	**55.18**	**3.07**	**55.18**
3	9.16	8.83	3.60	**5.54**	**39.52**	**5.54**	**39.52**
4	10.50	10.50	0.00	7.14	32.00	**6.52**	**37.90**
5	11.36	11.36	0.00	9.09	19.98	**8.10**	**28.70**
6	6.63	6.58	0.75	4.72	28.81	**4.49**	**31.76**
7	11.01	8.77	20.35	7.47	32.15	**7.20**	**34.60**
8	11.18	11.18	0.00	7.24	35.24	**6.30**	**43.65**
9	9.81	9.81	0.00	5.67	42.20	**5.65**	**42.40**
10	7.96	7.89	0.88	**5.66**	**28.89**	**5.66**	**28.89**
11	6.54	5.40	17.43	3.90	40.37	**3.30**	**49.54**
12	5.55	2.55	54.05	3.05	45.05	**2.60**	**53.15**

Quantitative Comparison For all weeks, Table 8.1 shows the MPLR and $\%\text{PS}_{\text{no BESS}}$. In this table we observe that the benchmark no BESS and simple BESS operation achieve similar MPLR in seven weeks. In contrast, both LRDFs clearly enable a lower MPLR compared to the benchmark no BESS achieving a peak shaving by at least 19.98% for LRDF$^{\text{fix}}$ and 28.70% for LRDF$^{\text{opt}}$ for all weeks. The comparison of the benchmark simple BESS operation and the LRDFs shows that the LRDFs achieve a lower MPLR and a higher peak shaving for almost all weeks. Outstanding is week 12, in which the benchmark simple BESS operation achieves a smaller MPLR and thus a higher peak shaving than the LRDFs. When comparing the LRDF$^{\text{opt}}$ with the LRDF$^{\text{fix}}$, we observe a lower MPLR and a higher peak shaving for the LRDF$^{\text{opt}}$ in eight weeks. Further, we observe that the MPLR highly depends on the considered week for the LRDFs and both benchmarks.

Impact of Line Restriction

To assess the impact of the line restriction in the mathematical formulation, we qualitatively and quantitatively compare the LRDF with the benchmark no LR. For the qualitative comparison, we analyse the dispatches and the corresponding BESS' SoE of the first and third level for week 5. For the quantitative comparison, we evaluate the percentage of differences in MPLR relative to the benchmark no LR, and the minimum, average, and maximum of the differences in the MPLR relative to the benchmark no LR.

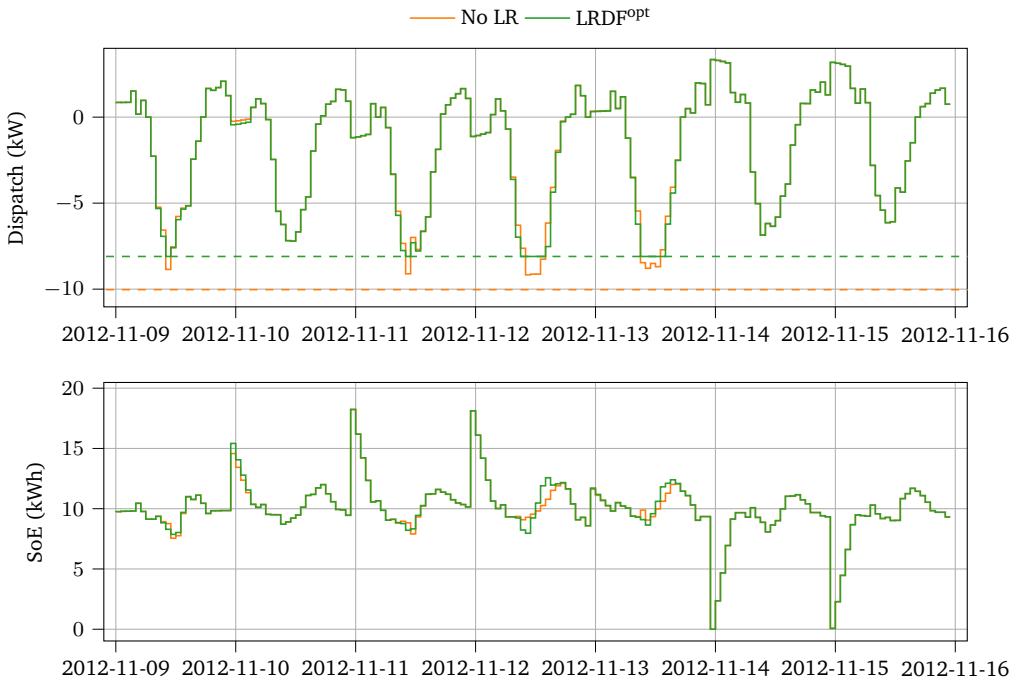

(a) The DS $p_{g_{DS}}$ and the corresponding SoE.

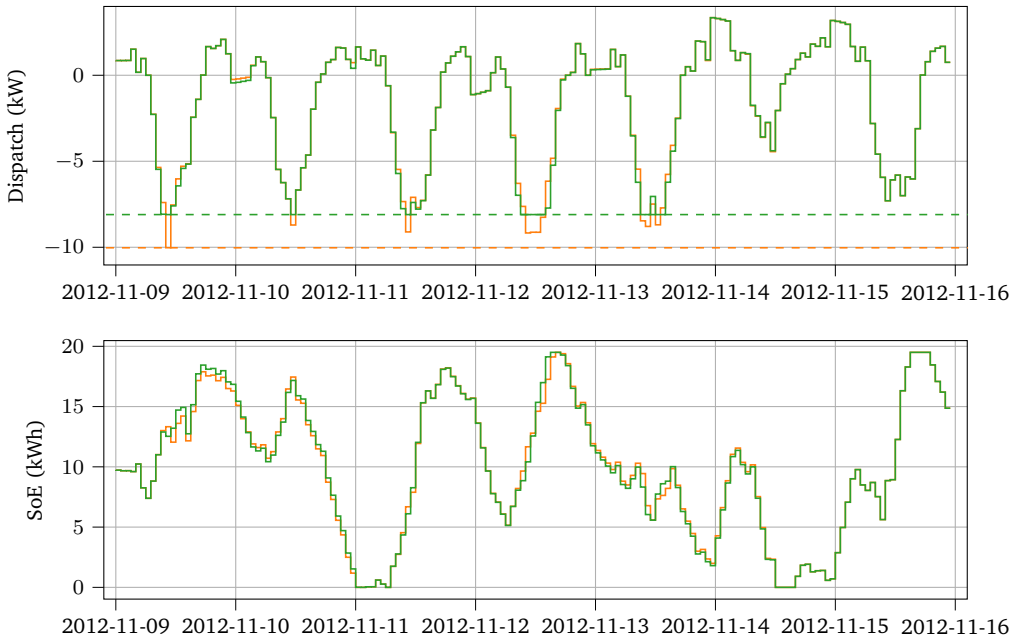

(b) The actual dispatch p_g and the corresponding SoE.

Fig. 8.2.: The dispatches and the corresponding BESS' state of energy for the first (a) and third level (b) of the benchmark no LR and the LRDF^{opt} for week 5 with the minimum possible line restriction of the benchmark no LR in dashed orange (10.03 kW) and of the LRDF in dashed green (8.10 kW).

Tab. 8.2.: The percentage of differences in the minimum possible line restriction in %, the minimum, the average, and the maximum of the differences in the minimum possible line restriction in kW of the LRDF relative to the benchmark no LR over all considered weeks and security level parameters ϵ_P.

ϵ_E	$\%\text{diff}_{\text{no LR}}$	$\min\{\text{diff}\}_{\text{no LR}}$	$\text{average}\{\text{diff}\}_{\text{no LR}}$	$\max\{\text{diff}\}_{\text{no LR}}$
0.10	90%	0.22	1.51	4.07
0.25	92%	0.09	1.53	4.05
0.40	67%	0.15	0.91	1.68
0.55	10%	0.12	0.31	0.40
0.70	8%	0.05	0.35	0.66
0.85	8%	0.05	0.35	0.66

Qualitative Comparison Figure 8.2 shows the results for week 5 of the benchmark no LR and the LRDF^{opt}. The line restriction of the LRDF^{opt} is set to the MPLR, i.e. 8.10 kW. The MPLR of the benchmark no LR and thus the maximum absolute value of the actual prosumption is 10.03 kW. For days 1, 2, 3, 4, and 5, we see a difference in the DS and the BESS' SoE. These differences are particularly visible during hours of high PV power generation, where the BESS' SoE of the LRDF^{opt} charges slightly more and thus shaves the peaks of the DS and the actual dispatch more compared to the benchmark no LR. During some of these hours, we observe slightly higher values of the relaxation parameter ϵ_{fix} for the LRDF^{opt}.

Quantitative Comparison Table 8.2 shows $\%\text{diff}_{\text{no LR}}$, $\text{minimum}\{\text{diff}\}_{\text{no LR}}$, $\text{average}\{\text{diff}\}_{\text{no LR}}$, and $\text{maximum}\{\text{diff}\}_{\text{no LR}}$ over all weeks and security level parameters ϵ_P for all considered security level parameters ϵ_E. In this table we can see that taking the line restriction into account reduces the maximum absolute value of the actual prosumption in at least 90% of the considered cases with an average of at least 1.51 kW for ϵ_E of 0.10 and 0.25. While considering the line restriction still has an impact for the majority of cases for ϵ_E of 0.40, this impact is reduced to at most 10% of cases for a greater ϵ_E. For these ϵ_E, we observe that the average reduction of the maximum absolute value of the actual prosumption is around 0.30 kW.

Sensitivity to Considered Uncertainty

In this subsection, we qualitatively and quantitatively investigate the sensitivity of the considered uncertainty. Therefore, we compare the LRDF with the benchmarks $\text{LRDF}_{\text{perf}}$ and $\text{LRDF}_{\text{point}}$. For the qualitative comparison, we examine the dispatches and the corresponding SoEs of the BESS of the first and third level for week 11. For the quantitative comparison, we compare the MPLR and the percentage share of MPLR relative to the benchmark $\text{LRDF}_{\text{perf}}$ for all weeks.

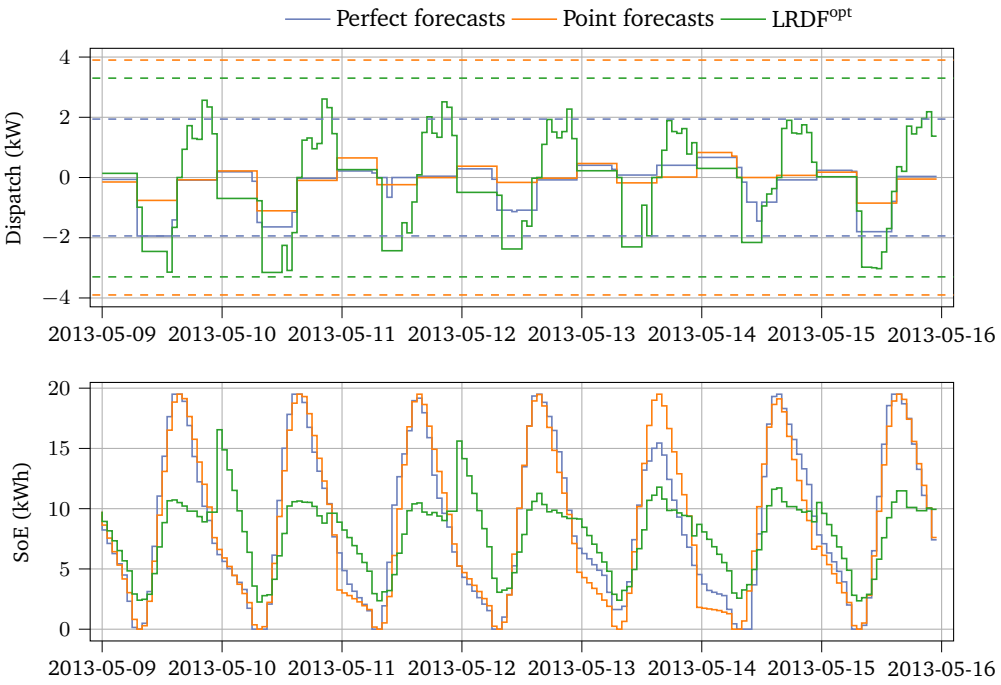

(a) The DS $p_{g_{DS}}$ and the corresponding SoE.

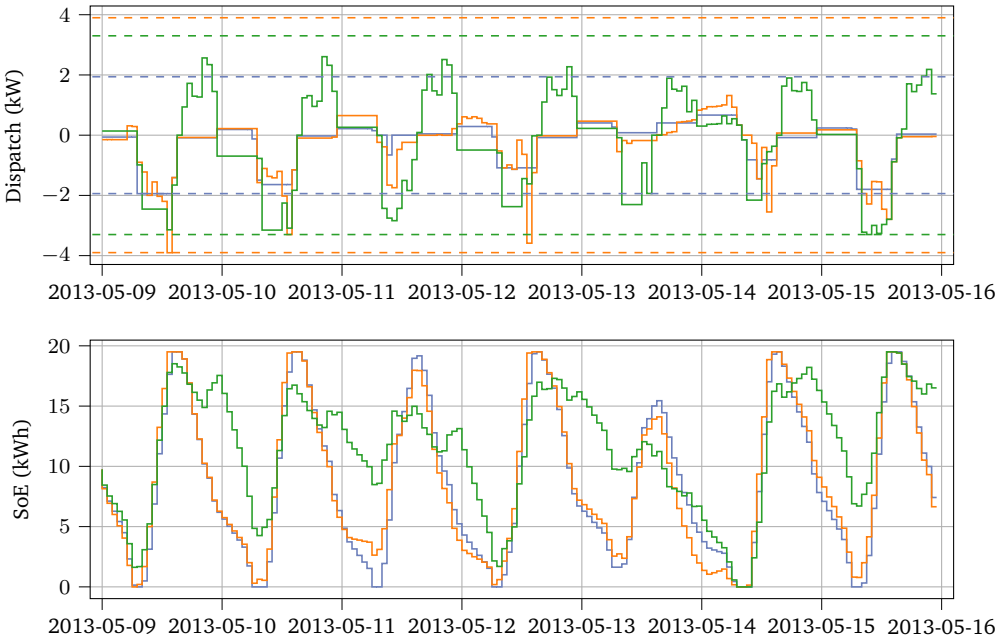

(b) The actual dispatch p_g and the corresponding SoE.

Fig. 8.3.: The dispatches and the corresponding BESS' state of energy for the first (a) and third level (b) of the benchmark $\text{LRDF}_{\text{perf}}$, the benchmark $\text{LRDF}_{\text{point}}$, and the LRDF^{opt} for week 11. The minimum possible line restriction of the benchmark $\text{LRDF}_{\text{perf}}$ in dashed blue (1.94 kW), of the benchmark $\text{LRDF}_{\text{point}}$ in dashed orange (3.90 kW), and of the LRDF^{opt} in dashed green (3.30 kW)

Tab. 8.3.: The minimum possible line restriction in kW of the benchmark $\text{LRDF}_{\text{perf}}$, the benchmark $\text{LRDF}_{\text{point}}$, the LRDF^{fix}, and the LRDF^{opt}, and the percentage share of minimum possible line restriction relative to the benchmark $\text{LRDF}_{\text{perf}}$ in % of the benchmark $\text{LRDF}_{\text{point}}$, the LRDF^{fix}, and the LRDF^{opt} for all considered weeks. Note that the higher the percentage of minimum possible line restriction relative to the benchmark $\text{LRDF}_{\text{perf}}$, the closer the minimum possible line restriction to the best possible solution.

Week	$\text{LRDF}_{\text{perf}}$	$\text{LRDF}_{\text{point}}$		LRDF^{fix}		LRDF^{opt}	
	MPLR	MPLR	$\%\text{share}_{\text{perf}}$	MPLR	$\%\text{share}_{\text{perf}}$	MPLR	$\%\text{share}_{\text{perf}}$
1	1.61	3.71	43.40	3.63	44.35	3.37	47.77
2	2.27	3.15	72.06	3.07	73.94	3.07	73.94
3	4.57	5.70	80.18	5.54	82.49	5.54	82.49
4	5.93	7.14	83.05	7.14	83.05	6.52	90.95
5	6.67	9.11	73.22	9.09	73.38	8.10	82.35
6	3.01	4.49	67.04	4.72	63.77	4.49	67.04
7	6.05	7.48	80.88	7.47	81.00	7.20	84.03
8	6.18	7.27	85.00	7.24	85.36	6.30	98.10
9	5.07	5.68	89.26	5.67	89.42	5.65	89.73
10	3.15	5.73	54.97	5.66	55.65	5.66	55.65
11	1.94	3.90	49.74	3.90	49.74	3.30	58.79
12	1.03	3.05	33.77	3.05	33.77	2.60	39.62

Qualitative Comparison Figure 8.3 shows the dispatches and the corresponding BESS' SoE for the two benchmarks and the LRDF_{opt} exemplary for week 11. The line restrictions are set to the respective MPLR, i.e. 1.94 kW for the benchmark $\text{LRDF}_{\text{perf}}$, 3.90 kW for the benchmark $\text{LRDF}_{\text{point}}$, and 3.30 kW for the LRDF^{opt}. In the first level, we see that the BESS of the LRDF^{opt} is never fully charged or discharged. In contrast, the BESS of the benchmark $\text{LRDF}_{\text{perf}}$ and the benchmark $\text{LRDF}_{\text{point}}$ reach the upper and lower BESS energy capacity limit on several hours. This results in a lower maximum absolute value of the DS for both benchmarks compared to the LRDF^{opt}. However, while the LRDF^{opt} can almost maintain the maximum absolute value of the DS with the actual dispatch, the benchmark $\text{LRDF}_{\text{point}}$ deviates especially during the PV power generation hours from its DS, resulting in a higher MPLR. Compared to the benchmark $\text{LRDF}_{\text{perf}}$, the actual SoE of the benchmark $\text{LRDF}_{\text{point}}$ is similar, with one crucial difference, namely that the BESS is charged to its upper limit $e_s^{\max} = 19.5$ earlier during the PV power generation hours.

Quantitative Comparison Table 8.3 shows the MPLR and $\%\text{share}_{\text{perf}}$ for all weeks. We describe three observations. First, we see that the LRDF^{opt} achieves a MPLR and thus a percentage share at least as well as the benchmark $\text{LRDF}_{\text{point}}$ for all weeks. However, there are no or only small differences between the LRDF^{opt} and the benchmark $\text{LRDF}_{\text{point}}$ in weeks 2, 6, 9, and 10. Second, we observe that the LRDF^{fix} performs inferior than the LRDF^{opt} in eight weeks. Additionally, the LRDF^{fix}

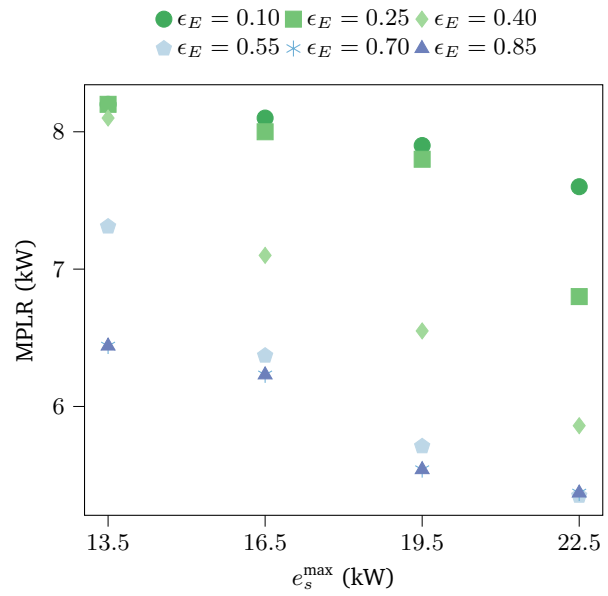

(a) Week 3

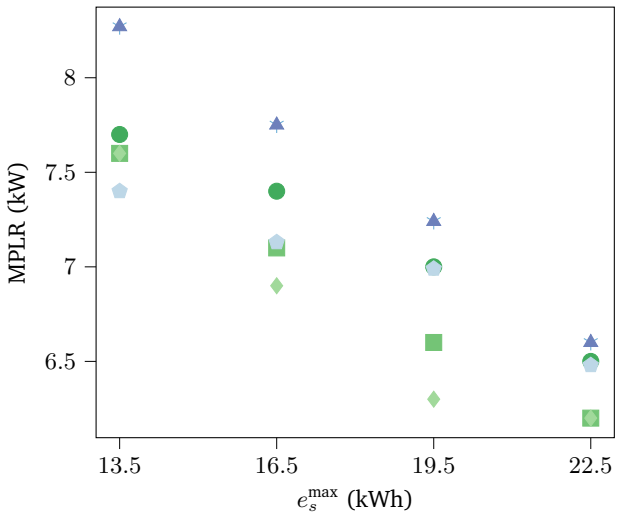

(b) Week 8

Fig. 8.4.: The minimal possible line restriction for different BESS energy capacities $e_s^{\max}$ and different security level parameter ϵ_E for week 3 and 8. Note that ϵ_P is set to 0.25.

performs inferior compared to the benchmark $\text{LRDF}_{\text{point}}$ in week 6. Finally, we observe that the percentage shares vary in the considered weeks. Outstanding are weeks 1 and 12, which result in low percentage shares for both the LRDFs and the benchmark $\text{LRDF}_{\text{point}}$.

Impact of Problem-Specific Parameters

While in the analyses above, the BESS energy capacity $e_s^{\max}$ and the security level parameters ϵ_P and ϵ_E are set to specific values, we analyse in this subsection the impact of these parameters on the MPLR. Figure 8.4 shows the MPLR of the LRDF for different BESS energy capacities $e_s^{\max}$ and security level parameters ϵ_E for weeks 3 and 8. We make three observations. First, we observe that the choice of the security level parameter ϵ_E can have an impact on the MPLR depending on the week. In contrast, the security level parameter ϵ_P has less impact on the MPLR, which is why we do not explicitly show the results. Second, the MPLR for most ϵ_E is decreasing with an increasing BESS energy capacity in both weeks. Third, the relation between BESS energy capacity and ϵ_E with respect to the best MPLR is not clear. While in week 3, there is a clear tendency for a bigger ϵ_E, such a clear tendency is not visible in week 8. In this week, we observe that a medium ϵ_E is beneficial with respect to the MPLR with a tendency to a smaller ϵ_E for a bigger BESS energy capacity.

8.3 Discussion

In this section, we discuss the findings of the results above, the limitations and further research.

8.3.1 Findings

We discuss the evaluation of the LRDF focusing on five aspects. First, we discuss the performance of the LRDF using a hierarchical OP for BESS operation. Second, we discuss the impact of considering the line restriction in the mathematical formulation. Third, we discuss the impact of using probabilistic forecasts. Fourth, we discuss the impact of the BESS energy capacity and the security level parameters. Finally, we return to the research question posed in this chapter and assess how the findings contribute to answering it.

First, regarding the performance of LRDF as hierarchical OP, the results show that including a scheduling and rescheduling level reduces the MPLR and thus increases the number of buildings a street line can serve. More specifically, compared to the benchmark simple BESS operation, the LRDF is beneficial because of the consideration of prosumption forecasts in addition to the actual prosumption values. Thus, the LRDF leaves BESS reserves to shave peaks for the whole period of PV power overgeneration. However, we also observe that the MPLR is dependent on

the week. These fluctuations may be caused by the varying prosumption profiles and the quality of the forecasts.

Second, regarding the impact of the line restriction in the mathematical formulation, the results show that the DS, the actual dispatch, and the corresponding SoEs can vary when considering the line restriction. Notably, negative peaks are shaved as a full PV power feed-in would violate the line restriction. This peak shaving comes with a slightly stronger relaxed security level $1 - \epsilon_E$ over ϵ_{fix}. However, the assumption in Section 8.1 of more imbalances is not reflected in the cost. More precisely, the average daily imbalance cost for the LRDF are lower or negligibly higher than for the benchmark no LR for all weeks and security levels considered. Together with the lower average daily DS cost for the LRDF due to less power exchange with the grid, the LRDF results in lower average daily total cost compared to the benchmark no LR. In the single-building scenario, these results demonstrate that the LRDF can respect and adapt to a line restriction. Since the single-building scenario is analogous to a multiple-building scenario with a fixed share of the street line capacity, these results can be generalised accordingly. Furthermore, the results show that the smaller the security level parameter ϵ_E, the greater the impact of the line restriction. This can be explained as follows: The smaller the security level parameter ϵ_E and thus the higher the reserve held for the prosumption energy uncertainty, the less the BESS can be used for peak shaving and thus the higher the potential for reducing the exchange with the grid. However, simply reducing the reserve held for the prosumption uncertainty may not result in a lower maximum absolute value of the actual dispatch, as actual prosumption values that deviate from its point forecast, especially at the end of PV power generation hours, may result in high peaks.

Third, regarding the impact of using probabilistic forecasts, the results indicate that considering probabilistic forecasts in the mathematical formulation of the three-level DF considering probabilistic forecasts can reduce line overloadings compared to point forecasts. However, the LRDF does not reach the MPLR of the DF considering perfect forecasts, which is an upper but unrealistic bound for the given setup. Furthermore, we observe different performances of the LRDF within the considered weeks. In eight out of twelve weeks the LRDF achieves a MPLR over 60% of the best possible solution. In the remaining weeks, which fall in the Australian winter months, we observe an underconfidence in calibration, particularly for the quantile forecasts of $q_{E_l(k+1)}$, while maintaining a similar sharpness to the quantile forecasts of other weeks. This suggests that the forecasts may be too conservative, overestimating the uncertainty. As a consequence, the LRDF may hold more reserve for the prosumption energy uncertainty in the BESS preventing a reduction of the MPLR.

Fourth, regarding the impact of the BESS energy capacity and the security level parameters, we observe that a higher BESS energy capacity results in a lower

MPLR, which makes sense because a higher BESS energy capacity can reduce the exchange between the LRDF and the grid. For the security level parameter ϵ_E, there is a trade-off for the operation of the BESS between reserve for the prosumption energy uncertainty and usage to reduce the MPLR. Therefore, a higher security level parameter ϵ_E may result in a lower MPLR. However, this strongly depends on the characteristics of the probabilistic forecasts of $F_{\Delta E_l(k+1)}$. More precisely, if the actual values align with the probabilistic forecasts, it may be beneficial to use a bigger ϵ_E. This is the case for week 3, which has a good calibration, sharpness, and CRPS. However, no such interpretable explanation can be found for week 8. These results imply that choosing the security level parameter ϵ_E for a specific BESS energy capacity with respect to the MPLR can be complex and should not be based solely on forecast quality metrics such as the CRPS. Additional weeks with more complex metrics could be evaluated to further understand the relationship. The impact of the security level parameters is further highlighted by the differences in performance between the LRDF with weekly optimal security level parameters and the LRDF with fixed security level parameters over all weeks. The results show that an inappropriate choice of security level parameters can lead to lower performance of the LRDF and even lower performance than when considering point forecasts. This highlights the critical role of a good choice of the security level parameters.
Finally, regarding the research question

RQ5: *How to consider the line restriction and mitigate line overloadings for the dispatchable feeder considering probabilistic forecasts?*

we can say that adding a fixed, time-independent technical restriction in the mathematical formulation of the three-level DF considering probabilistic forecasts can reduce line overloadings in the single-building scenario. Both the three-level operation and the consideration of probabilistic forecasts can be beneficial with respect to the MPLR. The extent of these benefits depends on the characteristics of the forecasts, the BESS energy capacity, and the security level parameters.

8.3.2 Limitations and Further Research

In the following, we examine the limitations and suggest directions for further research considering four aspects.
First, since our results highlight the critical role of the forecasts, further research could explore the impact of different forecasts on the MPLR. In this context, the choice of the security level parameter ϵ_E depending on the forecast could be elaborated.

Second, our evaluation is conducted on a weekly basis, which could be extended to a full year, including extreme cases, to obtain a more generalisable MPLR.
Third, the evaluation of the LRDF is limited to a single building with a fixed share of the street line. Future research could extend this scenario to include multiple buildings with a flexible share via the joint optimisation of the buildings coupled by the line restriction. This could include distributed optimisation to ensure data privacy, and individual cost functions for each building to take into account for individual objectives [40].
Finally, while we circumvent the infeasibility of the OP as explained in Section 8.1 by using the MPLR, further investigation is required when using a technical restriction of the street line, such as the choice of the BESS energy capacity and additional flexibility providing measures.

Part IV

Conclusion and Future Work

9 Conclusion

This thesis focuses on the dispatchable feeder (DF), which is a concept for making aggregated renewable energy sources (RES) and loads dispatchable using battery energy storage systems (BESS). As such, it is formulated as a stochastic optimisation problem using forecasts of the RES generation and loads as inputs. Consequently, both the forecasts and the mathematical formulation of the optimisation problem have an impact on the performance of the DF. Therefore, this thesis considers both aspects.

More precisely, in Chapter 4, we evaluate the DF's performance based on point forecasts with different characteristics obtained using different loss functions on a dataset of 300 residential buildings. As evaluation metrics we consider the average daily costs of the dispatch schedule, the imbalances, and the weighted sum of both. The results show that the forecast characteristics influence the forecast value for the DF and that this influence depends on the BESS energy capacity and the prosumption data. Thus, to improve the performance of the DF, it is beneficial to carefully consider the forecast characteristics, taking into account the considered forecast value, the BESS energy capacity, and the prosumption data. Moreover, achieving the best forecast value may require looking beyond the typical forecast characteristics determined by standard loss functions.

In Chapter 5, we introduce a framework to automatically select the forecast method with respect to the forecast value for the DF considering point forecasts based on meta-learning. The selection task is treated as a classification problem and a classifier is trained based on labels referring to the forecast method generating the forecast with the highest forecast value for the DF. This classifier outputs either the label of one forecast method or probabilities for each forecast method, which are used to generate an ensemble forecast. The results show that our framework reduces the average daily total cost and improves the accuracy compared to selecting the same forecast method for each building. Compared to manually selecting the forecasting method for each building, the proposed framework leads to a similar average daily total cost requiring noticeably less computational effort. In particular, using the classifier to generate ensemble forecasts is more beneficial with respect to the average daily total cost than using the classifier to select one forecast method.

In Chapter 6, we evaluate the DF's performance based on probabilistic forecasts

with different characteristics. Specifically, we modify the probabilistic forecasts to have either a bias or a different dispersion. Equivalent to the point forecast evaluation, we consider several average daily costs as forecast value. The results show that the forecast characteristics can influence the forecast value. Additionally, the results underline the strong relation between the security level parameters for the reformulated power and energy chance constraints and the dispersion of the forecast, and suggest that a coordination of the three leads to lower average daily cost.

In Chapter 7, we compare the performance of the DF considering point forecasts and the DF considering probabilistic forecasts over several buildings, using forecasts with different characteristics. More specifically, we consider both point forecasts and the probabilistic forecasts from Chapter 4 and Chapter 6 respectively, which lead to a high forecast value for the DF, as well as standard point and probabilistic forecasts. The results show that while the DF considering value-oriented probabilistic forecasts achieves the lowest total cost with imbalance cost factor $\alpha = 10$, the total cost with imbalance cost factor $\alpha = 2$ is comparable for all considered DFs. For this total cost, the best performing DF depends on the specific building. Additionally, the consideration of value-oriented point forecasts can result in total costs with imbalance cost factor $\alpha = 10$ that are similar to unmodified probabilistic forecasts, indicating that value-oriented point forecasts can compensate to some extent for the lack of integration of the prosumption uncertainty in the mathematical formulation.

Finally, in Chapter 8, we extend the mathematical formulation of the DF considering probabilistic forecasts to include the technical restriction of the street line, which we call line-restricted dispatchable feeder (LRDF). For the single-building scenario, the results on a selected building show that the LRDF can reduce line overloadings compared to a simple BESS management and DF without line restriction. Additionally, the results show that the consideration of probabilistic forecasts can be more beneficial in reducing line overloadings than the consideration of point forecasts. Thereby, the performance depends on the probabilistic forecast and the chosen security level parameters of the reformulated power and energy chance constraints.

10 Future Work

In addressing the research questions set out in Section 3.1 with the evaluations and frameworks presented, potential for future work emerged. Although some of these ideas for future work are mentioned in the individual chapters, these suggestions are expanded upon here. What follows is an overview of these ideas, grouped into three main categories.

Extension of the Forecast Evaluation and Forecast Method Selection

In order to broaden the application and robustness of the forecast evaluations and the proposed forecast method selection, several extensions could be made. These could include:

- Further forecast values, such as the minimum possible line restriction, and additional problem-specific parameters, such as the energy cost function parameters used in the computation of the dispatch schedule, could be considered.
- Both the forecast evaluation and the value-oriented forecast method selection could be extended and applied to other stochastic OPs.
- An online value-oriented forecast method selection could be developed, that continuously reclassifies the best forecast method based on current information.
- A value-oriented recalibration of probabilistic forecasts could be developed with respect to the performance of the DF considering probabilistic forecasts.
- Forecast methods could be specifically trained to generate forecasts with high forecast value for the DF, as demonstrated in [16].
- The forecast evaluation could be extended to advanced machine learning methods, such as foundation models and other approaches to generate the cumulative distribution function forecasts could be considered [136].

Extension of Mathematical Formulation of the Dispatchable Feeder

The mathematical formulation of the DF could be extended to include additional uncertainties and aspects. These could include:

- Uncertainty could be incorporated into the OP for rescheduling via model predictive control [130] and into the energy cost function used for the computation of the dispatch schedule.
- Additional aspects, such as demand-side management, a dynamic energy cost function, and more realistic models of the BESS and the grid, could be integrated into the formulation.
- Additional devices, such as heat pumps and electric vehicles, could be incorporated into the mathematical formulation.
- The mathematical formulation could be extended to multi-objective optimisation to handle multiple conflicting objectives, such as minimising energy cost while also minimising imbalance cost or maximising BESS efficiency [147].
- A multi-building scenario, i.e. multiple buildings sharing the same point of common coupling to the grid, could be considered to account for inter-building effects, to explore the achievement of collective objectives such as peak shaving [131], and to assess the scalability of the DF.

Further Extensions

In addition to extending the forecasting and the mathematical formulation, other extensions could be made. These could include:

- The real-world implementation of the DF, as discussed in [17], could be carried out to assess its performance in practice, taking into account temporal resolutions of seconds to minutes to address rapid fluctuations and real-time operational needs.
- The security level parameters for the reformulated power and energy chance constraints of the DF considering probabilistic forecasts could be optimally selected.
- An optimal sizing of the BESS power and energy capacity could be developed to ensure proper operation of the DF.

Bibliography

[1] K. Abdulla, K. Steer, A. Wirth, and S. Halgamuge. “Improving the on-line control of energy storage via forecast error metric customization”. *Journal of Energy Storage* 8 (Nov. 2016), pp. 51–59.

[2] M. A. Abdullah, K. M. Muttaqi, D. Sutanto, and A. P. Agalgaonkar. “An Effective Power Dispatch Control Strategy to Improve Generation Schedulability and Supply Reliability of a Wind Farm Using a Battery Energy Storage System”. *IEEE Transactions on Sustainable Energy* 6.3 (July 2015), pp. 1093–1102.

[3] A. F. Agarap. “Deep Learning using Rectified Linear Units (ReLU)”. *arXiv preprint arXiv:1803.08375* (Feb. 2019).

[4] R. Alvarenga, H. Herbaux, and L. Linguet. “On the Added Value of State-of-the-Art Probabilistic Forecasting Methods Applied to the Optimal Scheduling of a PV Power Plant with Batteries”. *Energies* 16.18, 6543 (Jan. 2023).

[5] B. Amos and J. Z. Kolter. “OptNet: Differentiable Optimization as a Layer in Neural Networks”. *arXiv preprint arXiv:1703.00443* (2017).

[6] J. A. E. Andersson, J. Gillis, G. Horn, J. B. Rawlings, and M. Diehl. “CasADi: a software framework for nonlinear optimization and optimal control”. *Mathematical Programming Computation* 11.1 (Mar. 2019), pp. 1–36.

[7] R. R. Appino. “Scheduling of energy storage using probabilistic forecasts and energy-based aggregated models”. *Dissertation, Karlsruher Institut für Technologie (KIT)* (2019).

[8] R. R. Appino, J. Á. González Ordiano, R. Mikut, T. Faulwasser, and V. Hagenmeyer. “On the use of probabilistic forecasts in scheduling of renewable energy sources coupled to storages”. *Applied Energy* 210 (Jan. 2018), pp. 1207–1218.

[9] L. Ardizzone, J. Kruse, S. Wirkert, et al. “Analyzing Inverse Problems with Invertible Neural Networks”. *arXiv preprint arXiv:1808.04730* (Feb. 2019).

[10] P. Artzner, F. Delbaen, J.-M. Eber, and D. Heath. “Coherent Measures of Risk”. *Mathematical Finance* 9.3 (1999), pp. 203–228.

[11] D. Bansal, R. T. Q. Chen, M. Mukadam, and B. Amos. “TaskMet: Task-Driven Metric Learning for Model Learning”. *arXiv preprint arXiv:2312.05250* (Dec. 2023).

[12] L. Baringo and M. Rahimiyan. *Virtual Power Plants and Electricity Markets: Decision Making Under Uncertainty*. Cham: Springer International Publishing, 2020.

[13] R. Bartlett, A. Wachter, and L. Biegler. “Active set vs. interior point strategies for model predictive control”. *Proceedings of the 2000 American Control Conference. ACC (IEEE Cat. No.00CH36334)*. Chicago, IL, USA: IEEE, 2000, 4229–4233 vol.6.

[14] M. Beichter, N. Friederich, J. Pinter, et al. “Decision-focused fine-tuning of time series foundation models for dispatchable feeder optimization”. *Energy and AI* 21, 100533 (2025). DOI: 10.1016/j.egyai.2025.100533.

[15] M. Beichter, K. Phipps, M. M. Frysztacki, et al. “Net load forecasting using different aggregation levels”. *Energy Informatics* 5.1, 19 (Sept. 2022).

[16] M. Beichter, D. Werling, B. Heidrich, et al. “Decision-Focused Retraining of Forecast Models for Optimization Problems in Smart Energy Systems”. *Proceedings of the 15th ACM International Conference on Future and Sustainable Energy Systems, Association for Computing Machinery*. e-Energy ’24 (2024), pp. 170–181. DOI: 10.1145/3632775.3661952.

[17] S. Beichter, M. Beichter, D. Werling, et al. “Towards a Real-World Dispatchable Feeder”. *2023 8th IEEE Workshop on the Electronic Grid (eGRID)*. Oct. 2023, pp. 1–6. DOI: 10.1109/eGrid58358.2023.10380834.

[18] R. J. Bessa, V. Miranda, A. Botterud, and J. Wang. “‘Good’ or ‘bad’ wind power forecasts: a relative concept”. *Wind Energy* 14.5 (2011), pp. 625–636.

[19] L. T. Biegler and V. M. Zavala. “Large-scale nonlinear programming using IPOPT: An integrating framework for enterprise-wide dynamic optimization”. *17th European Symposium on Computer Aided Process Engineering, Computers & Chemical Engineering* 33.3 (Mar. 2009), pp. 575–582.

[20] G. E. P. Box and G. M. Jenkins. *Time Series Analysis: Forecasting and Control*. Holden-Day, 1970.

[21] L. Breiman, J. Friedman, R. A. Olshen, and C. J. Stone. *Classification and Regression Trees*. New York: Chapman and Hall/CRC, Oct. 2017.

[22] P. J. Brockwell and R. A. Davis. *Introduction to Time Series and Forecasting*. Springer Texts in Statistics. Cham: Springer International Publishing, 2016.

[23] R. G. Brown. *Exponential Smoothing for Predicting Demand*. Little, 1956.

[24] R. Buizza. “Accuracy and Potential Economic Value of Categorical and Probabilistic Forecasts of Discrete Events”. *American Meteorological Society* (Sept. 2001).

[25] Bundesministerium für Wirtschaft und Energie. *Erneuerbare-Energien-Gesetz (EEG 2014)*. (2014).

[26] H.-J. Bungartz, S. Zimmer, M. Buchholz, and D. Pflüger. *Modeling and Simulation: An Application-Oriented Introduction*. Springer Undergraduate Texts in Mathematics and Technology. Berlin, Heidelberg: Springer, 2014.

[27] M. L. Bynum, G. A. Hackebeil, W. E. Hart, et al. *Pyomo — Optimization Modeling in Python*. Vol. 67. Springer Optimization and Its Applications. Cham: Springer International Publishing, 2021.

[28] X. Cai, M. I. Hejazi, and D. Wang. “Value of Probabilistic Weather Forecasts: Assessment by Real-Time Optimization of Irrigation Scheduling”. *Journal of Water Resources Planning and Management* 137.5 (Sept. 2011), pp. 391–403.

[29] G. Calafiore and M. Campi. “Uncertain convex programs: randomized solutions and confidence levels”. *Mathematical Programming* 102.1 (Jan. 2005), pp. 25–46.

[30] D. Carneiro, M. Guimarães, M. Carvalho, and P. Novais. “Using meta-learning to predict performance metrics in machine learning problems”. *Expert Systems* 40.1, e12900 (2023).

[31] A. Charnes and W. W. Cooper. “Chance-Constrained Programming”. *Management Science* 6.1 (1959), pp. 73–79.

[32] W. Charytoniuk, M. Chen, P. Kotas, and P. Van Olinda. “Demand forecasting in power distribution systems using nonparametric probability density estimation”. *IEEE Transactions on Power Systems* 14.4 (Nov. 1999), pp. 1200–1206.

[33] T. Chen and C. Guestrin. “XGBoost: A Scalable Tree Boosting System”. *Proceedings of the 22nd ACM SIGKDD International Conference on Knowledge Discovery and Data Mining*. KDD ’16. New York, NY, USA: Association for Computing Machinery, Aug. 2016, pp. 785–794.

[34] T.-H. Chung, V. Rostami, H. Bastani, and O. Bastani. “Decision-Aware Learning for Optimizing Health Supply Chains”. *arXiv preprint arXiv:2211.08507* (Nov. 2022).

[35] J. Coignard, M. Janvier, V. Debusschere, et al. “Evaluating forecasting methods in the context of local energy communities”. *International Journal of Electrical Power & Energy Systems* 131, 106956 (Oct. 2021).

[36] A. J. Conejo, M. Carrión, and J. M. Morales. *Decision Making Under Uncertainty in Electricity Markets*. Vol. 153. International Series in Operations Research & Management Science. Boston, MA: Springer US, 2010.

[37] F. Conte, S. Massucco, G.-P. Schiapparelli, and F. Silvestro. “Day-Ahead and Intra-Day Planning of Integrated BESS-PV Systems Providing Frequency Regulation”. *IEEE Transactions on Sustainable Energy* 11.3 (July 2020), pp. 1797–1806.

[38] T. Cover and P. Hart. “Nearest neighbor pattern classification”. *IEEE Transactions on Information Theory* 13.1 (Jan. 1967), pp. 21–27.

[39] M. David, J. Boland, L. Cirocco, P. Lauret, and C. Voyant. “Value of deterministic day-ahead forecasts of PV generation in PV + Storage operation for the Australian electricity market”. *Solar Energy* 224 (Aug. 2021), pp. 672–684.

[40] M. Diekerhof, F. Peterssen, and A. Monti. “Hierarchical Distributed Robust Optimization for Demand Response Services”. *IEEE Transactions on Smart Grid* 9.6 (Nov. 2018), pp. 6018–6029.

[41] G. Dileep. “A survey on smart grid technologies and applications”. *Renewable Energy* 146.C (2020), pp. 2589–2625.

[42] L. Dinh, J. Sohl-Dickstein, and S. Bengio. “Density estimation using Real NVP”. *arXiv preprint arXiv:1605.08803* (Feb. 2017).

[43] P. L. Donti, B. Amos, and J. Z. Kolter. “Task-based End-to-end Model Learning in Stochastic Optimization”. *arXiv preprint arXiv:1703.04529* (Apr. 2019).

[44] A. N. Elmachtoub and P. Grigas. “Smart "Predict, then Optimize"”. *arXiv preprint arXiv:1710.08005* (Nov. 2020).

[45] EURELECTRIC. *Flexibility and Aggregation: Requirements for Their Interaction in the Market*. Tech. rep. Jan. 2014.

[46] S. Fang and H. Wang. “Basics for Optimization Problem”. *Optimization-Based Energy Management for Multi-energy Maritime Grids*. Singapore, 2021, pp. 31–45.

[47] M. A. Fotouhi Ghazvini, G. Lipari, M. Pau, et al. “Congestion management in active distribution networks through demand response implementation”. *Sustainable Energy, Grids and Networks* 17, 100185 (Mar. 2019).

[48] M. Al-Gabalawy, N. S. Hosny, and A. R. Adly. “Probabilistic forecasting for energy time series considering uncertainties based on deep learning algorithms”. *Electric Power Systems Research* 196, 107216 (July 2021).

[49] T. Gneiting, F. Balabdaoui, and A. E. Raftery. “Probabilistic forecasts, calibration and sharpness”. *Journal of the Royal Statistical Society: Series B (Statistical Methodology)* 69.2 (2007), pp. 243–268.

[50] J. Á. González Ordiano, S. Waczowicz, M. Reischl, R. Mikut, and V. Hagenmeyer. “Photovoltaic power forecasting using simple data-driven models without weather data”. *Computer Science - Research and Development* 32.1 (Mar. 2017), pp. 237–246.

[51] F. M. Gonzalez-Longatt and J. Luis Rueda, eds. *PowerFactory Applications for Power System Analysis*. Power Systems. Cham: Springer International Publishing, 2014.

[52] I. Goodfellow, Y. Bengio, and A. Courville. *Deep Learning*. MIT Press, 2016.

[53] C. W. J. Granger. “Prediction with a Generalized Cost of Error Function”. *OR* 20.2 (1969), pp. 199–207.

[54] L. Gröll. “Klassifikation von Optimierungsproblemen”. *at - Automatisierungstechnik* 66.11 (Nov. 2018), pp. 903–927.

[55] A. Groß, C. Wittwer, and M. Diehl. “Stochastic model predictive control of photovoltaic battery systems using a probabilistic forecast model”. *European Journal of Control* 56 (Nov. 2020), pp. 254–264.

[56] S. Haben, M. Voss, and W. Holderbaum. *Core Concepts and Methods in Load Forecasting: With Applications in Distribution Networks*. Cham: Springer International Publishing, 2023.

[57] S. Haben, J. Ward, D. Vukadinovic Greetham, C. Singleton, and P. Grindrod. “A new error measure for forecasts of household-level, high resolution electrical energy consumption”. *International Journal of Forecasting* 30.2 (Apr. 2014), pp. 246–256.

[58] C. R. Harris, K. J. Millman, S. J. van der Walt, et al. “Array programming with NumPy”. *Nature* 585.7825 (Sept. 2020), pp. 357–362.

[59] W. E. Hart, J.-P. Watson, and D. L. Woodruff. “Pyomo: modeling and solving mathematical programs in Python”. *Mathematical Programming Computation* 3.3 (Sept. 2011), pp. 219–260.

[60] T. Hastie, R. Tibshirani, and J. H. Friedman. *The elements of statistical learning: data mining, inference, and prediction*. Second edition, corrected at 12th printing 2017. Springer Series in Statistics. New York, NY: Springer, 2017.

[61] B. Heidrich. “Challenges in Deep Learning Based Forecasting of Time Series with Calendar-driven Periodicities”. *Dissertation, Karlsruher Institut für Technologie (KIT)* (2024).

[62] B. Heidrich, M. Hertel, O. Neumann, V. Hagenmeyer, and R. Mikut. “Using conditional Invertible Neural Networks to perform mid-term peak load forecasting”. *IET Smart Grid* 7.4 (Aug. 2024), pp. 460–472.

[63] B. Heidrich, K. Phipps, O. Neumann, et al. “ProbPNN: Enhancing Deep Probabilistic Forecasting with Statistical Information”. *arXiv preprint arXiv:2302.02597* (Feb. 2023).

[64] H. Hersbach, B. Bell, P. Berrisford, et al. “The ERA5 global reanalysis”. *Quarterly Journal of the Royal Meteorological Society* (May 2020).

[65] C. C. Holt. “Forecasting seasonals and trends by exponentially weighted moving averages”. *International Journal of Forecasting* 20.1 (Jan. 2004), pp. 5–10.

[66] H. Holttinen, A. Tuohy, M. Milligan, et al. “The Flexibility Workout: Managing Variable Resources and Assessing the Need for Power System Modification”. *IEEE Power and Energy Magazine* 11.6 (Nov. 2013), pp. 53–62.

[67] T. Hong, P. Pinson, S. Fan, et al. “Probabilistic energy forecasting: Global Energy Forecasting Competition 2014 and beyond”. *International Journal of Forecasting* 32.3 (July 2016), pp. 896–913.

[68] R. A. Howard. *Dynamic programming and Markov processes*. Technology Press of Massachusetts Institute of Technology, 1960.

[69] P. J. Huber. “Robust Estimation of a Location Parameter”. *The Annals of Mathematical Statistics* 35.1 (Mar. 1964), pp. 73–101.

[70] R. J. Hyndman and G. Athanasopoulos. *Forecasting: Principles and Practice (3rd ed)*. Melbourne, Australia: OTexts, 2021.

[71] International Energy Agency. “Global EV Outlook 2023: Trends in Batteries”. *International Energy Agency* (2023).

[72] P. Kall and S. Wallace. “Stochastic Programming”. *Journal of the Operational Research Society* 46 (Jan. 1994).

[73] I. Kalogeropoulos and H. Sarimveis. “Predictive control algorithms for congestion management in electric power distribution grids”. *Applied Mathematical Modelling* 77 (Jan. 2020), pp. 635–651.

[74] G. Kara, A. Tomasgard, and H. Farahmand. “Characterizing flexibility in power markets and systems”. *Utilities Policy* 75, 101349 (Apr. 2022).

[75] N. Karmarkar. “A new polynomial-time algorithm for linear programming”. *Proceedings of the 16th Annual ACM symposium on Theory of Computing*. STOC ’84. New York, NY, USA: Association for Computing Machinery, 1984, pp. 302–311.

[76] J. Kennedy and R. Eberhart. “Particle swarm optimization”. *Proceedings of ICNN’95 - International Conference on Neural Networks*. Vol. 4. Nov. 1995, 1942–1948 vol.4.

[77] I. Khabibrakhmanov, S. Lu, H. F. Hamann, and K. Warren. “On the usefulness of solar energy forecasting in the presence of asymmetric costs of errors”. *IBM Journal of Research and Development* 60.1, 7:1–7:6 (Jan. 2016).

[78] A. J. King and S. W. Wallace. *Modeling with Stochastic Programming*. Springer Series in Operations Research and Financial Engineering. New York, NY: Springer, 2012.

[79] D. P. Kingma and J. Ba. “Adam: A Method for Stochastic Optimization”. *arXiv preprint arXiv:1412.6980* (Jan. 2017).

[80] S. Klaiber, P. Bretschneider, S. Waczowicz, et al. “A contribution to the load forecast of price elastic consumption behaviour”. *2015 IEEE Eindhoven PowerTech* (June 2015), pp. 1–6.

[81] B. P. Koirala, E. Koliou, J. Friege, R. A. Hakvoort, and P. M. Herder. “Energetic communities for community energy: A review of key issues and trends shaping integrated community energy systems”. *Renewable and Sustainable Energy Reviews* 56 (Apr. 2016), pp. 722–744.

[82] M. Korpaas, A. T. Holen, and R. Hildrum. “Operation and sizing of energy storage for wind power plants in a market system”. *14th Power Systems Computation Conference, International Journal of Electrical Power & Energy Systems 25.8* (Oct. 2003), pp. 599–606.

[83] J.-P. Kreiß and G. Neuhaus. *Einführung in die Zeitreihenanalyse*. Statistik und ihre Anwendungen. Berlin/Heidelberg: Springer-Verlag, 2006.

[84] V. Kuleshov, N. Fenner, and S. Ermon. “Accurate Uncertainties for Deep Learning Using Calibrated Regression”. *Proceedings of the 35th International Conference on Machine Learning*. PMLR, July 2018, pp. 2796–2804.

[85] I. Lampropoulos, P. Garoufalis, P. P. van den Bosch, and W. L. Kling. “Hierarchical predictive control scheme for distributed energy storage integrated with residential demand and photovoltaic generation”. *IET Generation, Transmission & Distribution* 9.15 (2015), pp. 2319–2327.

[86] A. H. Land and A. G. Doig. “An Automatic Method of Solving Discrete Programming Problems”. *Econometrica* 28.3 (1960), pp. 497–520.

[87] U. Langenmayr, W. Wang, and P. Jochem. “Unit commitment of photovoltaic-battery systems: An advanced approach considering uncertainties from load, electric vehicles, and photovoltaic”. *Applied Energy* 280, 115972 (Dec. 2020).

[88] Y. LeCun, Y. Bengio, and G. Hinton. “Deep learning”. *Nature* 521.7553 (May 2015), pp. 436–444.

[89] G. Li and H.-D. Chiang. “Toward Cost-Oriented Forecasting of Wind Power Generation”. *IEEE Transactions on Smart Grid* 9.4 (July 2018), pp. 2508–2517.

[90] O. Lindberg, D. Lingfors, J. Arnqvist, D. Van Der Meer, and J. Munkhammar. “Day-ahead probabilistic forecasting at a co-located wind and solar power park in Sweden: Trading and forecast verification”. *Advances in Applied Energy* 9 (Feb. 2023), p. 100120.

[91] O. Lindberg, R. Zhu, and J. Widén. “Quantifying the value of probabilistic forecasts when trading renewable hybrid power parks in day-ahead markets: A Nordic case study”. *Renewable Energy* 237, 121617 (Dec. 2024).

[92] J. Lofberg. “YALMIP : a toolbox for modeling and optimization in MATLAB”. *2004 IEEE International Conference on Robotics and Automation (IEEE Cat*. Sept. 2004, pp. 284–289.

[93] M. Lubin, O. Dowson, J. D. Garcia, et al. “JuMP 1.0: recent improvements to a modeling language for mathematical optimization”. *Mathematical Programming Computation* 15.3 (Sept. 2023), pp. 581–589.

[94] J. Luoma, P. Mathiesen, and J. Kleissl. “Forecast value considering energy pricing in California”. *Applied Energy* 125 (July 2014), pp. 230–237.

[95] J. Mandi, V. Bucarey, M. M. K. Tchomba, and T. Guns. “Decision-Focused Learning: Through the Lens of Learning to Rank”. *Proceedings of the 39th International Conference on Machine Learning*. PMLR, June 2022, pp. 14935–14947.

[96] A. Mashlakov, T. Kuronen, L. Lensu, A. Kaarna, and S. Honkapuro. “Assessing the performance of deep learning models for multivariate probabilistic energy forecasting”. *Applied Energy* 285, 116405 (Mar. 2021).

[97] W. McKinney. “Data Structures for Statistical Computing in Python”. *Proceedings of the 9th Python in Science Conference* (2010), pp. 56–61.

[98] S. Meisenbacher, M. Turowski, K. Phipps, et al. “Review of automated time series forecasting pipelines”. *WIREs Data Mining and Knowledge Discovery* 12.6, e1475 (2022).

[99] J. M. Morales, A. J. Conejo, H. Madsen, P. Pinson, and M. Zugno. “Integrating Renewables in Electricity Markets: Operational Problems”. *International Series in Operations Research & Management Science 205, Springer US* (2014).

[100] A. H. Murphy. “What Is a Good Forecast? An Essay on the Nature of Goodness in Weather Forecasting”. *Weather and Forecasting* (June 1993).

[101] K. R. Mylne. “Decision-making from probability forecasts based on forecast value”. *Meteorological Applications* 9.3 (Sept. 2002), pp. 307–315.

[102] U. R. Nair, M. Sandelic, A. Sangwongwanich, et al. “Grid Congestion Mitigation and Battery Degradation Minimisation Using Model Predictive Control in PV-Based Microgrid”. *IEEE Transactions on Energy Conversion* 36.2 (June 2021), pp. 1500–1509.

[103] E. Namor, F. Sossan, R. Cherkaoui, and M. Paolone. “Control of Battery Storage Systems for the Simultaneous Provision of Multiple Services”. *IEEE Transactions on Smart Grid* 10.3 (May 2019), pp. 2799–2808.

[104] S. M. Nosratabadi, R.-A. Hooshmand, and E. Gholipour. “A comprehensive review on microgrid and virtual power plant concepts employed for distributed energy resources scheduling in power systems”. *Renewable and Sustainable Energy Reviews* 67 (Jan. 2017), pp. 341–363.

[105] A. Paszke, S. Gross, F. Massa, et al. “PyTorch: An Imperative Style, High-Performance Deep Learning Library”. *arXiv preprint arXiv:1912.01703* (Dec. 2019).

[106] F. Pedregosa, G. Varoquaux, A. Gramfort, et al. “Scikit-learn: Machine Learning in Python”. *Journal of Machine Learning Research* 12.85 (2011), pp. 2825–2830.

[107] F. Petropoulos, D. Apiletti, V. Assimakopoulos, et al. “Forecasting: theory and practice”. *International Journal of Forecasting* 38.3 (July 2022), pp. 705–871.

[108] K. Phipps. “Quantifying and Interpreting Uncertainty in Time Series Forecasting”. *Dissertation, Karlsruher Institut für Technologie (KIT)* (2024).

[109] K. Phipps, B. Heidrich, M. Turowski, et al. “Generating probabilistic forecasts from arbitrary point forecasts using a conditional invertible neural network”. *Applied Intelligence 54* (Apr. 2024).

[110] K. Phipps, S. Lerch, M. Andersson, et al. “Evaluating ensemble post-processing for wind power forecasts”. *Wind Energy* 25.8 (2022), pp. 1379–1405.

[111] P. Pinson, J. Juban, and G. N. Kariniotakis. “On the Quality and Value of Probabilistic Forecasts of Wind Generation”. *2006 International Conference on Probabilistic Methods Applied to Power Systems*. Stockholm, Sweden: IEEE, June 2006, pp. 1–7.

[112] J. Pinter, F. Zahn, M. Beichter, R. Mikut, and V. Hagenmeyer. “Probabilistic Day-Ahead Battery Scheduling based on Mixed Random Variables for Enhanced Grid Operation”. *arXiv preprint arXiv:2411.12480* (Nov. 2024).

[113] J. Platt. “Probabilistic Outputs for Support Vector Machines and Comparisons to Regularized Likelihood Methods”. *Advances in Large Margin Classifier* 10.3 (June 2000), pp. 61–74.

[114] D. Putz, M. Gumhalter, and H. Auer. “The true value of a forecast: Assessing the impact of accuracy on local energy communities”. *Sustainable Energy, Grids and Networks* 33, 100983 (Mar. 2023).

[115] S. Rass, S. Schauer, S. König, and Q. Zhu. “Mathematical Decision Making”. en. *Cyber-Security in Critical Infrastructures: A Game-Theoretic Approach*. Advanced Sciences and Technologies for Security Applications. Cham: Springer International Publishing, 2020, pp. 43–78.

[116] E. L. Ratnam, S. R. Weller, C. M. Kellett, and A. T. Murray. "Residential load and rooftop PV generation: an Australian distribution network dataset". *International Journal of Sustainable Energy* 36.8 (Sept. 2017), pp. 787–806.

[117] I. Rechenberg and M. Eigen. *Evolutionsstrategie: Optimierung technischer Systeme nach Prinzipien der biologischen Evolution*. Problemata 15. Stuttgart-Bad Cannstadt: Frommann-Holzboog, 1973.

[118] J. Riley. *Understanding Metadata: What is Metadata, and What is it For?: A Primer*. NISO, Jan. 2017.

[119] U. Sadana, A. Chenreddy, E. Delage, et al. "A Survey of Contextual Optimization Methods for Decision Making under Uncertainty". *arXiv preprint arXiv:2306.10374* (June 2023).

[120] D. Salinas, V. Flunkert, J. Gasthaus, and T. Januschowski. "DeepAR: Probabilistic forecasting with autoregressive recurrent networks". *International Journal of Forecasting* 36.3 (July 2020), pp. 1181–1191.

[121] K. Schwenk. "A Smart Charging Assistant for Electric Vehicles Considering Battery Degradation, Power Grid and User Constraints". *Dissertation, Karlsruher Institut für Technologie (KIT)* (2022).

[122] K. Schwenk, S. Meisenbacher, B. Briegel, et al. "Integrating Battery Aging in the Optimization for Bidirectional Charging of Electric Vehicles". *IEEE Transactions on Smart Grid* 12.6 (Nov. 2021), pp. 5135–5145.

[123] R. J. Serfling. *Approximation theorems of mathematical statistics*. Wiley Series in Probability and Statistics. New York, NY: Wiley, 2002.

[124] S. Shah, A. Perrault, B. Wilder, and M. Tambe. "Leaving the Nest: Going Beyond Local Loss Functions for Predict-Then-Optimize". *arXiv preprint arXiv:2305.16830* (May 2023).

[125] S. Shah, K. Wang, B. Wilder, A. Perrault, and M. Tambe. "Decision-Focused Learning without Differentiable Optimization: Learning Locally Optimized Decision Losses". *arXiv preprint arXiv:2203.16067* (Nov. 2022).

[126] F. Sossan, E. Namor, R. Cherkaoui, and M. Paolone. "Achieving the Dispatchability of Distribution Feeders Through Prosumers Data Driven Forecasting and Model Predictive Control of Electrochemical Storage". *IEEE Transactions on Sustainable Energy* 7.4 (Oct. 2016), pp. 1762–1777.

[127] F. Sossan and M. Paolone. "Integration and Operation of Utility-Scale Battery Energy Storage Systems: the EPFL's Experience". *IFAC Workshop on Control of Transmission and Distribution Smart Grids CTDSG 2016, IFAC-PapersOnLine* 49.27 (Jan. 2016), pp. 433–438.

[128] E. Stai, L. Reyes-Chamorro, F. Sossan, J.-Y. Le Boudec, and M. Paolone. "Dispatching Stochastic Heterogeneous Resources Accounting for Grid and Battery Losses". *IEEE Transactions on Smart Grid* 9.6 (Nov. 2018), pp. 6522–6539.

[129] T. S. Talagala, R. J. Hyndman, and G. Athanasopoulos. "Meta-learning how to forecast time series". *Journal of Forecasting* 42.6 (2023), pp. 1476–1501.

[130] W. R. D. Tarnate, F. Ponci, and A. Monti. “Uncertainty-Aware Model Predictive Control for Residential Buildings Participating in Intraday Markets”. *IEEE Access* 10 (2022), pp. 7834–7851.

[131] M. Treutlein, M. Schmidt, R. Hahn, et al. “Generating peak-aware pseudo-measurements for low-voltage feeders using metadata of distribution system operators”. *arXiv preprint arXiv:2409.19713* (Sept. 2024).

[132] M. Turowski. “Data-Driven Methods for Managing Anomalies in Energy Time Series”. *Dissertation, Karlsruher Institut für Technologie (KIT)* (2023).

[133] V. N. Vapnik. *The Nature of Statistical Learning Theory*. New York, NY: Springer, 2000.

[134] M. Vasile, ed. *Optimization Under Uncertainty with Applications to Aerospace Engineering*. Cham: Springer International Publishing, 2021.

[135] A. Vaswani, N. Shazeer, N. Parmar, et al. “Attention is all you need”. *Proceedings of the 31st International Conference on Neural Information Processing Systems*. NIPS’17. Long Beach, California, USA: Curran Associates Inc., 2017, pp. 6000–6010.

[136] J. Vossen, B. Feron, and A. Monti. “Probabilistic Forecasting of Household Electrical Load Using Artificial Neural Networks”. *2018 IEEE International Conference on Probabilistic Methods Applied to Power Systems (PMAPS)*. June 2018, pp. 1–6.

[137] A. Wächter and L. T. Biegler. “On the implementation of an interior-point filter line-search algorithm for large-scale nonlinear programming”. *Mathematical Programming* 106.1 (Mar. 2006), pp. 25–57.

[138] S. Waczowicz. “Konzept zur datengetriebenen Analyse und Modellierung des preisbeeinflussten Verbrauchsverhaltens”. *Dissertation, Karlsruher Institut für Technologie (KIT)* (2018).

[139] C. Wang, T. Bäck, H. H. Hoos, et al. “Automated Machine Learning for Short-term Electric Load Forecasting”. *2019 IEEE Symposium Series on Computational Intelligence (SSCI)*. Dec. 2019, pp. 314–321.

[140] X. Wang, K. Smith-Miles, and R. Hyndman. “Rule induction for forecasting method selection: Meta-learning the characteristics of univariate time series”. *Lattice Computing and Natural Computing (JCIS 2007) / Neural Networks in Intelligent Systems Design (ISDA 2007), Neurocomputing* 72.10 (June 2009), pp. 2581–2594.

[141] Y. Wang and L. Wu. “Improving economic values of day-ahead load forecasts to real-time power system operations”. *IET Generation, Transmission & Distribution* 11.17 (2017), pp. 4238–4247.

[142] M. Weber, M. Turowski, H. K. Çakmak, et al. “Data-Driven Copy-Paste Imputation for Energy Time Series”. *IEEE Transactions on Smart Grid* 12.6 (Nov. 2021), pp. 5409–5419.

[143] D. Werling, M. Beichter, B. Heidrich, et al. “Automating Value-Oriented Forecast Model Selection by Meta-learning: Application on a Dispatchable Feeder”. *Energy Informatics, Lecture Notes in Computer Science, Springer Nature Switzerland* (2024), pp. 95–116. DOI: 10.1007/978-3-031-48649-4_6.

[144] D. Werling, M. Beichter, B. Heidrich, et al. “The Impact of Forecast Characteristics on the Forecast Value for the Dispatchable Feeder”. *Companion Proceedings of the 14th ACM International Conference on Future Energy Systems, e-Energy ’23, Association for Computing Machinery* (June 2023), pp. 59–71. DOI: 10.1145/3599733.3600251.

[145] D. Werling, B. Heidrich, H. K. Çakmak, and V. Hagenmeyer. “Towards line-restricted dispatchable feeders using probabilistic forecasts for PV-dominated low-voltage distribution grids”. *Proceedings of the 13th ACM International Conference on Future Energy Systems, e-Energy ’22, Association for Computing Machinery* (June 2022), pp. 395–400. DOI: 10.1145/3538637.3538868.

[146] W. van Westering and H. Hellendoorn. “Low voltage power grid congestion reduction using a community battery: Design principles, control and experimental validation”. *International Journal of Electrical Power & Energy Systems* 114, 105349 (Jan. 2020).

[147] N. Wirtz and A. Monti. “Battery Storage Utilization for Cost and Imbalance Reduction in a Balancing Group”. *2018 IEEE PES Innovative Smart Grid Technologies Conference Europe (ISGT-Europe)*. Oct. 2018, pp. 1–6.

[148] Y. Yang, S. Bremner, C. Menictas, and M. Kay. “Modelling and optimal energy management for battery energy storage systems in renewable energy systems: A review”. *Renewable and Sustainable Energy Reviews* 167, 112671 (Oct. 2022).

[149] J. H. Yi, R. Cherkaoui, and M. Paolone. “Dispatch-aware planning of energy storage systems in active distribution network”. *Electric Power Systems Research* 190, 106644 (2021).

[150] G. U. Yule. “On a Method of Investigating Periodicities in Disturbed Series, with Special Reference to Wolfer’s Sunspot Numbers”. *Philosophical Transactions of the Royal Society of London. Series A, Containing Papers of a Mathematical or Physical Character, Vol. 226, The Royal Society* (1927), pp. 267–298.

[151] H. Zhang. “The Optimality of Naive Bayes”. *Proceedings of the Seventeenth International Florida Artificial Intelligence Research Society Conference, FLAIRS 2004* (Jan. 2004).

[152] J. Zhang, Y. Wang, and G. Hug. “Cost-oriented load forecasting”. *Electric Power Systems Research* 205, 107723 (Apr. 2022).

[153] Y. Zhang, M. Jia, H. Wen, and Y. Shi. “Value-oriented Renewable Energy Forecasting for Coordinated Energy Dispatch Problems at Two Stages”. *arXiv preprint arXiv:2309.00803* (Sept. 2023).

[154] Y. Zhang, H. Wen, Y. Bian, and Y. Shi. “Deriving Loss Function for Value-oriented Renewable Energy Forecasting”. *arXiv preprint arXiv:2310.00571* (Oct. 2023).

[155] A. Zharmagambetov, B. Amos, A. Ferber, et al. “Landscape Surrogate: Learning Decision Losses for Mathematical Optimization Under Partial Information”. *arXiv preprint arXiv:2307.08964* (Nov. 2023).

[156] Y. Zhu, Z. Toth, R. Wobus, D. Richardson, and K. Mylne. “The Economic Value Of Ensemble-Based Weather Forecasts”. *American Meteorological Society* (Jan. 2002).

[157] Y. Zuo, Z. Yuan, F. Sossan, et al. “Performance assessment of grid-forming and grid-following converter-interfaced battery energy storage systems on frequency regulation in low-inertia power grids”. *Sustainable Energy, Grids and Networks* 27, 100496 (Sept. 2021).

List of Figures

List of Tables

Appendix

A

A.1 Dealing with Non-Convexity

While the non-convexity in the computation of the DS considering point forecasts, the rescheduling via MPC, and the calculation of the actual dispatch comes solely from the complementarity constraint of the BESS active power input

$$\bar{p}_s^+(k) \cdot \bar{p}_s^-(k) \geq -\zeta,$$

the reformulated energy chance constraint

$$1 - \epsilon_E - \epsilon_{\text{fix}}(k) - \epsilon_{\text{var}}(k) \leq F_{\Delta E_l(k+1)}\left(\bar{e}_s(k+1) - e_s^{\min}\right) - F_{\Delta E_l(k+1)}\left(\bar{e}_s(k+1) - e_s^{\max}\right)$$

additionally introduces non-convexity in the computation of the DS considering probabilistic forecasts. As a global minimum for non-convex OPs can not be guaranteed, it is important to pay awareness and potentially conduct further analysis for trustworthy solutions. In our case, we conduct the following analysis on selected data:

- Computation of DS considering point forecast / Rescheduling via MPC: We exclude the complementarity constraint, which results in a convex OP. For the selected data, the convex OP yields the same solutions as the original OP. This suggests that the original OP could be reformulated as a convex problem.
- Computation of DS considering probabilistic forecasts: We run the OP with different initial values with the same solutions as a result. However, this consistency of solutions does not ensure convergence to the global minimum, which can not be proved. Furthermore, we exclude the complementarity constraint, which leads to the same solutions as the original OP.
- Calculation of actual dispatch: The OP can be rewritten to a rule-based approach via

$$\texttt{If} \quad e_s^{\min} \leq e_s(k) + p_{g_{\text{ref}}}(k) - p_l(k) - \mu \cdot |p_{g_{\text{ref}}}(k) - p_l(k)| \leq e_s^{\max} \quad \texttt{and}$$

$$
\begin{aligned}
p_s^{\min} \leq p_{g_{\text{ref}}}(k) - p_l(k) \leq p_s^{\max}: \\
p_s(k) = p_{g_{\text{ref}}}(k) - p_l(k) \\
\texttt{elif } p_{g_{\text{ref}}}(k) - p_l(k) > 0: \\
p_s(k) = \min\left\{p_s^{\max}, \frac{e_s^{\max} - e_s(k)}{1-\mu}\right\} \\
\texttt{elif } p_{g_{\text{ref}}}(k) - p_l(k) < 0: \\
p_s(k) = \max\left\{p_s^{\min}, -\frac{e_s^{\min} - e_s(k)}{1+\mu}\right\}.
\end{aligned}
$$

The comparison of the solutions of the rule-based approach and the OP shows that the OP returns the global minimum. For formatting consistency within the implementation, we use the formulation as OP. Note that the exclusion of the complementarity constraint of the BESS active power input results in a different solution.

A.2 Parameter Specifications of the Optimisation Problems for the Dispatchable Feeder

Tab. A.1.: The parameter specifications of the optimisation problems for the dispatchable feeder in Equation (2.23), Equation (2.24), Equation (2.25) and Equation (2.26) if not specified otherwise.

Parameter	Value
Δt	1 (hour)
k_0	index of time interval starting at 12 PM
k_b	index of time interval starting at 12 AM
m	6 (hour)
$\mathcal{K}$	$\{k_b, ..., k_b + 29\}$
c^+_{quad}	0.05 (€/kWh^2)
c^+_{lin}	0.3 (€/kWh)
c^-_{quad}	0.05 (€/kWh^2)
c^-_{lin}	0.15 (€/kWh)
$p_s^{\min}$	-5 (kW)
$p_s^{\max}$	5 (kW)
$e_s^{\min}$	0 (kWh)
$e_s^{\max}$	19.5 (kWh)
μ	0.05
$\bar{e}_s^{k_b}$	day 1: $\frac{e_s^{\max}}{2}$ (kWh)
	all other days: estimated[1]
γ	1e-8
c_{fix}	50
c_{var}	[0.1, 0.2, 0.4, 1000000,...,100000]

A.3 Estimation of State of Energy at k_b

For the day-ahead computation of the DS, an estimate of the SoE at k_b is required. Therefore, as in [8], this SoE is estimated based on the current SoE at k_0 and the prosumption forecasts. For this estimation, the same OP as in Equation (2.26) is run for each time index between k_0 and k_b, i.e. twelve times with the specifications in Table A.1, using the mean prosumption forecasts $\hat{\bar{p}}_l(k)$ generated at k_0 instead of the actual prosumption values $p_l(k)$.

[1]The initial state of energy $\bar{e}_s^{k_b}$ for all other days is estimated as described in Appendix A.3.

A.4 Comparison of Modification for Bias and of Dispersion for Security Level Parameters $\epsilon_P = 0.1$, $\epsilon_E = 0.3$

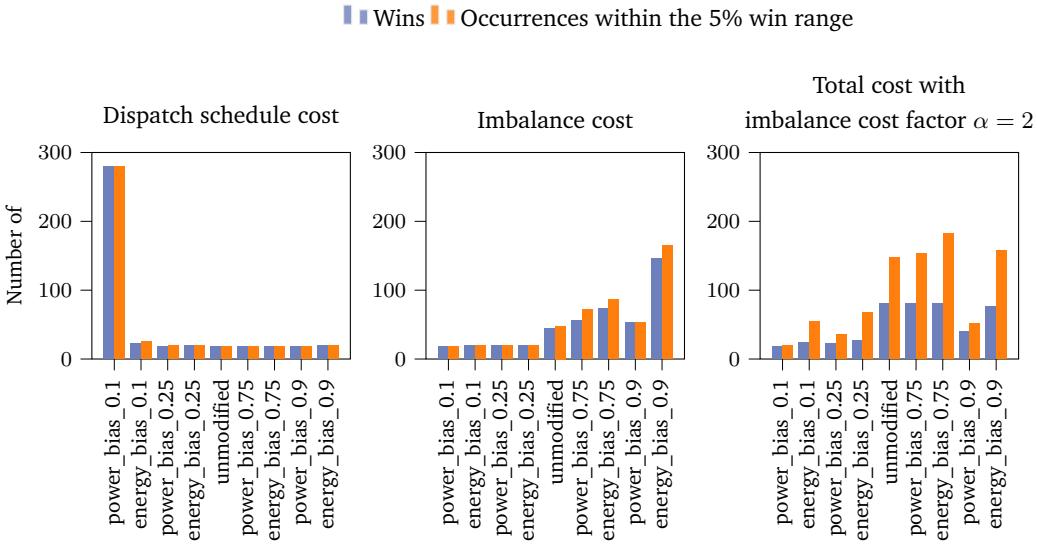

(a) Modification for bias

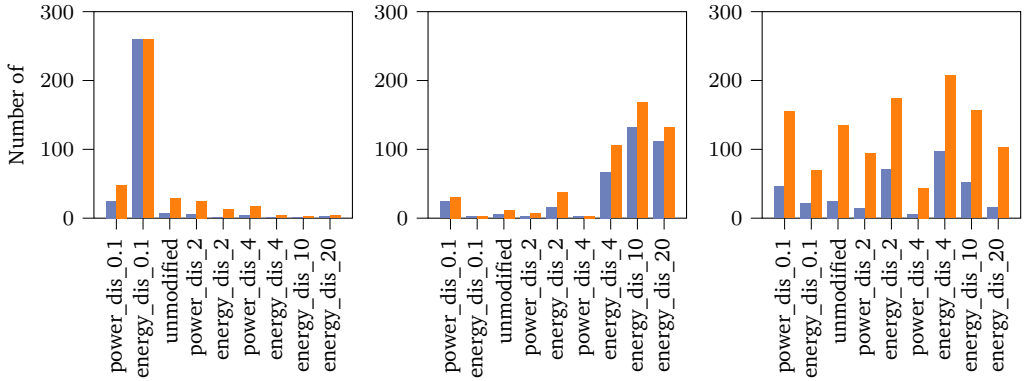

(b) Modification of dispersion

Fig. A.1.: The wins and the occurrences within the 5% win range for the considered average daily cost, i.e. the dispatch schedule cost (left), the imbalance cost (middle), and the total cost with imbalance cost factor $\alpha = 2$ (right) and the security level parameters $\epsilon_P = 0.1$, $\epsilon_E = 0.3$ for the considered modifications for a bias (a) and the considered modifications of the dispersion (b). Note that more wins and more occurrences within the 5% win range are better.

A.5 The Dispatch Schedule Costs and the Imbalance Costs for the Comparison of Different Dispatchable Feeders

Tab. A.2.: The average daily dispatch schedule costs and the average daily imbalance costs in € for the $DF_{\text{v-o point}}$, the $DF_{\text{v-o prob,total 2}}$, the $DF_{\text{v-o prob,total 10}}$, the $DF_{\text{MSE point}}$, the $DF_{\text{unmod prob,total 2}}$, and the $DF_{\text{unmod prob,total 10}}$. The average daily costs are averaged over the last year and over all buildings with IDs greater than 200. For the average daily costs, lower values are better. Further average daily costs are displayed in Table 7.2.

Approaches	DS	Imbalance
$DF_{\text{v-o point}}$	3.87	0.59
$DF_{\text{v-o prob,total 2}}$	4.20	0.53
$DF_{\text{v-o prob,total 10}}$	4.23	0.46
$DF_{\text{MSE point}}$	3.29	0.80
$DF_{\text{unmod prob,total 2}}$	3.36	0.80
$DF_{\text{unmod prob,total 10}}$	3.83	0.53

A.6 Security Level Parameter Specifications for the Line-Restricted Dispatchable Feeder

Tab. A.3.: The security level parameters ϵ_P and ϵ_E used in Chapter 8 for each considered week.

Week	ϵ_P	ϵ_E
1	0.40	0.55
2	0.55	0.70
3	0.55	0.70
4	0.40	0.55
5	0.40	0.10
6	0.70	0.70
7	0.40	0.25
8	0.25	0.40
9	0.40	0.70
10	0.40	0.55
11	0.25	0.40
12	0.25	0.70

A.7 Evaluation of the Line-Restricted Dispatchable Feeder for Different Sets of Forecasts

Tab. A.4.: The minimum possible line restriction in kW and the percentage share of minimum possible line restriction relative to the benchmark $LRDF_{perf}$ in % of the benchmark $LRDF_{point}$, the $LRDF^{fix}$, and the $LRDF^{opt}$ and the percentage of peak shaving relative to the benchmark no BESS in % of the $LRDF^{fix}$ and the $LRDF^{opt}$ for all considered weeks and the four additional generated set of forecasts.

(a) Set 1

Week	$LRDF_{point}$		$LRDF^{fix}$			$LRDF^{opt}$		
	MPLR	$\%share_{perf}$	MPLR	$\%PS_{no\ BESS}$	$\%share_{perf}$	MPLR	$\%PS_{no\ BESS}$	$\%share_{perf}$
1	3.53	45.61	3.51	42.55	45.87	3.51	42.55	45.87
2	3.82	59.42	3.82	44.23	59.42	3.12	54.45	72.76
3	5.94	76.94	5.95	35.04	76.81	5.94	35.15	76.97
4	7.01	84.59	7.01	33.24	84.59	6.90	34.29	85.94
5	8.13	82.04	8.11	28.61	82.24	8.11	28.61	82.24
6	4.96	60.69	4.96	25.19	60.69	4.96	25.19	60.69
7	9.49	63.75	9.57	13.08	63.22	9.49	13.81	63.75
8	6.84	90.35	7.00	37.39	88.29	6.60	40.97	93.64
9	6.40	79.22	6.40	34.76	79.22	6.40	34.76	79.22
10	6.84	46.05	6.70	15.83	47.01	6.10	23.37	51.64
11	3.66	53.01	3.64	44.34	53.30	2.30	64.83	84.35
12	3.00	34.33	3.00	45.95	34.33	2.70	51.35	38.15

(b) Set 2

Week	$LRDF_{point}$		$LRDF^{fix}$			$LRDF^{opt}$		
	MPLR	$\%share_{perf}$	MPLR	$\%PS_{no\ BESS}$	$\%share_{perf}$	MPLR	$\%PS_{no\ BESS}$	$\%share_{perf}$
1	3.84	41.93	3.74	38.79	43.05	3.74	38.79	43.05
2	3.67	61.85	3.17	53.72	71.61	3.07	55.18	73.94
3	6.20	73.71	5.90	35.59	77.46	5.90	35.59	77.46
4	7.18	82.59	7.08	32.57	83.76	6.80	35.24	87.21
5	9.10	73.30	9.10	19.8	73.30	9.10	19.8	73.30
6	4.66	64.59	4.43	33.18	67.95	4.43	33.18	67.95
7	8.97	67.45	8.97	18.53	67.45	10.10	8.27	59.90
8	7.31	84.54	7.50	32.92	82.40	7.30	34.70	84.66
9	6.43	78.85	6.61	32.62	76.70	6.40	34.76	79.22
10	5.66	55.65	5.66	28.89	55.65	5.66	28.89	55.65
11	3.93	49.36	3.90	40.37	49.74	3.90	40.37	49.74
12	3.21	32.09	3.08	44.50	33.44	2.40	56.76	42.92

(c) Set 3

Week	$LRDF_{point}$		$LRDF^{fix}$			$LRDF^{opt}$		
	MPLR	$\%share_{perf}$	MPLR	$\%PS_{no\ BESS}$	$\%share_{perf}$	MPLR	$\%PS_{no\ BESS}$	$\%share_{perf}$
1	5.26	30.61	5.08	16.86	31.69	5.08	16.86	31.69
2	3.45	65.80	2.96	56.79	76.69	2.96	56.79	76.69
3	5.74	79.62	5.59	38.97	81.75	5.59	38.97	81.75
4	7.25	81.79	7.14	32.00	83.05	7.10	32.38	83.52
5	8.49	78.56	8.38	26.23	79.59	8.11	28.61	82.24
6	5.15	58.45	4.65	29.86	64.73	4.65	29.86	64.73
7	8.77	68.99	9.69	11.99	62.44	8.77	20.35	68.99
8	7.40	83.51	7.30	34.70	84.66	7.10	36.49	87.04
9	7.01	72.33	7.03	28.34	72.12	6.58	32.93	77.05
10	5.67	55.56	5.66	28.89	55.65	5.66	28.89	55.65
11	3.90	49.74	3.69	43.58	52.57	3.69	43.58	52.57
12	3.42	30.12	3.12	43.78	33.01	3.00	45.95	34.33

(d) Set 4

Week	$LRDF_{point}$		$LRDF^{fix}$			$LRDF^{opt}$		
	MPLR	$\%share_{perf}$	MPLR	$\%PS_{no\ BESS}$	$\%share_{perf}$	MPLR	$\%PS_{no\ BESS}$	$\%share_{perf}$
1	4.64	34.70	4.26	30.28	37.79	4.26	30.28	37.79
2	3.77	60.21	3.63	47.01	62.53	2.90	57.66	78.28
3	6.03	75.79	6.06	33.84	75.41	5.90	35.59	77.46
4	7.27	81.57	7.05	32.86	84.11	6.90	34.29	85.94
5	8.11	82.24	8.11	28.61	82.24	8.11	28.61	82.24
6	4.78	62.97	5.13	22.62	58.67	4.71	28.96	63.91
7	8.17	74.05	8.49	22.89	71.26	8.17	25.79	74.05
8	6.96	88.79	6.77	39.45	91.29	6.69	40.16	92.38
9	6.02	84.22	6.50	33.74	78.00	5.92	39.65	85.64
10	5.66	55.65	5.66	28.89	55.65	5.66	28.89	55.65
11	3.90	49.74	3.90	40.37	49.74	3.59	45.11	54.04
12	3.29	31.31	3.15	43.24	32.70	2.60	53.15	39.62

Colophon

This thesis was typeset with LaTeX 2_ε. It uses the *Clean Thesis* style developed by Ricardo Langner. The design of the *Clean Thesis* style is inspired by user guide documents from Apple Inc.

Download the *Clean Thesis* style at `http://cleanthesis.der-ric.de/`.